University of Alberta

Phase Behavior and Thermophysical Properties of Peace River Bitumen + Propane mixtures

by

Yoann DINI

A thesis submitted to the Faculty of Graduate Studies and Research in partial fulfillment of the requirements for the degree of

Master of Science
in
Chemical and Materials Engineering
Department of Chemical and Materials Engineering

©Yoann DINI
Summer 2015
Edmonton, Alberta

Abstract

Oil sands bitumen is increasingly recovered by injecting steam into reservoirs using the energy intensive Steam assisted gravity drainage (SAGD) process. Interest in improving recovery and energy efficiencies have led to an interest in injecting light hydrocarbons along with or instead of steam as a basis for the development of improved production technologies. Propane and mixtures including propane as a principal component are among the leading potential injectants. In this work, the phase behavior, phase composition and phase densities of propane + Peace River bitumen mixtures are studied using a variable-volume X-ray view cell in the temperature range between 303 K and 393 K at pressures ranging from 1 to 6 MPa. This apparatus permits the study of mixtures that are opaque to visible light and provides real time phase volume and liquid phase density measurements. Pressure-temperature at fixed composition, and pressure-composition at fixed temperature phase diagrams, and temperature-composition and pressure-temperature phase projections are presented, along with the saturated compositions and densities of the co-existing bitumen saturated propane liquid (L1) and propane saturated bitumen liquid (L2) phases. The phase behavior of this pseudo binary mixture can be categorized as Type III according to the van Konynenburg-Scott nomenclature. One of the key findings is the unexpected magnitude of the volumes of mixing, particularly for the L1 phase. Saturated L1 and L2 phases are both significantly less dense than liquid water phases at the same temperatures and pressures. The data set is expected to provide a benchmark for process development and process design calculations for ongoing bitumen production and de-asphalting applications.

Acknowledgements.

Table of Contents

List of Tables

List of Figures

List of Abbreviations and Symbols

Symbol	Unit	Description
Λ	nm	Wave lengh of the X-ray beam
P	$Kg.m^{-3}$	Density
M	$m^2.kg^{-1}$	Mass attenuation coefficient of a mixture
μ_i	$m^2.kg^{-1}$	Mass attenuation coefficient of elemental i
Δx	M	Distance
ABVB		Athabasca Vacuum residue
I	Shade of grey	Intensity
L		Liquid
L1		Low density liquid phase
L2		High density liquid phase
L1V		Low density liquid phase-vapor
L2V		High density liquid phase-vapor
L1L2V		Low density liquid phase-heavier liquid phase-vapor
L2V/L2		Boundary which separate High density liquid-vapor and High density liquid regions
L1V/L1		Boundary which separate Low density liquid-vapor and Low density liquid regions
L1L2V/L1L2		Boundary which separate Low density liquid phase- High density liquid phase-vapor and Low density liquid phase-High density liquid phase region
Mole Fraction	Mole fraction	Composition
P	MPa	Pressure
PRB		Peace River Bitumen
PT		Pressure-Temperature
Px		Pressure-Composition

T	K	Temperature
V		Vapor
Wt. fraction	Weight fraction	Composition

Chapter 1: Introduction

1.1 Oil sands

Canada has one of the largest reserves of oil including conventional and unconventional oil in the world. Conventional oils are liquid at reservoir pressure and temperature. Unconventional oils comprising oil sands, oil shale and tight oil are typically immobile within reservoirs and are harder to produce. However, the reserves of unconventional oil are bigger than the reserves of conventional oil, and there are geopolitical and regional incentives for unconventional oil production and processing.

In Alberta, more than 170 billions barrels of unconventional oil can be produced economically with current technologies. The three big reserves of oil sands are in the Athabasca Wabiskaw-McMurray, Cold Lake Clearwater, and Peace River Bluesjy-Gething basins. They occupy an area of 142,000 km^2. The preferred production methods vary by site. Two types of production processes exist to recover these reserves: open pit mining, which is very similar to coal mining, and in-situ production methods. Most of the in-situ production technologies are based on Steam-Assisted Gravity Drainage (SAGD) developed by Butler and co-workers during the 1970s [1,2]. This process consists of injecting high-pressure steam into reservoirs in order to decrease the crude oil viscosity and permit pumping. In Canada, the crude oil produced from oil sands is commonly called bitumen. Bitumen composition varies within a basin by depth and geographically by location. The composition of bitumen produced also varies depending on the extraction process used. This is one of the reasons why this oil is not very well defined and why new technology development associated with this resource type is complicated. For example, laboratory based studies rely on samples extracted from cores or field pilots and it is not obvious if these samples are representative of the hydrocarbon resource as a whole or even from the specific rock from which they are extracted. Nevertheless, it is still very important to study the properties of these samples individually to gain an appreciation for the spectrum of properties and phase behaviors exhibited and to modify or develop new technologies that meet increasingly stringent environment regulations.

1.2 Bitumen Sample

Produced bitumen thermophysical properties depend on many parameters that change with the extent of bacterial degradation, their locality and solvents used during in-situ production or open pit mining prior to sample extraction. Samples resemble one another to varying degrees but are not identical and none possess properties that are identical to the thermophysical properties of the unproduced bitumen in reservoirs. Like all crude oils, bitumen is ill-defined. Ill-defined components include boiling fractions, molar mass distributions or so-called solubility classes, such as those obtained from SARA analysis, that comprise innumerable components and where even if the values among samples are comparable, they may exhibit different thermophysical properties. However, even if the properties of bitumen samples differ, and they are not precisely characterized, there are still many similarities among them.

Bitumen has a high density and a high viscosity and comprises large hydrocarbon molecules with significant aromatic carbon, sulfur and oxygen contents. Bitumen has a density between 964 and 1015 $kg.m^{-3}$ and a viscosity of approximately 100,000 mPa.s, which is one thousand times more than a light crude oil. This work focuses on the phase behavior of Peace River bitumen. It has 0.06 wt. fraction of sulfur, 0.0015 wt. fraction of nitrogen and 73 ppm Nickel [3]. Moreover, bitumen contains a lot of aggregated organic molecules called asphaltenes. For example, Peace River bitumen contains 18.1 wt. fraction C5 asphaltenes. The asphaltene fraction is composed of a multitude of molecules that include polynuclear aromatic rings and high concentrations of heteroatoms. Asphaltenes form large and dense flocs in n-alkanes that can be used to remove this fraction that also includes most of the heteroatoms and the heavy metals present in the bitumen during production or refining. The Peace River bitumen sample obtained from Shell Canada was produced using the Steam Assisted Gravity Drainage (SAGD) process and was subjected to desalting. Thus clays (if present initially), salt and water were removed from the bitumen.

Several in-situ production methods have been applied or proposed for the production of bitumen from reservoirs. The commercially successful processes use steam to heat reservoirs and reduce bitumen viscosity so that it flows (Steam Assisted Gravity Drainage

(SAGD), Cyclic Steam Stimulation (CSS)). In situ combustion processes have been proposed, as have ambient temperature solvent injection processes. SAGD + solvent hybrid processes are seen as a potential economically viable emerging technology.

The SAGD technology was developed by Butler during the 1970's [1,2]. In this process, steam is injected into a reservoir through an upper horizontal well. On heating to more than 523 K, the viscosity of the bitumen decreases and it flows downward by gravity to a lower horizontal production well. Bitumen remains denser than liquid water at these temperatures [4]. This process requires a lot of energy to heat the reservoir, has high CO2 emissions, and the recovery factor is variable and low < 50% [5]. Even so, SAGD is the only technology that is economically viable at the present time.

There are significant economic and environmental drivers to improve this process. Research into improving efficiency, and decreasing the energy consumption and the CO_2 emissions is ongoing. One of the ways to improve this technology is to add a solvent along with less and lower pressure steam. The Expanding Solvent-SAGD (ES-SAGD) [6] process is one such example. This process includes the injection of a small quantity of solvent, such as hexane along with steam. By adding solvent to bitumen the viscosity of the bitumen decreases further than achievable by temperature increase alone. In small scale studies, ES-SAGD improves the rate of oil recovery compared to SAGD [7]. However care must be taken to ensure that the bitumen + solvent mixture remains more dense than water under production conditions [4], to ensure that the hydrocarbon rich-fluid remains single phase. Frequently, asymmetric hydrocarbon mixtures form more than one liquid phase such as alcohol + n-alkanes mixtures [8] or aniline + n-alkane mixtures [9]. Clearly, for such processes to be successful, a detailed understanding of the phase behavior of solvent + bitumen mixtures is required as is a detailed understanding of fluid density under subsurface conditions and in surface processes from water recovery for steam generation to pipelining to refining.

Asphaltenes are commonly removed prior to upgrading to minimize pipework and vessel fouling. In deasphalting units, asphaltenes are typically separated from bitumen or

vacuum residue by adding an alkane solvent such as propane, n-butane, n-pentane, n-hexane or n-heptane. The asphaltenes and some of the non-asphaltenic materials report to one phase (an asphaltene rich phase) and the balance of the bitumen and the added solvent report to another phase. The solvent is then recovered by distillation. In this way, the solvent can be recovered for reuse. Solvents such as propane and butane are less efficient at separating hard to refine asphaltenes from the balance of the bitumen but are easier to recover, and are less prone than larger alkanes to loss in the reservoir by sorbing on clays for example [10]. Phase diagrams for bitumen + n-alkane mixtures are clearly a required enabling technology for understanding and optimizing the complex functional relationships between the de-asphalting and production environments.

The high viscosity and the high density of bitumen is also a problem for transportation because, at atmospheric temperature and pressure, bitumen does not flow. The solution is to heat bitumen or add solvent in order to decrease the viscosity. To ship hydrocarbons through pipelines the shipped oil must meet certain specifications. The density should be less than 940 kg.m^{-3} and the viscosity should be lower than 350 mm^2.s^{-1} at 311 K [11]. To meet these specifications, bitumen producers blend bitumen with natural gas condensate (diluted bitumen or DILBIT), a common approach, or partially refine the bitumen (synthetic crude oil or SCO), a less common approach [12]. Again, understanding the impacts of light hydrocarbon addition to bitumen on the density, viscosity and phase behavior of blends is pivotal to the optimization of DILBIT preparation and transport.

1.3 Objectives

As described briefly above, there are many processes in which bitumen from diverse sources is blended with light hydrocarbons. As bitumen properties are variable, there is a need to understand the spectrum of the phase behavior and thermophysical properties of bitumen + solvent mixtures. In this research the phase behavior and properties of Peace River Bitumen + propane are explored. Propane is not commonly used as a solvent in the oil production or refining sectors. However, there is significant industrial interest in knowing whether propane could be a suitable candidate for envisaged integrated

processes for bitumen production, transport and refining. Extant studies on propane + bitumen phase behavior only address specific conditions and a phase diagram is not available in the literature. For example, Badamchi-Zadeh et al. [13] made measurement from 283 K to 333 K, and from 600 kPa to 1700 kPa with propane weight fractions ranging from 0 to 0.261 and Frauenfeld et al. [14], made measurements at 288 K and 292 K over a range of pressure from 110 kPa to 517 kPa and identified two liquid phases above ~ 0.20 wt. fraction propane.

The specific objectives of this work include:

1. Modification of the x-ray view cell to facilitate volatile liquid injection,
2. Calibration and validation of sensors and measurement methods for pressure, temperature, volume and density, for low density fluids,
3. Completion of a phase diagram for propane + Peace River bitumen in the form of pressure-temperature and pressure-composition phase diagrams and projections based on the conjugate method.
4. Provision of data for the saturated phase properties (density, volume) as a function of global composition, pressure and temperature.

The balance of the thesis comprises four chapters. Chapter 2 comprises a literature review of the phase behavior of binary and pseudo binary mixtures of hydrocarbons, the phase behavior of propane + hydrocarbons and bitumen + solvents and bitumen + light n-alkane. Chapter 3 presents the experimental apparatus and the calibration and validation experiments. Chapter 4 shows the results and the discussion of the experiment propane + Peace River Bitumen. The conclusions and perspective are presented in Chapter 5.

Chapter 2: Literature review

2.1 Phase behavior basics

Van Konynenburg and Scott [15] classified the phase behaviors of binary mixtures of organic molecules on the basis of the shape and unique features of critical loci in the pressure-temperatures projections. Figure 2.1 shows the main characteristics of the six possible Types of binary phase behavior.

For Type I phase behavior, the critical points of the light component and the heavy component are joined by a continuous liquid-vapor critical locus. This Type occurs when the two components are miscible. In this case, the two compounds of the binary mixture should be chemically similar and should possess similar critical temperatures and pressures. For example, mixtures of light gases have this Type of behavior. Typical examples of Type I phase diagram are argon + krypton (Shouten et al., 1975 [16]), methane + ethane, methane + propane (Wichterle and Kobayashi, 1972 [17,18]) and carbon dioxide + n-pentane (Besserer and Robinson, 1973 [19]).

Type II phase behavior shows a liquid-liquid immiscibility region at low temperatures. A continuous liquid-vapor critical locus goes from one of the pure component critical point to the other pure component critical point. A second critical locus is present starting at the liquid-liquid critical point and going at very high pressures. The intersection between this critical curve and the three-phase line (LLV line) at low temperature and pressure is called an Upper Critical End Pont (UCEP). Octane or dodecane + carbon dioxide (Weng and Lee, 1992 [20] and Hottovy et al., 1981 [21]) and ethane + ammonia or n-butane + ammonia (Brunner, 1988 [22]) are examples of Type II phase behavior.
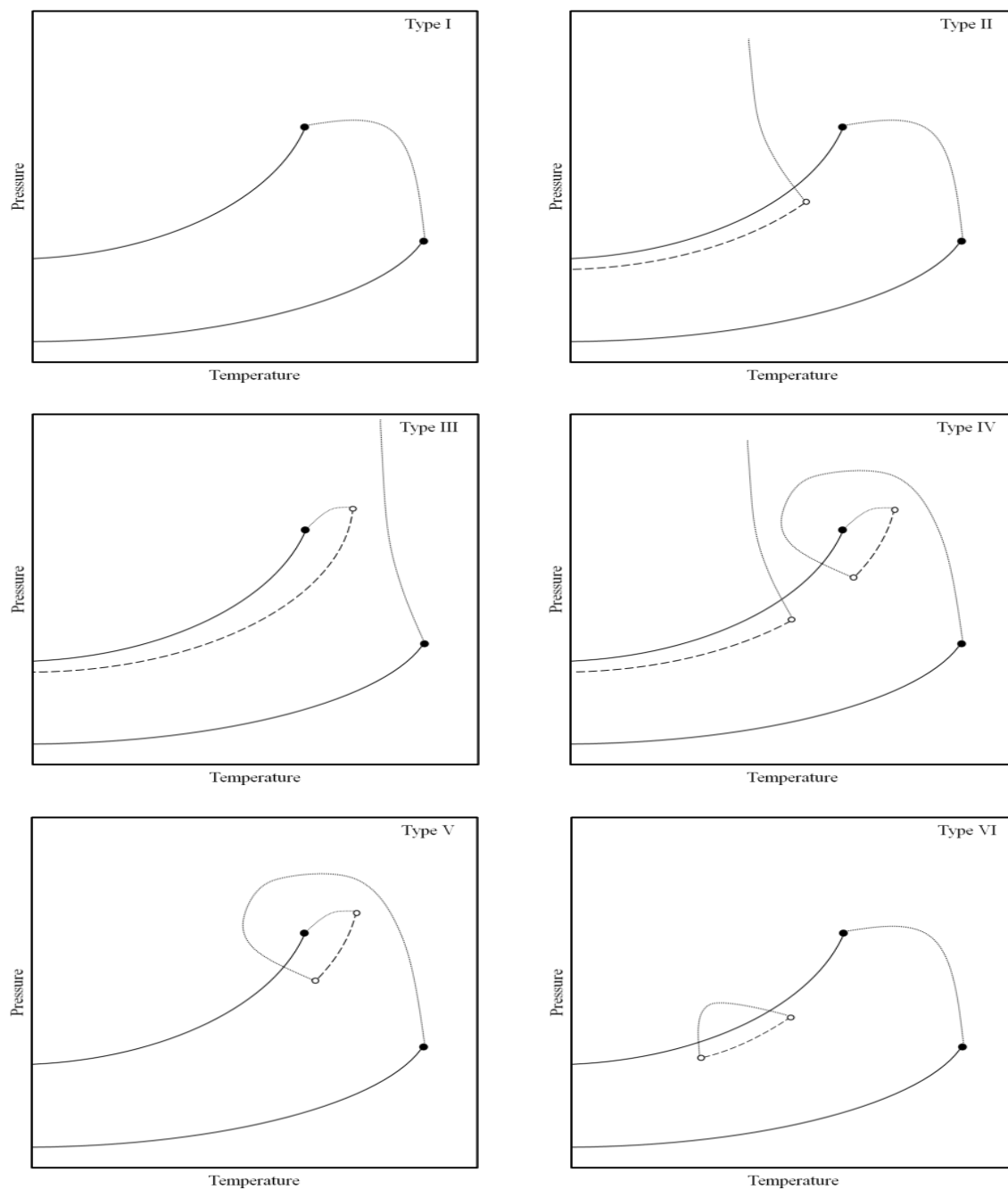
Figure 2.1. The Types of phase behavior found in binary mixtures of organic compounds. The solid curves are the pure compound vapor pressures. The dashed lines are the LLV/LL boundary pressures. The dotted lines represent the critical loci. The dark circles are the pure compound critical points. The upper and lower critical end point are the empty circles.

Type III phase behavior is observed in the case of a binary mixture with a high immiscibility. The difference with Type II is that the pure component critical points are not linked by a critical locus. In this case, the liquid-liquid-vapor curve intersects the liquid-vapor critical locus. The second critical locus starts at the critical point of the heavy component and continue at higher pressure and lower temperature. Methanol + ethane (Brunner, 1985 [23]). Methane + ammonia (Brunner, 1988 [22]), Tetradecane + carbon dioxide and water + propane (De Loos et al. 1980 [24]) are typical Type III binaries.

Type IV is quite similar to Type II. A liquid-liquid-vapor region is present at low temperature up to the first UCEP. After this point the two components are miscible but as the temperature increases another immiscibility zone appears. A Lower Critical End Point (LCEP) and an UCEP limit this region. There are three critical loci, one that goes from the critical point of the heavy component to the LCEP, another that links the light component critical point to the second UCEP, and the last critical locus goes from the first UCEP to the infinite. Tridecane + carbon dioxide (Enick et al., 1985 [25]) and methane +1-hexene (Davenport et al., 1966 [26]) are systems that present Type IV phase behavior.

Type V phase behavior is similar to Type IV phase behavior at high temperatures. It has an immiscibility zone at high temperature with an LCEP and an UCEP. However the components are miscible at low temperatures. Methane + n-hexane presents this Type of behavior (Davenport and Rowilson 1963 [27]) as well as ethane + ethanol (Kuenen and Robson, 1899 [28]).

Type VI is not common in nature. It is similar to Type I with a continuous critical locus that links the two critical points of the pure components. However, at low temperature, liquid-liquid-vapor phase behavior is observed that is limited by an UCEP and a LCEP. These two points are connected by a liquid-liquid critical locus. Water + 2-butoxyethanol shows Type VI phase behavior (Schneider, 1968 [29]).

2.2 Propane + Hydrocarbon Phase Behavior

The phase behavior of propane with different Types of hydrocarbon molecules provides a good background for understanding and interpreting phase behavior observations with propane + bitumen mixtures. Propane is part of the n-alkane chemical family. Peters et al. (1989) [30] showed that propane is miscible with n-alkanes up to n=29. For a carbon numbers less than 30 n-alkane + propane mixtures are Type I binaries. For carbon numbers greater than 30, Type V phase behavior is observed. The phase behavior of propane + aromatics differs (Peters et al. (1989) [31]). Depending on the aromatic molecules, Type II, III or IV phase behavior is observed. For example phenanthrene + propane (Breure et al. 2011 [32]) and triphenylemethane + propane Peters et al. 1995 [33]) show Type III phase behavior. Martinez et al (2011) [34] showed that mixtures of propane + three polynuclear aromatic hydrocarbons: dibenzothiofene, anthracene and carbazol exhibit LLV phase behavior. Polyethylene and poly(ethylene-co-methylacrylate) + propane show Type III phase behavior (Meilchen et al. 1991 [35]). Gregg et al. (1994) [36] worked on mixtures of propane + different Types of polyisobutylene (PIB). Propane + CH3-PIB-CH3 and CH3-PIB-OH show Type IV behavior and propane + OH-PIB-OH shows Type III behavior. As bitumen is a mixture of large and polar hydrocarbon molecules including molecules with heteroatoms these studies with model compounds suggest that propane + bitumen should exhibit Type II, III or IV phase behavior.

2.3 The Phase behavior of bitumen and bitumen fractions + Diluent Mixtures

Although these mixtures are better analogues for bitumen + propane mixtures than the model compound mixtures, there are few studies regarding the phase behavior of heavy oil + propane mixtures and extant phase diagram related data tend to be fragmentary. Mehrotra and Svcreck (1988) [37] dissolved gases such as nitrogen, methane, ethane, and carbon dioxide into different Alberta bitumens such as Cold Lake Bitumen. They discovered that each component has a specific solubility in the bitumen. Nitrogen has the lowest solubility, followed by methane, then carbon dioxide and ethane, which has the

highest solubility among these gases. The results obtained by Frauenfeld et al. (2002) [14] are consistent with these outcomes. They also showed that the solubility of ethane is lower than the solubility of propane in bitumen, and that for high concentrations of propane two liquid phases were observed. Similarly, three phases behavior were observed for bitumen + CO_2 mixtures Khaleghi (2011) [38].

At low temperatures, a solid phase can also appear yielding solid-liquid-liquid-vapor equilibrium. This solid phase can be a classical one based on waxes or other molecular components or it can be due to the aggregation of asphaltenes arising from n-alkane addition. In this latter case, asphaltene-rich (colloid + molecular liquid) phases are readily formed.

The phase behavior of Athabasca Vacuum residue (ABVB) + n-alkanes (pentane, n-heptane, n-decane and n-dodecane) has also been studied (Zou et al. 2007 [39]). This vacuum residue is the 797 K + boiling fraction of Athabasca bitumen and it includes ~ 0.32 wt. fraction pentane asphaltenes. The results are exemplified in Figure 2.2. This figure shows pressure-temperature phase diagrams, at fixed composition, for mixtures of vacuum residue with respectively pentane, heptane, decane and dodecane. The Athabasca Vacuum residue mass fractions are roughly similar in the four cases (0.25 and 0.30 wt. fraction) and the phase diagrams have the same trend. They have an L1L2V region in common that goes from low temperatures to approximately the critical point of the n-alkane. The pressure of the LLV bubble curve decreases with the increase of the n-alkane carbon number. Moreover, the range of compositions where the three phases coexist decreases with the increase of the n-alkane carbon number. A further point, highlighted in Figure 2.3, is the appearance of a four-phase region L1L2L3V and a L2L3V region in the pressure-composition phase diagram. The additional dense phase, L3, is an asphaltene-rich phase. This phase arises due to asphaltene flocculation. To date, this has only been noted with Athabasca bitumen + n-pentane mixtures.

Based on prior studies, including those cited in Chapter 1 on the behavior of bitumen + propane mixtures, a liquid-liquid-vapor region, extending from low temperatures up to

temperatures and pressures greater than the critical temperature and pressure of propane is expected. Further, a four phases region can also be anticipated for propane + bitumen mixtures. Thus the observed phase behavior in this case may include a colloidal behavior in addition to conventional Type III like phase behavior. Further, based on Abedi et al.'s work (1998) [40], L2 phase densities are expected to be larger than predicted by the ideal mixing rule, at low temperature.
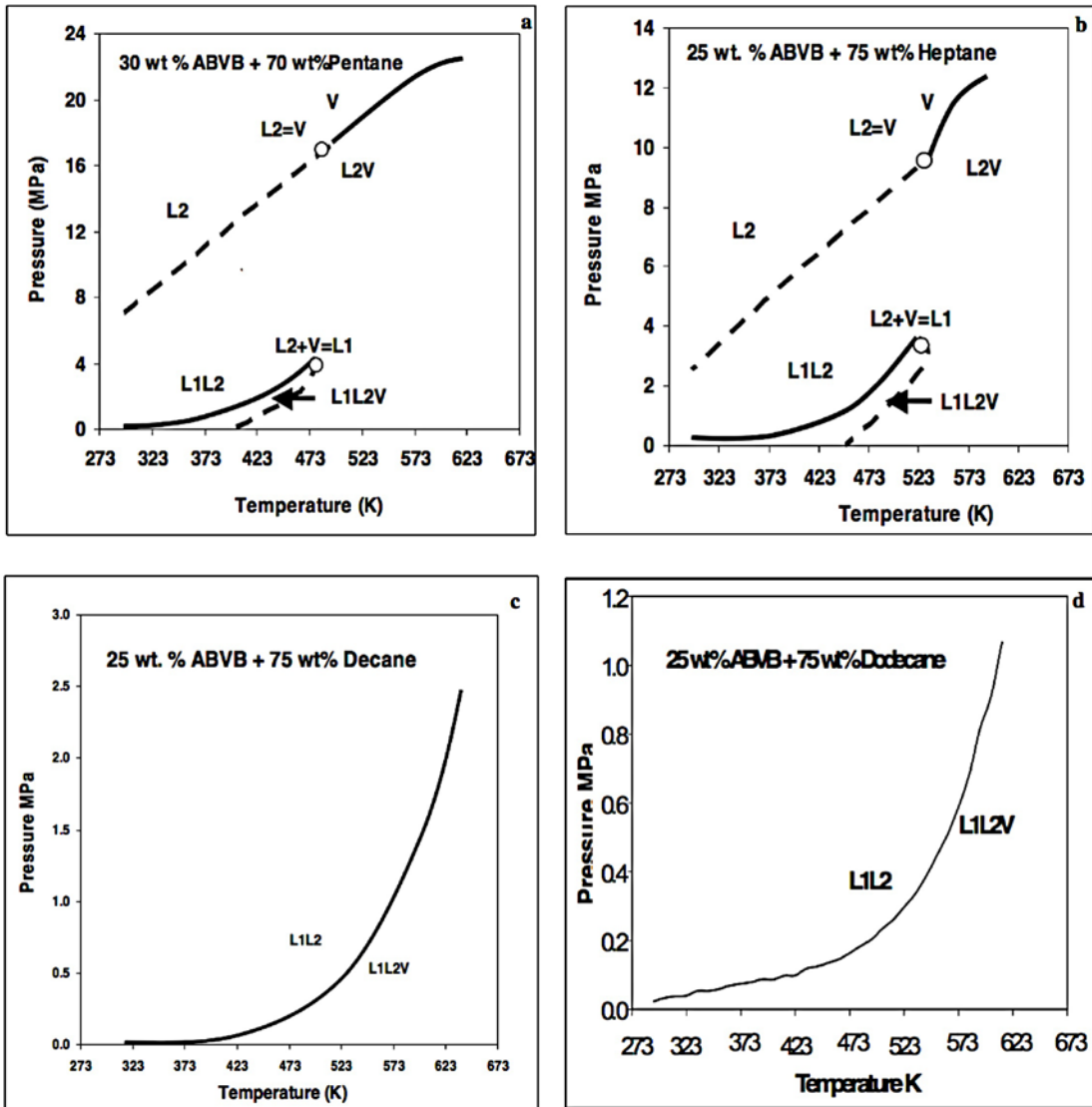
Figure 2.2. Pressure-temperature phase diagram at fixed composition for Athabasca Vacuum residue + n-alkane mixtures: (a) + 0.70 wt, fraction pentane; (b) + 0.75 wt. fraction heptane; (c) + 0.75 wt. fraction decane; (d) + 0.75 wt. fraction dodecane. [39]
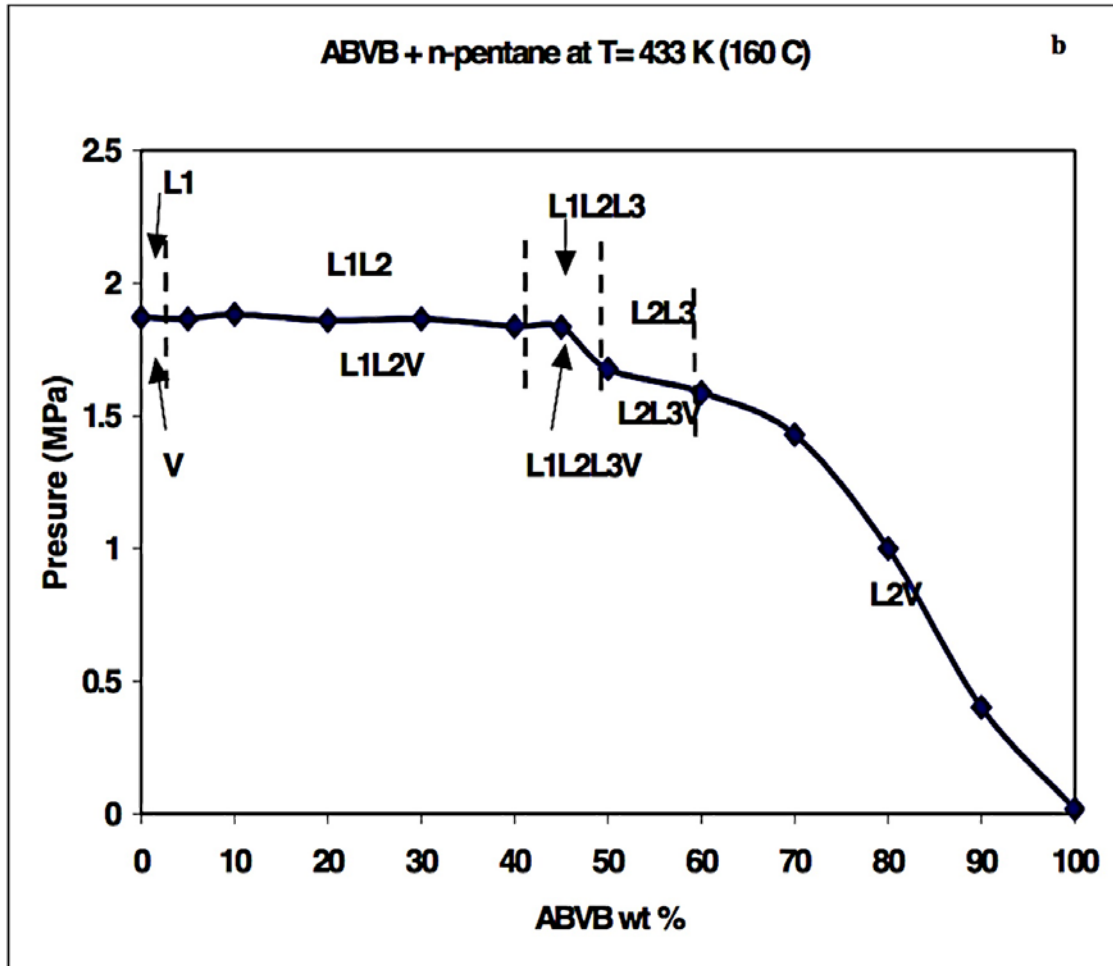
Figure 2.3. Bubble pressures for Athabasca Vacuum residue + pentane mixtures at 433 K [39]

12

Chapter 3: Experimental

3.1 Materials

The Peace River bitumen sample was produced and dewatered by Shell Canada and comes from the Peace River region of Alberta, Canada. Peace River bitumen SARA analysis is shown in Table 3.1 and the elemental analysis is presented in Table 3.2. The propane was provided by PRAXAIR with a purity of 99.5%. A detailed composition, including impurities for propane is shown in Table 3.3.

Table 3.1. SARA analysis for Peace River bitumen [3]

Sample	Saturates	Aromatics	Resins	C5 asphaltenes
	Wt. fraction			
Peace River bitumen	0.196	0.159	0.454	0.191

Table 3.2. Elemental analysis of Peace River Bitumen [3]

Element	Elemental analysis (wt. fraction)
C	0.8176
H	0.1006
S	0.0658
N	0.0037
O	0.0122

Table 3.3. Propane composition

Molecules	Mass concentration (wt. %)
Propane	99.5
Isobutene	<0.3
Ethane	<0.06
Propylene	<0.04
Methane	<0.03
n-Butane	<0.002

3.2 X-ray View Cell Apparatus

The phase behavior of propane + Peace River Bitumen was studied using a custom X ray View Cell developed for opaque mixtures such as bitumen and heavy oil. The equipment, used in numerous studies, is described in detail elsewhere (Abedi et al., 1999 [41]). Key features are described here. A schematic of the X-rays view cell is presented in Figure 3.1.

The view cell consists of a hollow opened-ended beryllium cylinder. This metal was chosen because it is transparent to X-rays and is dimensionally stable at high temperatures. The internal volume of the cylinder is approximately 200 mL. A variable volume bellows is attached to the upper end cap. The internal volume of the cell can be adjusted by changing the volume of the bellows. High-pressure nitrogen is used to inflate or deflate the bellows. The cell also includes a magnetic stirrer and a beryllium insert placed at the bottom of the cell. The feed lines are attached at the top of the cell and they are used to inject gas or liquid and to remove air once the cell is assembled. These tubes possess a volume of 10 mL. The injection line is represented by a syringe in Figure 3.1 because prior to the current work, a syringe was used to inject liquid through this port. In this work, the port is connected to a propane liquefaction unit described in section 3.3.

The cell is placed in a lead-lined cabinet between a polychromatic X-ray source and an X-ray sensitive camera. The polychromatic X-ray beam is emitted from a point source tungsten-target. A camera captures the transmitted X-rays and turns their intensity into a black and white digital image using a 256 point grey scale. These images are monitored and recorded using a computer. The heating system is made of two electrical heating jackets monitored by a PID (proportional, integral, derivative) controller. The temperature inside the cell is monitored and controlled using a RTD (resistance temperature detector). The temperature of exterior wall of the view cell is monitored by a K-type thermocouple. During experiments, two pressure transducers monitor the pressure. One is directly connected to the inside of the cell and the other is connected to the nitrogen side of the bellows. Both pressure transducers have an operating range of 0 - 27.6 MPa.
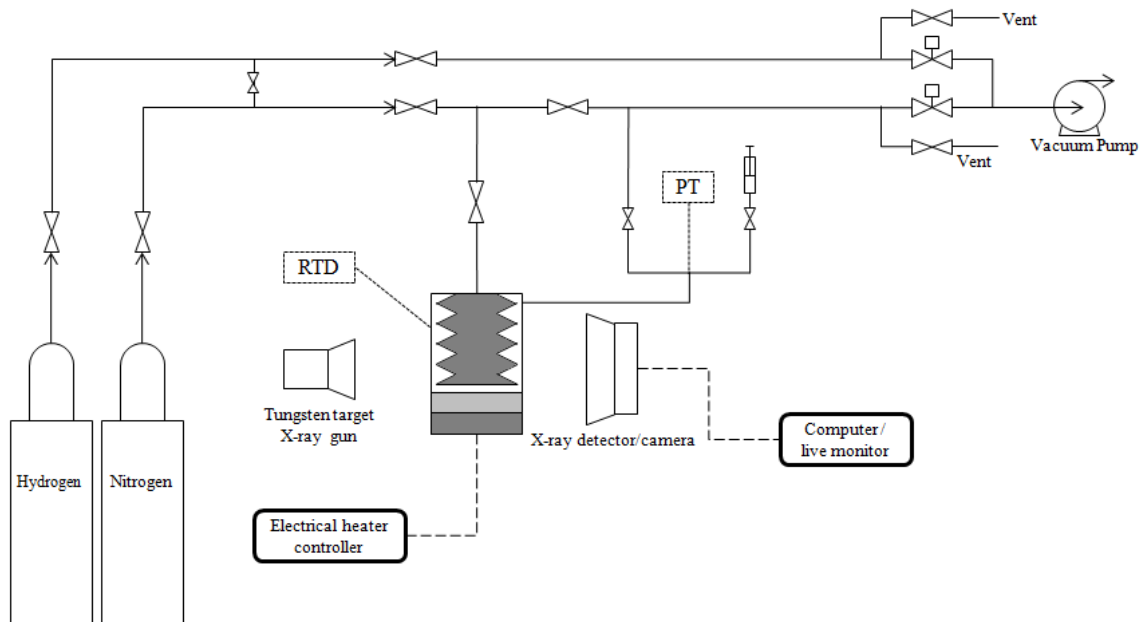
Figure 3.1. X-ray view cell apparatus schematic

Once the bitumen has been added to the cell and before starting an experiment, air is removed from the system. A vacuum pump is used to reduce the pressure in the view cell and the connected tubes to < 14 kPa. Then a leak test is performed. The view cell is pressurized with hydrogen to 10.5 MPa for one hour at room temperature. The condition

for success for the leak test is to have a pressure drop of less than 0.02 MPa in one hour. Following a leak test, the cell is re-evacuated and propane is introduced into the cell.

Pressures, volumes and densities are calibrated using pure liquids such as water or ethanol for which properties are well known, and in this case, using propane and Peace River bitumen. A beryllium insert is added at the bottom of the cell to reduce the cross section area and increase the volume measurement accuracy for small volumes of dense liquid phases. The precision of the pressure, volume and density measurements is discussed in detailed in section 3.7 and 3.8.

3.3 Apparatus Modification

3.3.1 Propane liquefaction unit

In this work, propane had to be liquefied prior to injection into the view cell in order to explore high propane mass fraction mixtures. The view cell had not been used in this way previously. A liquefaction unit was designed, built and tested. Key features of the design include intrinsic safety (the unit and associated piping is rated to at least 3.45 MPa at room temperature, a pressure much greater than the corresponding vapor pressure of propane ~ 0.7 MPa) and the ability to measure the quantity of propane injected into the view cell accurately. A schematic of the unit is shown in Figure 3.2 and an annotated photo showing details of the liquefaction cell is shown in Figure 3.3. Propane vapor transfers from the storage cylinder to the liquefaction unit, comprising a sight glass (Pentair, N7 series), as a low-pressure saturate vapor. The sight glass is inside a clear plastic tank and surrounded by a cooling fluid. 273 K water was a convenient choice in this case. The propane condenses rapidly with this arrangement. More than 25 mL of propane liquefies in less than 5 minutes. Once sufficient propane is condensed, the valves between the propane cylinder and the liquefaction unit are closed and some or all of the propane is transferred to the view cell by opening the connecting valves. The volume of liquid in the sight glass was calibrated carefully as a function of elevation using ethanol as the working fluid. The amount of propane transferred from the unit (as a saturated

liquid at 273 K) was determined by elevation difference measurements. It is necessary to insulate a number of transfer lines and valves adjacent to the liquefaction unit to avoid reboiling of the propane. This feature is indicated in Figure 3.2, but is not shown in Figure 3.3, so that the equipment details can be seen.
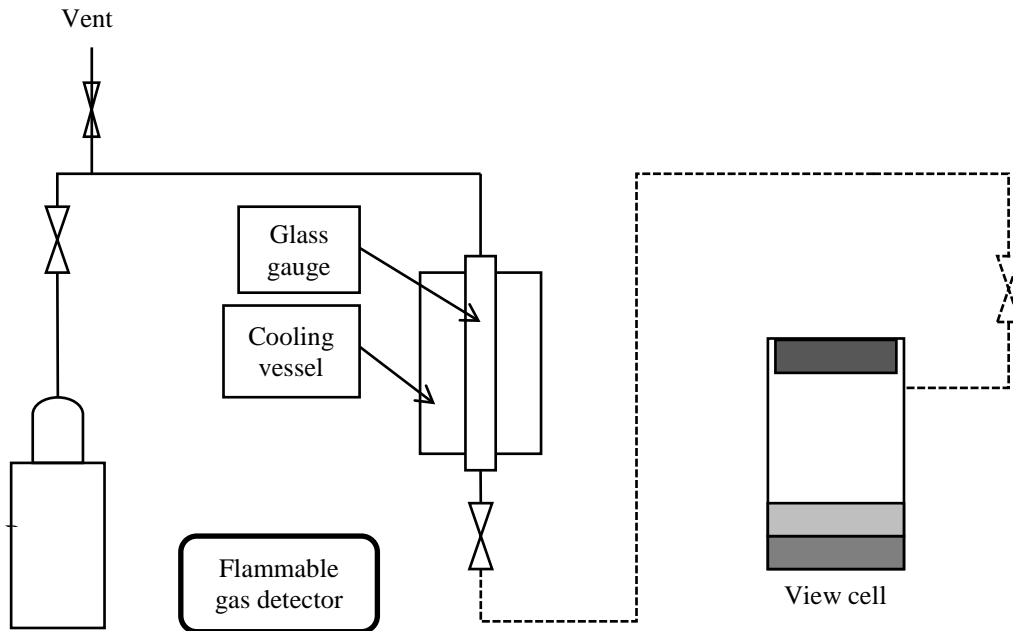
Figure 3.2. Schematic of the propane liquefaction unit. The dashed lines are heated.

The procedure for transferring propane from the liquefaction unit to the view cell is as follows:

1. All lines and vessels from the propane cylinder to the view cell evacuated.
2. The valve between the liquefaction unit and the view cell is closed and the propane cylinder valve is opened.
3. A water-glycol mixture at 268 K is poured into cooling section of the liquefaction unit.
4. When the propane meniscus reaches the top of the glass tube, the exact elevation is recorded and the valve between the view cell and the gage is then opened. The difference in pressure, between the cylinder and the cell, drives the propane into the cell.

5. The valve below the gauge is closed and then the final elevation is then recorded.
6. The tubing between the liquefaction unit and the view cell is then heated to ~ 350 K to ensure complete transfer of the propane in order to remove all the liquid propane in the tubes.
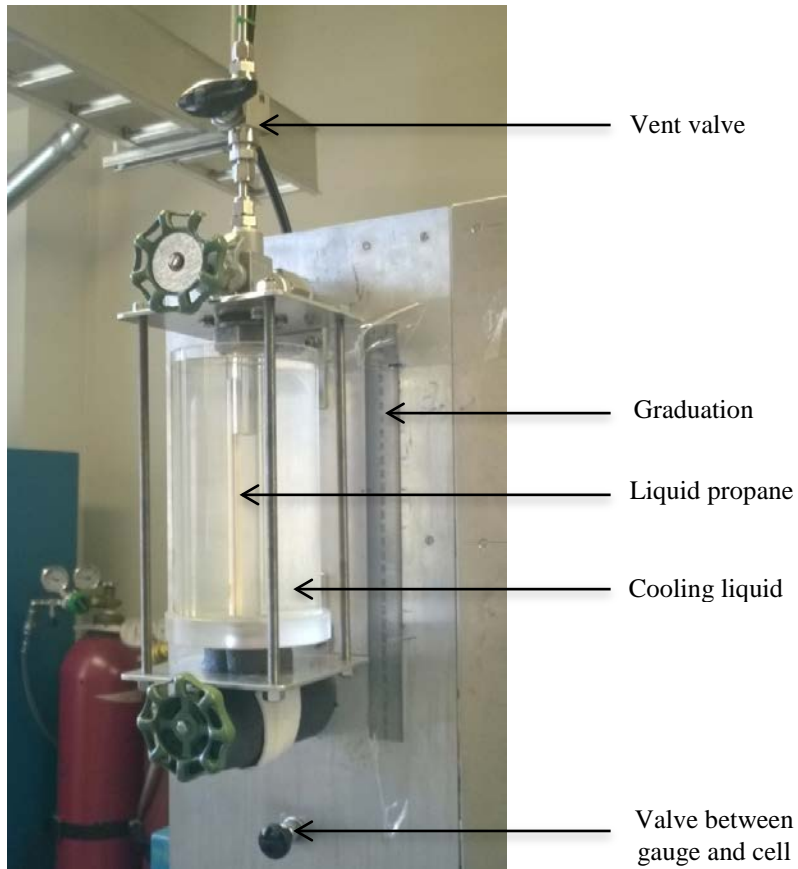
Figure 3.3. Picture of the propane liquefaction unit

Safety precautions include:
1. A flammable gas detector placed adjacent to the propane liquefaction unit and close to the floor liquefaction unit that operates continuously,
2. Leak testing of the apparatus with a sensitive portable flammable gas detector is performed prior to each experiment.

3.3.2 Installation of Heating Tape on Feed and Transfer Lines

The tubes and valves connected directly to the view cell have an internal volume of 10 mL. They are not heated by the heating jacket and remain at ~ 300 K. The pressure inside these lines is equal to the pressure inside the cell and they must be heated to prevent condensation of propane during low temperature experiments. For high-temperature phase equilibrium measurements (Amani, 2013 [42]), this effect is mitigated because larger masses are charged to the cell and prior to high temperature measurements, this space is filled with water liquid, or a low molar mass compound as a liquid or a gas and the global composition in the view cell is adjusted accordingly. For the present study, it was not possible to address this issue in the same way because the condensation kinetics near room temperature are slow relative to the time frame of the experiments. Heating tape was installed on the tubes and valves. By setting the temperature at 433 K, a temperature above the critical temperature of propane and the range of experimental measurements during the all experiments, condensation was eliminated, and this volume was included in the cell vapor volume.

3.4 X-ray absorption physics

With reference to Figure 3.4, the intensity of a transmitted X-ray beam passing through a sample of thickness Δx and density ρ is:

$$I(\lambda) = I_0(\lambda) \exp(-\mu(\lambda)\Delta x \rho) \tag{3-1}$$

where I_0 is the initial X-ray intensity of the beam and μ is the apparent mass attenuation coefficient at wave length λ.
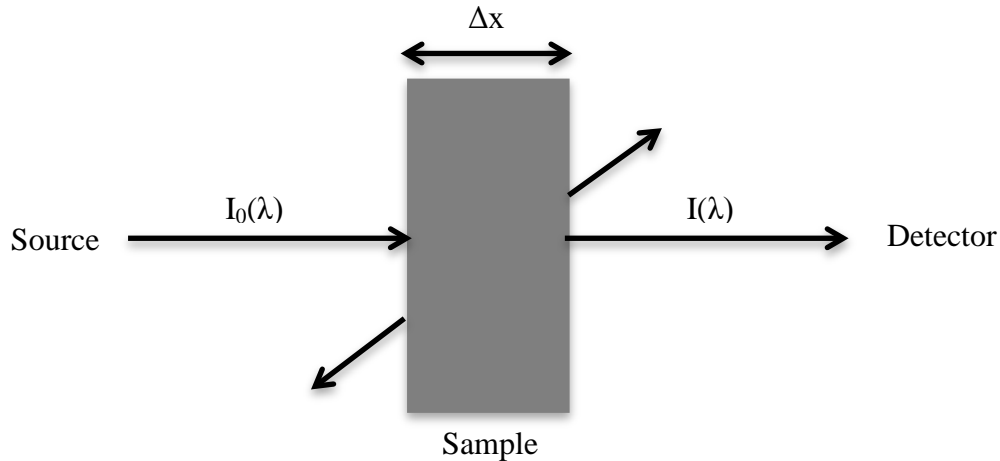
Figure 3.4. Schematic of X-ray absorption

High energy X-rays are absorbed by the core electrons of elements. Thus, the absorption of X-rays does not come from the chemical or physical state of an element but depends only on the kind and the proportion of an element. The mass attenuation coefficient depends on wavelength. The mass attenuation coefficient as a function of the wavelength is available for every element [43]. For molecules or mixtures, the mass attenuation coefficient is the sum of the element contributions.

$$\mu(\lambda) = \sum_i \omega_i \, \mu_i(\lambda) \tag{3-2}$$

where ω_i is the weight fraction of the atomic constituents of a compound. Transmitted intensities can be translated to densies through careful calibration. An internal standard, and bounding densities for bitumen and propane in this case are required as shown in section 3.8.

3.5 X-ray image analysis

The intensity of the transmitted X-rays depends on the density (over a fixed distance) and the composition. The number of phases, their volumes, and their densities can be determined from the images with careful calibration. At equilibrium, composite images comprising an average of 300 individual video stills obtained over a three-minute period

are processed. These images are composed of a 664 by 988 pixel array with 256 potential shades of gray. Figure 3.5 shows an example of the picture obtained from the X-ray view cell with the different inserts and zones.
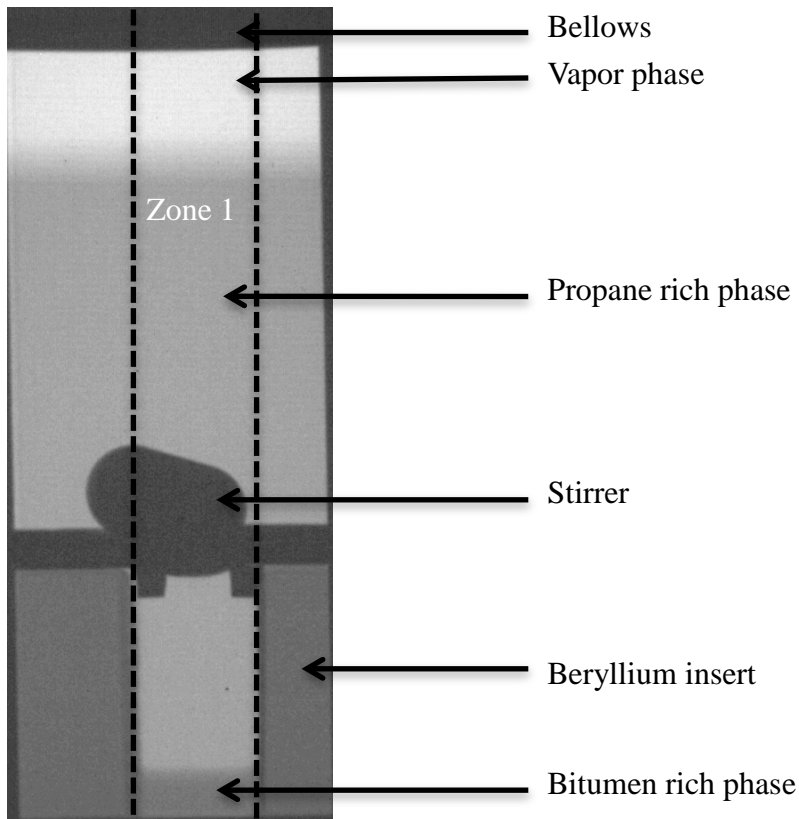
Figure 3.5. Composit**e** X–ray image of bitumen + 0.742 wt. fraction propane at 294.4 K and 1.06 MPa.

On the X-ray image in Figure 3.5, liquid-liquid-vapor phase behavior is clearly seen. For volume measurements, zone 1 is analyzed via a Matlab code as presented in Figure 3.6. Furthermore, the X-rays intensities are recorded in every picture and will permit to obtain the liquid densities.
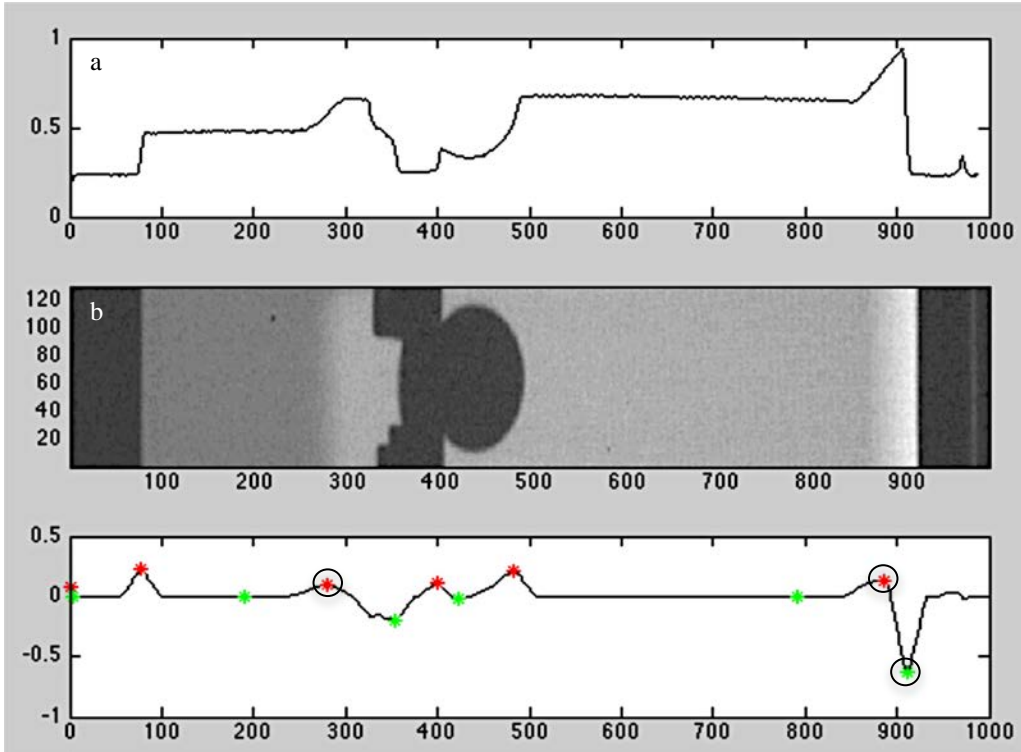
Figure 3.6. Matlab analysis of Zone 1 of Figure 3.3: a) X-ray intensity with elevation, b) composite image, c) the derivative of X-ray intensity with elevation. The circles with the red asterisks indicate liquid-liquid and liquid-vapor interfaces. The circle with the green asterisk indicates the bellows position.

A typical composite image and interface analysis are shown in Figure 3.6. Three points are required to define the phase volumes for liquid-liquid-vapor phase behavior: the position of the bitumen-rich and propane-rich liquid phase interface, the position of the propane-rich liquid vapor interface and the elevation of the bellows. The phase diagram for Peace River bitumen + propane is constructed in a systematic way based on the analysis of dozens of such images obtained for a broad range of temperatures/pressures and compositions.

3.6 Phase Boundary Construction Method

3.6.1 Extrapolation to saturated pressure

The view cell does not give the LV/L and LLV/LL phase boundaries directly. These boundaries are determined indirectly by extrapolating vapor phase volume as a function of pressure, at pressures near the bubble pressure, to a value of zero. At low vapor phase volumes, volume becomes linear function of pressure. Experiment of 1-methylnaphtalene + water at 563K (Amani et al., 2013 [44]) illustrates this point. Figure 3.7 shows the linearity of the pressure with the volume of vapor. It also illustrates the trend obtained from the Peng-Robinson equation of state for the same mixture at the same condition. For this case, the model was not fit to the vapor volume data. Only the trend is important. Even so, the equation of state and the linear model the difference between the predicted and measured LLV/LL bubble pressure is less than 3%.
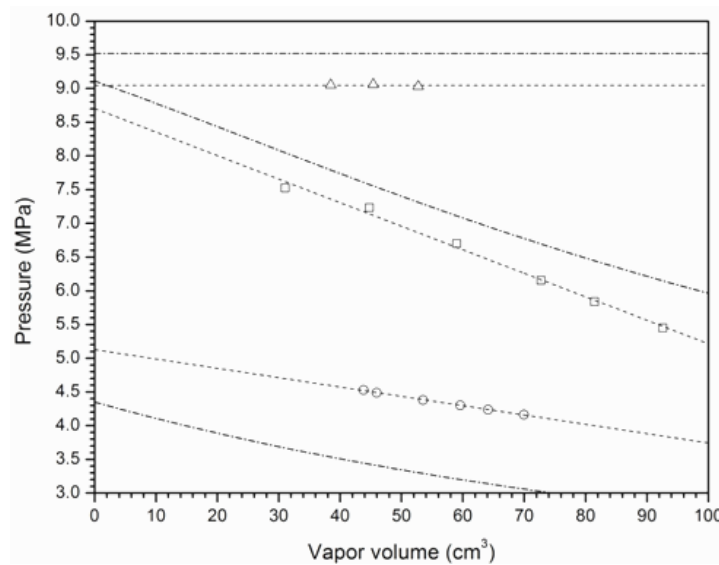
Figure 3.7. At 573 K, vapor phase volumes of the LLV/LL boundary are shown by triangles for 0.789 wt. fraction 1-methylnaphthalene + water and squares for 0.783 wt. fraction 1-methylnaphthalene + water. For the LV/L boundary with 0.963 wt. fraction 1-methylnaphthalene + water, it is shown by circle. The points are the experimental data, their extrapolated data are the dotted line and the dash-dot line is the trend shown by the Peng-Robinson equation of state [44].

This method is also used for LV/L and LLV/LL phase boundary identification in this work. At fixed composition and temperature, three values of pressure and vapor phase

volume are taken and then a linear model is used to extrapolate to the saturated liquid(s) pressure.

3.6.2 Experiment procedures and phase diagram construction

Each phase equilibrium experiment is made at fixed composition. The cell is heated from 303 K to 393 K and measurements are made at 10 K intervals. Pressures are recorded after the temperature stabilizes. Then three images are taken at increasingly higher pressures, as exemplified in Figure 3.8 for n-decane + propane (0.66 mole fraction) at 372.8 K. The gas phase volumes and pressures corresponding to images 1-3 of Figure 3.8 are listed in Table 3.4 and plotted in Figure 3.9. For this example, the saturated pressure for the mixture of 0.66 mole fraction propane + n-decane at 372.5 K is 2.44 ± 0.05 MPa. This agrees with the related literature value 2.39 MPa (Reamer and Sage 1966 [45]) as detailed in section 3.7.3. This method is repeated at every temperature and every composition. The values obtained are the basis for pressure-temperature (P-T) phase diagrams at fixed composition and pressure-composition (P-x) phase diagrams at fixed temperature.
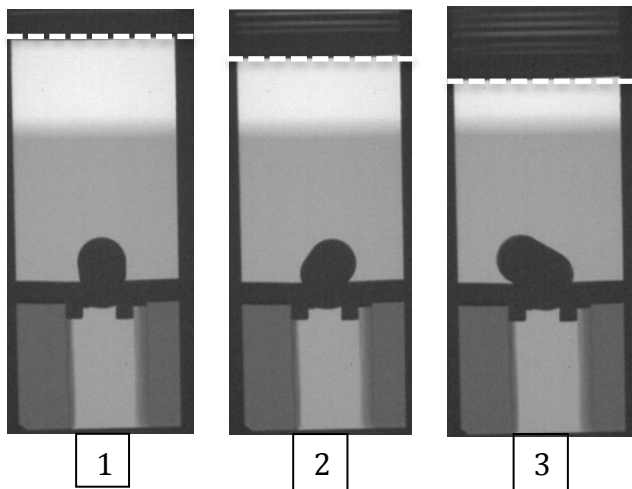
Figure 3.8. Three different positions of the bellows for T=372.5 K and for a mixture n-decane + propane (66 mole fraction). The dash lines show the position of the bellows.

Table 3.4: Pressures and vapor volumes at 372.8 K of a mixture of n-decane + propane (0.66 mole fraction)

Picture	Pressure (MPa)	Vapor Volume (mL)
1	2.11	68.1
2	2.15	60.5
3	2.16	56.3
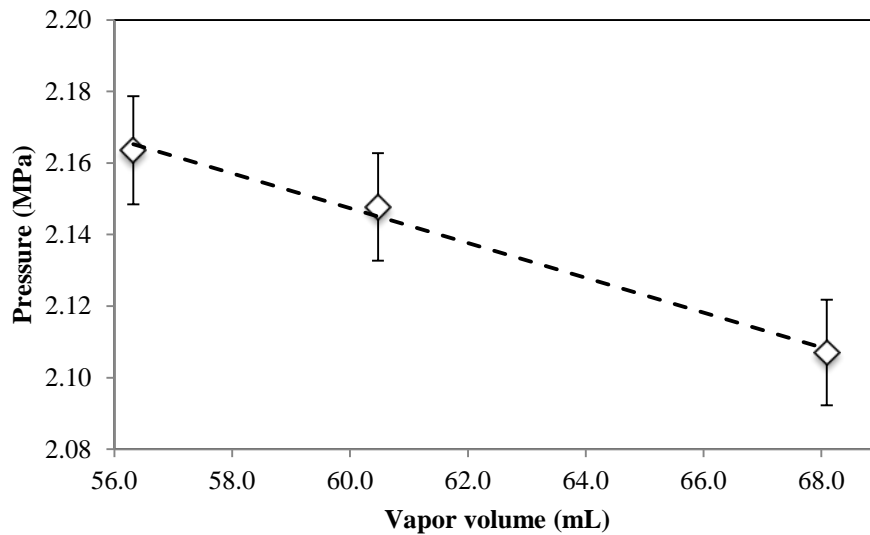
Figure 3.9. Pressure vs gas phase volume at 372.8 K for a mixture of n-decane + propane (0.66 mole fraction). The diamonds are the measured pressures and the dashed line is the linear model

The extrapolated saturation pressures are then smoothed at fixed global composition using a Clausius-Clapeyron type equation:

$$P \sim A * Exp\left(\frac{B}{T}\right) \tag{3-3}$$

where the pressure is in MPa and T is in kelvin and A, B are adjustable parameters. In this way, uncertainties are smoothed and it is possible to prepare P-x at constant

temperature diagrams, even if the data at fixed compositions are not obtained at identical temperatures. All of the phase diagrams reported in Chapter 4, were prepared using smoothed saturated pressure data.

3.7 Apparatus Calibration

3.7.1 Volume Calibration

From the view cell geometry, Figure 3.10, the 988 pixels difference between the base and upper end of the cell can be divided into three zones. In the zone below the stirrer, the volume associated with a one pixel change in elevation is 0.03 mL and above the stirrer it is 0.1 mL. Precise volume measurement in the transition zone proved to be difficult due to the complicated shape of the inserts such as the stirrer and the plate. Volumes were not measured in this zone. A calibration curve was prepared by injecting 5 mL aliquots of water with a syringe. Before any injection the mass of water in the syringe was carefully weighted with a high precision balance. The data are shown in Table 3.5, and plotted in Figure 3.11.
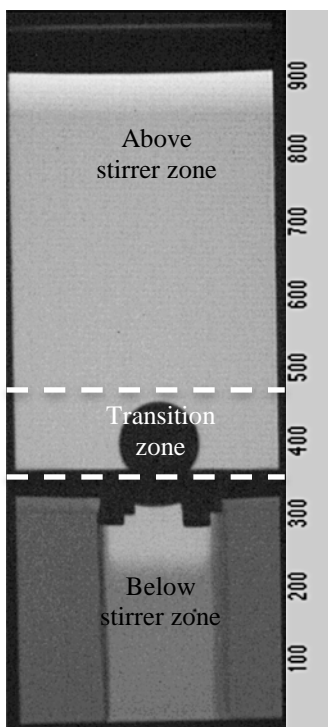
Figure 3.10. Volume zones and corresponding pixel boundaries.

Table 3.5. Relation between the pixel elevation and volume

Pixel height	Volume (mL)
221	4.97
404	10.03
436	15.04
496	20.10
559	25.11
608	30.11
657	35.17
707	40.32
758	45.38
812	50.46
862	55.48
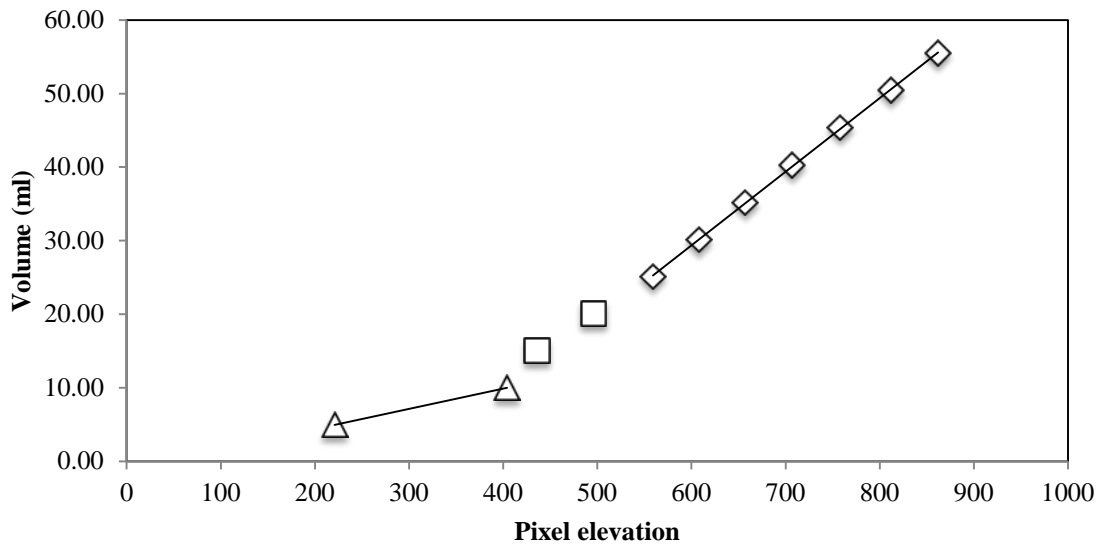
Figure 3.11. Liquid volume vs pixel number. Empty squares correspond to the zone below the stirrer, the empty triangles to the transition zone and the empty diamonds to the zone above the stirrer.

3.7.2 Pressure and temperature calibrations

The pressure and temperature calibrations were done jointly using pure propane. Saturated pressure and temperature measurements were compared to literature values for pure propane [46]. To verify the accuracy of the pressure measurements, temperature measurements were assumed to be precise. The uncorrected pressure measurement uncertainty is less than ± 0.7 % (Table 3.6) which is somewhat larger than the stated precision of the pressure transducer (± 0.25 % of full scale). This outcome is acceptable because none of the uncertainties exceeds 0.02 MPa. To determine the maximum temperature uncertainty, measured vapor pressures were assumed to be precise and the measured temperatures were compared to the corresponding literature values for the measured propane vapor pressures. The maximum uncertainty of the temperature measurements is less than 0.1% or ± 0.4 K (Table 3.7). Given this accuracy, pressures and temperatures were smoothed but not otherwise modified prior to creating phase diagrams.

Table 3.6 Pressure measurements and their uncertainty

Temperature (K)	Measured Saturated pressure (MPa)	Literature bubble pressure (MPa)	Deviation (MPa)	% Deviation
295.4	0.89	0.89	0.00	0.3%
307.4	1.20	1.20	0.00	0.1%
318.8	1.56	1.56	0.01	0.4%
329.7	1.98	1.97	0.01	0.3%
340.6	2.48	2.46	0.02	0.7%
347.8	2.85	2.83	0.02	0.7%
359.5	3.54	3.52	0.02	0.5%
363.7	3.82	3.80	0.02	0.5%
369.9	4.23	4.25	0.02	0.5%

Table 3.7 Temperature uncertainty measurements

Propane bubble pressure (MPa)	Literature temperature (K)	Temperature (K)	Deviation (K)	% Deviation
0.89	295.5	295.4	0.1	0.04%
1.20	307.4	307.4	0.04	0.01%
1.56	319.0	318.8	0.2	0.06%
1.98	329.8	329.7	0.1	0.04%
2.48	340.9	340.6	0.3	0.10%
2.85	348.2	347.8	0.4	0.10%
3.54	359.8	359.5	0.3	0.07%
3.82	364.0	363.7	0.3	0.08%
4.23	369.6	369.9	0.3	0.08%

3.7.3 Extrapolated pressure accuracy

As saturated pressures are obtained by extrapolation, the accuracy of the saturated pressures requires validation. A mixture of n-decane + 0.66 mole fraction propane was chosen for method precision validation because the saturated pressures from the literature are well known (Reamer and Sage, 1966 [45]). This illustration was referred to in section 3.6.2. Temperature, pressure, vapor volume and extrapolated saturated pressure results are shown in Table 3.8 for a number of temperatures and these values are compared with the literature values in Table 3.9. The average deviation is 2%.

Table 3.8. Experimental phase behavior data for 0.66 mole fraction propane + n-decane

Temperature (K)	LV pressure (MPa)	Vapor phase volume (mL)	LV/L boundary pressure (MPa)*
293.3	0.495	64.4	0.55
293.3	0.498	61.1	
294.4	0.501	58.1	
332.3	1.165	65.6	1.29
332.2	1.173	62.3	
331.9	1.182	56.4	
355.0	1.671	67.6	1.85
354.7	1.689	62.4	
354.2	1.697	57.6	
372.8	2.107	68.1	2.44
372.5	2.148	60.5	
372.3	2.164	56.3	
392.2	2.647	63.8	3.14
392.2	2.699	57.0	
412.5	3.183	64.2	3.80
412.4	3.208	61.8	
412.2	3.254	56.8	
443.1	3.734	64.1	4.59
443.0	3.785	60.6	
442.9	3.836	56.4	

*Obtained by extrapolation

Table 3.9 Saturated pressure uncertainty

Temperature (K)	Experimental saturated pressure (MPa)	Literature saturated pressure (MPa) [45]	Deviation (MPa)	% Deviation
293.3	0.55	0.52	0.03	5.8%
332.3	1.29	1.26	0.03	2.4%
355.0	1.85	1.86	0.01	0.5%
372.5	2.44	2.39	0.05	2.1%
392.2	3.14	3.08	0.06	1.9%
412.4	3.80	3.84	0.04	1.0%
433.1	4.59	4.66	0.07	1.5%

3.8 Liquid Density Calibration

3.8.1 Peace River Bitumen Density

Before doing a calibration between the X-ray intensity of the liquid and its density, it is needed to precisely know the density of the pure compound. Propane and n-decane densities are very well known and are available from NIST [46]. However, as bitumen properties change with sample, a density measurement of this specific Peace River bitumen need to be done.

A Paar 5000 densitometer was used to measure the Peace River Bitumen density as a function of temperature. The experimental procedure including validation measurements and uncertainties is explained in detail by Stewart et al. (2014) [4]. Density data for Peace River Bitumen are shown in Table 3.10 and are plotted in Figure 3.12. Over this range of temperatures, the density of Peace River bitumen varies linearly with temperature.

Table 3.10. Peace River bitumen density

Temperature (K)	Density ± 0.03 (kg.m^{-3})
353.0	977.02
348.0	980.18
343.0	983.35
338.0	986.53
333.0	989.7
328.0	992.88
323.0	996.06
318.0	999.25
313.0	1002.45
308.0	1005.65
303.0	1008.86
298.0	1012.07
293.0	1015.29
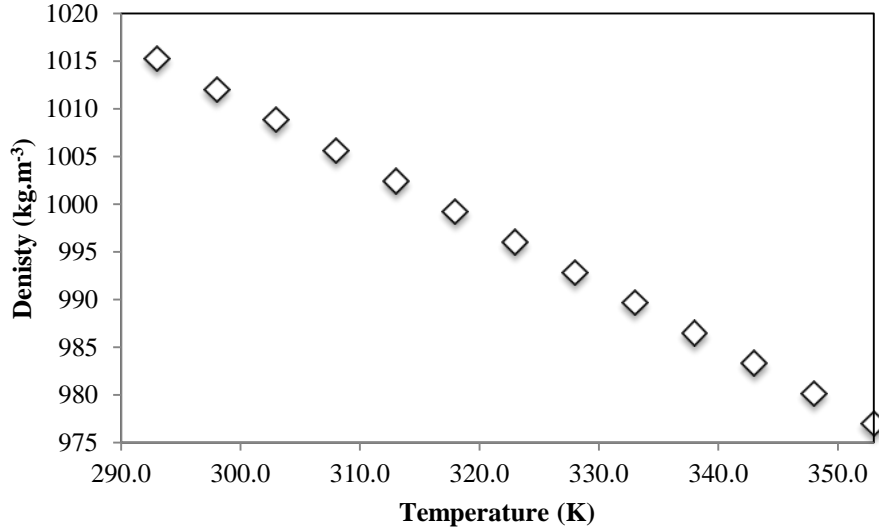
Figure 3.12. Peace River Bitumen density as a function of temperature. Diamonds are the experimental points

3.8.2 Density measurements using phase volumes

In this approach, liquid phase density is determined indirectly by knowing the mass charged to the cell and the liquid volume and by making a correction for the mass in the gas phase, in this case assumed to be pure propane (mass balance method). If two liquid phases are present, then only a bulk liquid density can be obtained. This method relies on careful volume calibration (section 3.7.1). The correction for water in the gas phase at ambient conditions is negligible. The density uncertainty for this best case, Table 3.11, is $\pm$ 3.1 kg.m^{-3} on average based on a water density of 998.2 kg.m^{-3}. The uncertainty for cases with significant correction arising from the gas phase is expected to be higher.

Table 3.11. Liquid density uncertainty based on measurements with water at 293 K.

Water injected mass (g)	Min volume (mL)	Max volume (mL)	Min density $(kg.m^{-3})$	Max density $(kg.m^{-3})$	Maximum density deviation from water density $(kg.m^{-3})$
4.96	4.94	5.00	992.2	1004.3	6.1
10.01	10.00	10.06	995.2	1001.2	3.0
25.06	25.01	25.21	994.2	1002.2	4.0
30.06	30.01	30.21	994.9	1001.5	3.3
35.11	35.07	35.27	995.4	1001.0	2.8
40.25	40.22	40.42	995.7	1000.7	2.5
45.3	45.28	45.48	996.0	1000.4	2.2
50.37	50.36	50.56	996.2	1000.2	2.0
55.38	55.38	55.58	996.4	1000.0	1.8

3.8.3 Density measurements using X-ray intensity

Densities can be determined directly by calibrating transmitted X-rays intensity. The basic theory is explained in section 3.4. To establish a reliable relationship between phase intensity and density, an internal intensity reference standard is required. The beryllium insert at the base of the cell provides a common grey scale reference for all experiments. Transmitted intensities of fluids are scaled using this common reference because transmitted intensity is sensitive to fluctuations in input voltage and current which fluctuate over time even if the set conditions remain fixed. One image is designated as a reference image. Transmitted intensities in other images are scaled relative to this reference image:

$$I_{scaled} = \frac{I_{Be\,image}}{I_{Be\,reference\,image}} * I_{image} \qquad (3\text{-}4)$$

where I_{image} is the measured liquid intensity, $I_{be\,image}$ is the intensity of the beryllium in the image, $I_{be\,reference\,image}$ is the intensity of beryllium in the reference image and I_{scaled} is the scaled intensity of the liquid phase.

The effective mass attenuation coefficient depends on phase composition, primarily due to variation in the scattering effect caused by the nanoparticulate asphaltene fraction. With reference to equation 3-1, a quadratic model:

$$\rho = -565.42 * LN(I_{Scaled})^2 + 4631.9 * LN(I_{Scaled}) - 8378.9 \qquad (3\text{-}5)$$

where ρ is the liquid density and I_{scaled} is the scaled intensity of the liquid phase, was fit to the bitumen, propane and n-decane density vs logarithm of intensity data as shown in Table 3.12 and plotted in Figure 3.13. The precision of the intensity measurements is $\pm$ 1 shade of grey. The transmitted intensity of bitumen $\sim$ 93 and liquid propane 169 at room temperature where the difference in density is $\sim$ 500 kg.m^{-3} provides a minimum measure of uncertainty. More typically the uncertainty of the density values is approximately $\pm$ 1% ($\pm$ 10 kg.m^{-3}).

Table 3.12. Transmitted intensity (70 kV and 1.30 mA) and density of reference fluids

Compound	Temperature (K)	Intensity (Shade of grey)	LN (Intensity)	Density (kg.m^{-3})	Density deviation (kg.m^{-3})
	314.0	94	4.543	1001.83	0.03
	326.4	96	4.564	993.95	0.03
	335.3	96	4.564	988.23	0.03
	342.5	96	4.564	983.68	0.03
Bitumen	353.1	98	4.585	976.93	0.03
	362.4	98	4.585	970.99	0.03
	376.1	98	4.585	962.23	0.03
	381.4	99	4.595	958.85	0.03
	391	99	4.595	952.73	0.03
N-decane	293	137	4.920	730.4	1.5
Propane	293	169	5.130	500.28	0.46
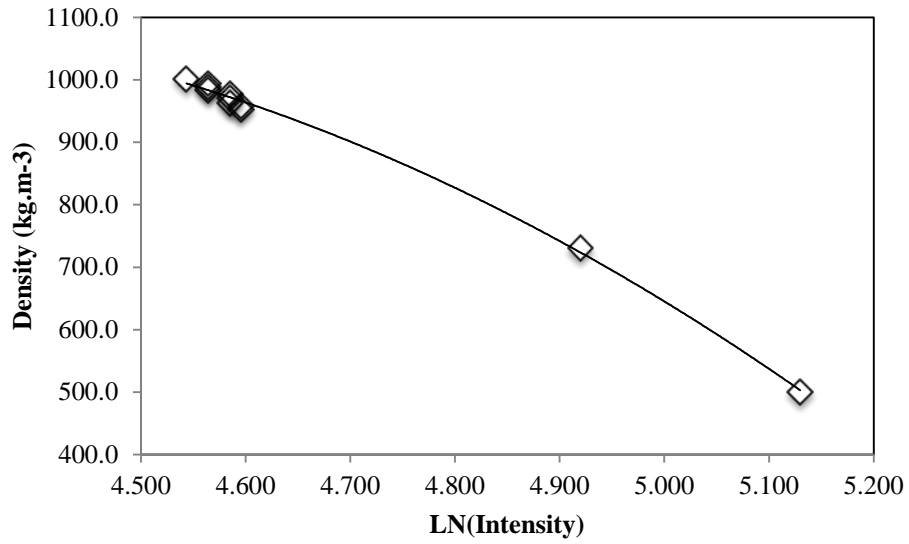
Figure 3.13. Density vs intensity calibration. Empty diamond points are the pure component densities and the solid line is the quadratic model (equation 3-5).

Chapter 4: Results and Discussion

Propane is employed as a combustible gas for energy generation. Some refineries use it as a diluent in deasphalting units. Others use it as a base to make propylene for plastic fabrication. Hence, propane does not have a high value compared to refinery products such as gas oil, diesel or kerosene. If it could be used in an integrated manner to improve production, transport and refining processes, this would add significant value. Furthermore, as shown in Table 4.1 propane possesses interesting properties compared to those of Peace River bitumen. As a diluent, it can be expected that mixtures of bitumen + propane possess low densities and viscosities relative to bitumen. The critical temperature, 369.89 K, and pressure, 4.25 MPa, of propane also fall within the range of production and separation processes.

Table 4.1 Properties comparison between propane and bitumen

Properties at 288.56 K	Propane	Peace River bitumen
Density (kg.m^{-3})	506.9	1014
Viscosity (Cp)	0.1072	7848

4.1 Phase behavior of propane + Peace River Bitumen

4.1.1 Phase diagram construction

Pressure-Temperature phase diagrams at fixed composition are constructed from images obtained from a single experiment. Illustrative images are shown in Figure 4.1a. This mixture, comprising Peace River Bitumen + 0.161 wt. fraction propane, exhibits one liquid phase from 303 K up to 393 K. From a single experiment at one composition, it is not possible to observe all phase behaviors that a specific mixture presents due to the limited pressure range accessible with each filling. It is also not possible to assess the phase behavior Type of a mixture over all or to assign appropriate designations to phases.

Pressure-composition phase diagrams at fixed temperature, constructed as composites of multiple pressure-temperature phase diagrams at fixed composition, that are then interpolated and extrapolated based on relative phase volumes, phase densities, pressures to determine limits of specific phase behaviors are required to assess phase behavior Type. Illustrated images, drawn from multiple experiments at 303 K and shown in Figure 4.1b span the low-density liquid + vapor composition region designated (L1V), the high-density liquid + vapor region designated (L2V) and the intermediate low-density liquid + high-density liquid + vapor region designated (L1L2V). These and other sets of images are analyzed in detail to identify key features of the phase diagrams. Delineation of the L1/L1L2, L2/L1L2, L1L2V/L1L2, L1V/L1 and L2V/L2 phase boundaries are the focus of this work. Identification of L1L2V/L2V boundaries is of lesser importance and L2V/V boundary is of tertiary importance. From the images in Figure 4.1b, the L1/L1L2 boundary is expected to be between 0.75 and 0.85 wt. fraction propane and that the L2/L1L2 phase boundary is expected to be between 0.25 and 0.39 wt. fraction propane. Much work goes into obtaining well-defined phase boundaries, on the basis of such images. Further, this work focuses on the temperature region 300 K to 400 K. The lower temperature limit is dictated by the operating range of the view cell. Above the upper temperature limit, only L2, L2V and V phase behavior is expected and above ~ 600 K the bitumen becomes thermally unstable.
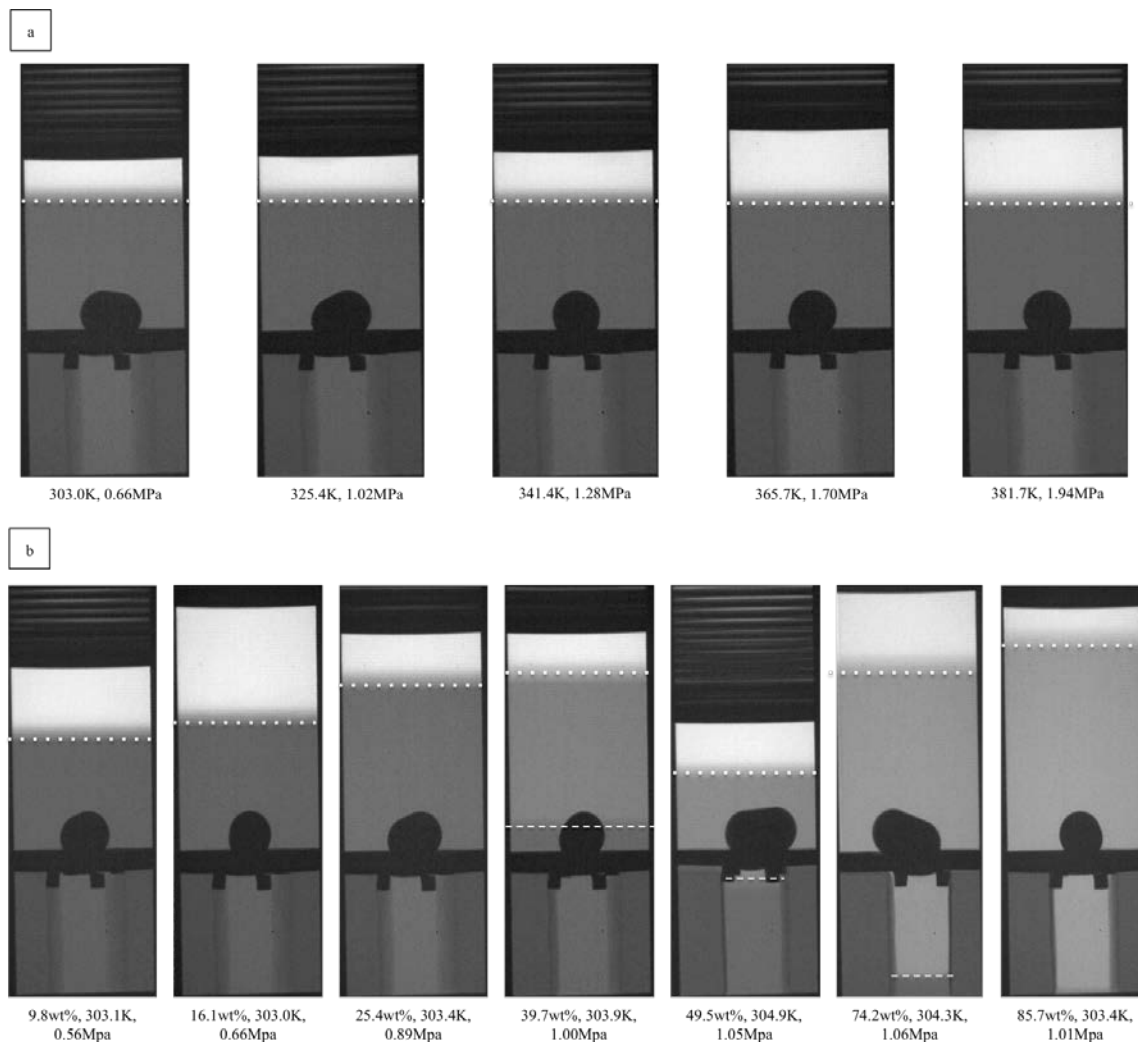
Figure 4.1 Typical X-ray images for Peace River Bitumen + propane mixtures: a) a series of Pressure-Temperature images at fixed composition (0.161 wt. fraction propane) ; b) a series of pressure composition images at fixed temperature images (~303 K). The dashed line indicates liquid/liquid interfaces and the dotted line indicates liquid/vapor interfaces.

Pressure-temperature phase diagrams at fixed propane wt. fraction are shown in Figure 4.3. The phase boundary pressures and the phase behavior observations are provided in Table 4.2.

At 0.098 wt. fraction, 0.161wt. fraction and 0.254 wt. fraction propane, only one liquid phase is observed and the bubble pressure increases toward the vapor pressure of propane as the propane wt. fraction is increased. This bitumen rich liquid phase is designated L2. At 0.397 wt. fraction, 0.495 wt. fraction and 0.742 wt. fraction of propane two liquid phases are observed and the relative amount of the low-density propane-rich liquid phase

(L1) increases as the wt. fraction of propane is increased. However, the bubble pressure of the mixtures is independent of propane wt. fraction and equal to the vapor pressure of propane. This suggests that the vapor phase is essentially pure propane. Above ~ 373 K, only a dense liquid (L2) and a propane-rich vapor are observed. This means that there is an upper critical end point for L1L2V phase behavior (L1=V+L2) in the phase diagram. At 0.857 wt. fraction propane, Figure 4.3g, a small amount of L2 phase is present at 303 K and 313 K and from 323 to 363 K only the L1 phase is observed. Between 363 K and 373 K, the L1 phase disappears and L2V, L2, V phase behavior is observed as shown in Figure 4.2. Depending on the temperature, at high pressure, either the L2 phase or the V phase disappears, indicating a critical point on the two phase to one phase boundary at 377 K ± 4K.

| 372.8 K, 4.13 MPa | 373.0 K, 4.21 MPa | 372.7 K, 4.29 MPa |
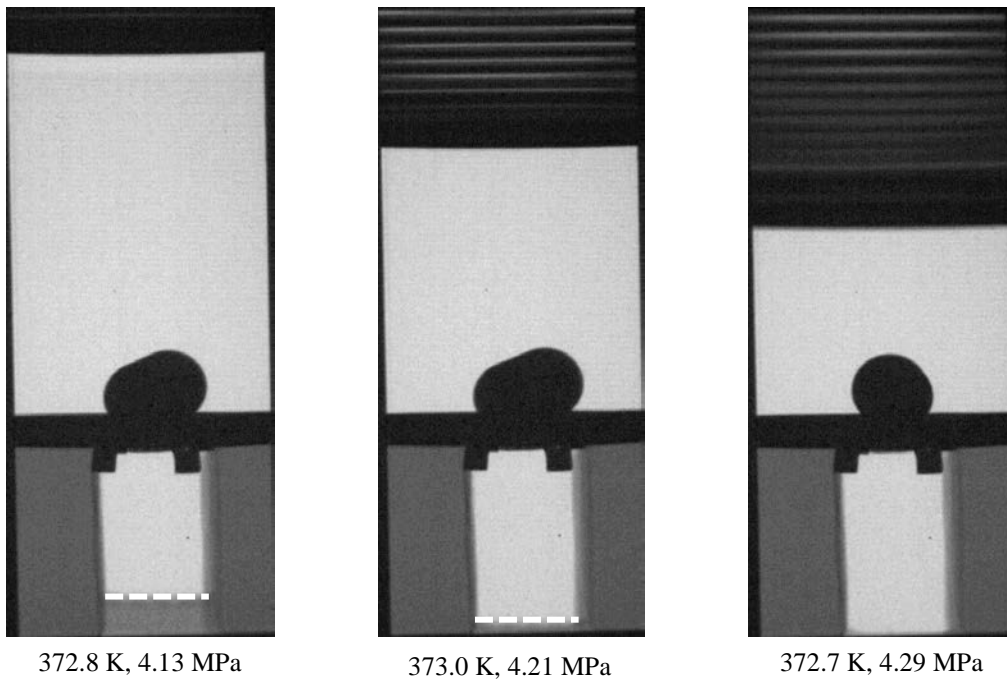
Figure 4.2. X-rays images of bitumen + 0.742 wt. fraction propane at 373 K. The white dashed line shows the L2V interface.
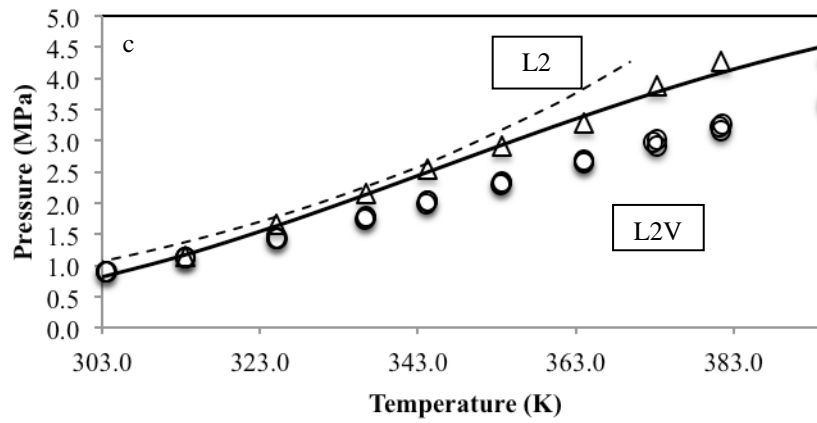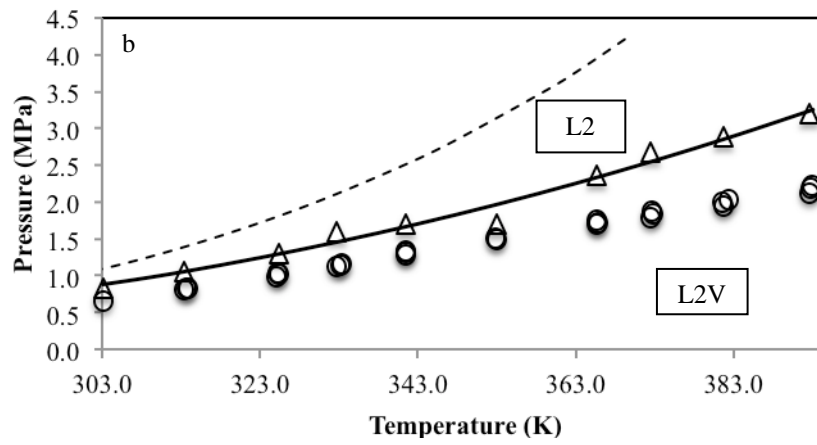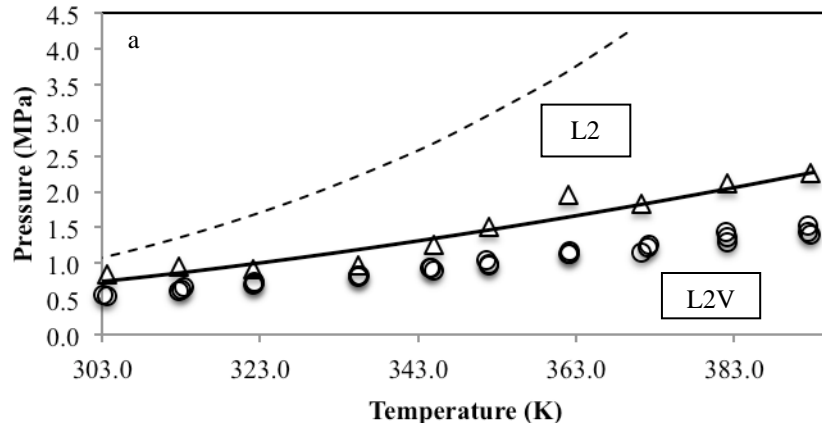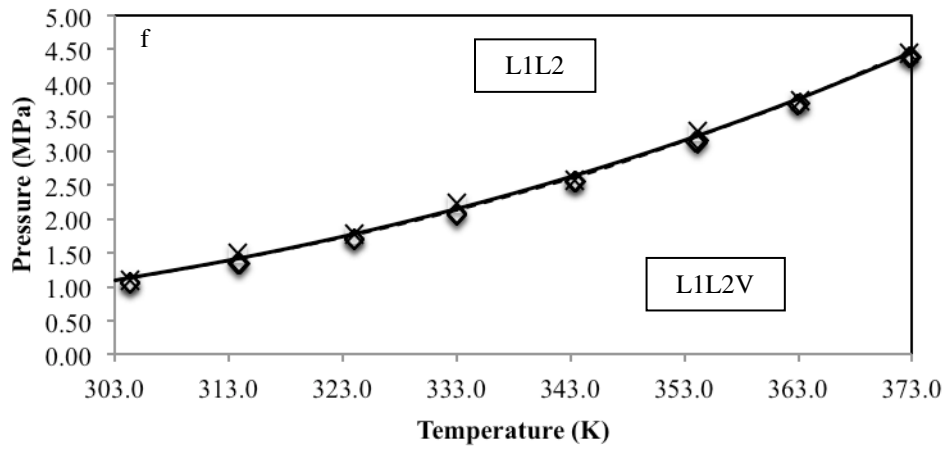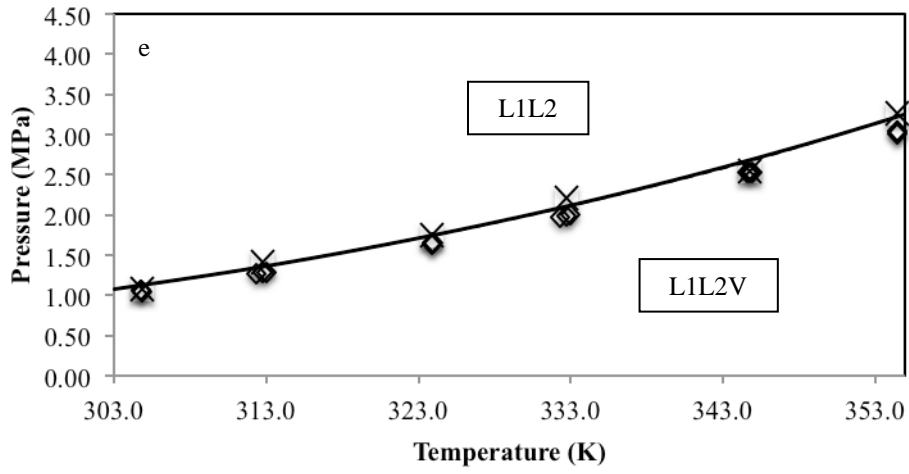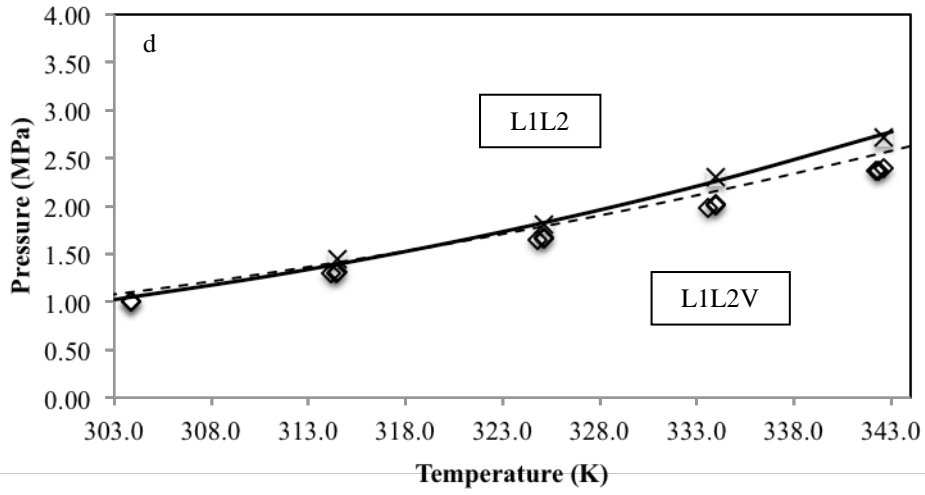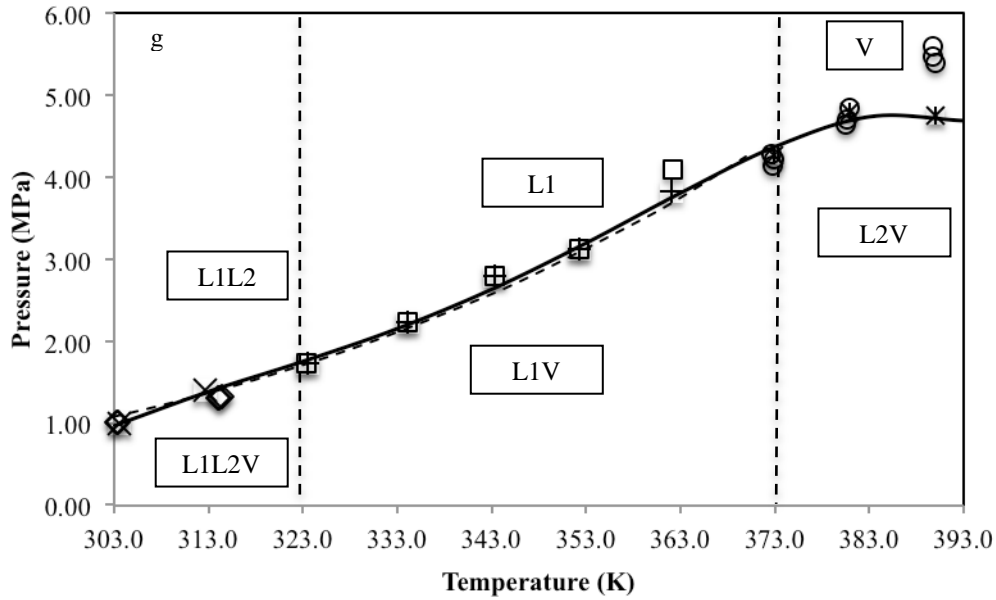
Figure 4.3. Pressure-Temperature diagrams at fixed composition for Peace River bitumen + propane at various propane wt. fraction: a) 0.098 wt. fraction, b) 0.161 wt. fraction, c) 0.254 wt. fraction, d) 0.354 wt. fraction, e) 0.495 wt. fraction, f) 0.742 wt. fraction, g) 0.857 wt. fraction. The propane vapor pressure is shown as a dashed line. Measured pressures are designated by empty circles in the L2V region, empty diamonds in the L1L2V region and empty squares in the L1V region. Points on LLV/LL boundaries are designated by cross points. Points on the L2V/L2 boundary are empty triangles points. Points on the L1V/L1 are plus points. Points on the L2V/V boundary are star points. The solid line shows smoothed LV/L and LLV/LL boundaries.

Table 4.2. L1L2V/L1L2, L2V/L2, L1V/L1 and L2V/V phase boundaries for Peace River bitumen (PRB) + propane mixtures

PRB (0.902 wt. fraction) + Propane (0.098 wt. fraction)		
Temperature (K)	Pressure (MPa)	Boundary
303.1	0.84	L2V/L2
313.0	0.96	L2V/L2
322.1	0.92	L2V/L2
335.3	0.97	L2V/L2
345.0	1.25	L2V/L2
351.9	1.51	L2V/L2
372.0	1.83	L2V/L2
382.1	2.12	L2V/L2
392.7	2.25	L2V/L2

43

PRB (0.839 wt. fraction) + Propane (0.161 wt. fraction)

Temperature (K)	Pressure (MPa)	Boundary
302.9	0.84	L2V/L2
313.6	1.06	L2V/L2
325.1	1.31	L2V/L2
333.2	1.60	L2V/L2
341.4	1.70	L2V/L2
365.7	2.37	L2V/L2
372.6	2.67	L2V/L2
381.7	2.88	L2V/L2
392.8	3.20	L2V/L2

PRB (0.746 wt. fraction) + Propane (0.254 wt. fraction)

Temperature (K)	Pressure (MPa)	Boundary
303.5	0.85	L2V/L2
313.6	1.14	L2V/L2
325.1	1.65	L2V/L2
336.4	2.15	L2V/L2
344.2	2.54	L2V/L2
353.6	2.90	L2V/L2
364.1	3.28	L2V/L2
373.3	3.87	L2V/L2
381.4	4.26	L2V/L2

PRB (0.603 wt. fraction) + Propane (0.397 wt. fraction)		
Temperature (K)	Pressure (MPa)	Boundary
303.9	1.02	L1L2V/L1L2
314.5	1.44	L1L2V/L1L2
325.1	1.81	L1L2V/L1L2
334.9	2.29	L1L2V/L1L2
342.6	2.71	L1L2V/L1L2
354.8	3.35	L1L2V/L1L2
363.2	3.78	L2V/L2
383.3	5.41	L2V/L2
392.5	6.26	L2V/L2

PRB (0.505 wt. fraction) + Propane (0.495 wt. fraction)		
Temperature (K)	Pressure (MPa)	Boundary
304.9	1.07	L1L2V/L1L2
312.8	1.40	L1L2V/L1L2
323.9	1.74	L1L2V/L1L2
332.8	2.21	L1L2V/L1L2
344.8	2.54	L1L2V/L1L2
354.5	3.26	L1L2V/L1L2
365.0	4.31	L1L2V/L1L2
372.8	4.97	L2V/L2
382.2	5.61	L2V/L2
392.8	6.38	L2V/L2

PRB (0.258 wt. fraction) + Propane (0.742 wt. fraction)		
Temperature (K)	Pressure (MPa)	Boundary
304.3	1.09	L1L2V/L1L2
313.8	1.49	L1L2V/L1L2
324.0	1.77	L1L2V/L1L2
333.0	2.24	L1L2V/L1L2
343.3	2.57	L1L2V/L1L2
354.1	3.30	L1L2V/L1L2
363.2	3.74	L1L2V/L1L2

PRB (0.143 wt. fraction) + Propane (0.857 wt. fraction)		
Temperature (K)	Pressure (MPa)	Boundary
303.4	1.00	L1L2V/L1
323.5	1.73	L1L2V/L1
334.2	2.23	L1V/L1
343.7	2.79	L1V/L1
352.4	3.12	L1V/L1
362.6	3.76	L1V/L1
372.8	4.31	L2V/V
380.7	4.85	L2V/V
389.8	5.75	L2V/V

4.1.2 Saturated L2 Composition Identification

Temperature dependent compositions of the L2 phase at the L2/L1L2 boundary are identified from the intersection of the composition dependent bubble pressure curves with the composition independent bubble curves starting from low propane wt. fraction. Table 4.3 shows the experimental L2V/L2 phase behavior boundary pressures. These pressures are essentially linear with composition as shown in Figure 4.4. Linear correlations of these values intersect the bubble pressures of propane at the values shown in Table 4.4 and plotted in Figure 4.5. Figure 4.5 shows that within the uncertainty of the interpolations a fixed value, 0.28 ± .03 mass fraction propane, accurately reflects the saturated composition of the L2 phase from 303 K to 370 K.

Table 4.3: Comparison of saturated pressures in the L2V/L2 region and the bubble pressures of propane

Temperature (K)	Bitumen + 0.098 wt. fraction propane Pressure (MPa)	Bitumen + 0.161 wt. fraction propane Pressure (MPa)	Bitumen + 0.254 wt. fraction propane Pressure (MPa)	Propane Pressure (MPa)
313	0.88	1.05	1.16	1.36
323	1.02	1.25	1.55	1.71
333	1.17	1.46	1.99	2.11
343	1.33	1.71	2.44	2.58
353	1.50	1.97	2.91	3.12
363	1.68	2.26	3.35	3.75
369	1.79	2.44	3.61	4.18
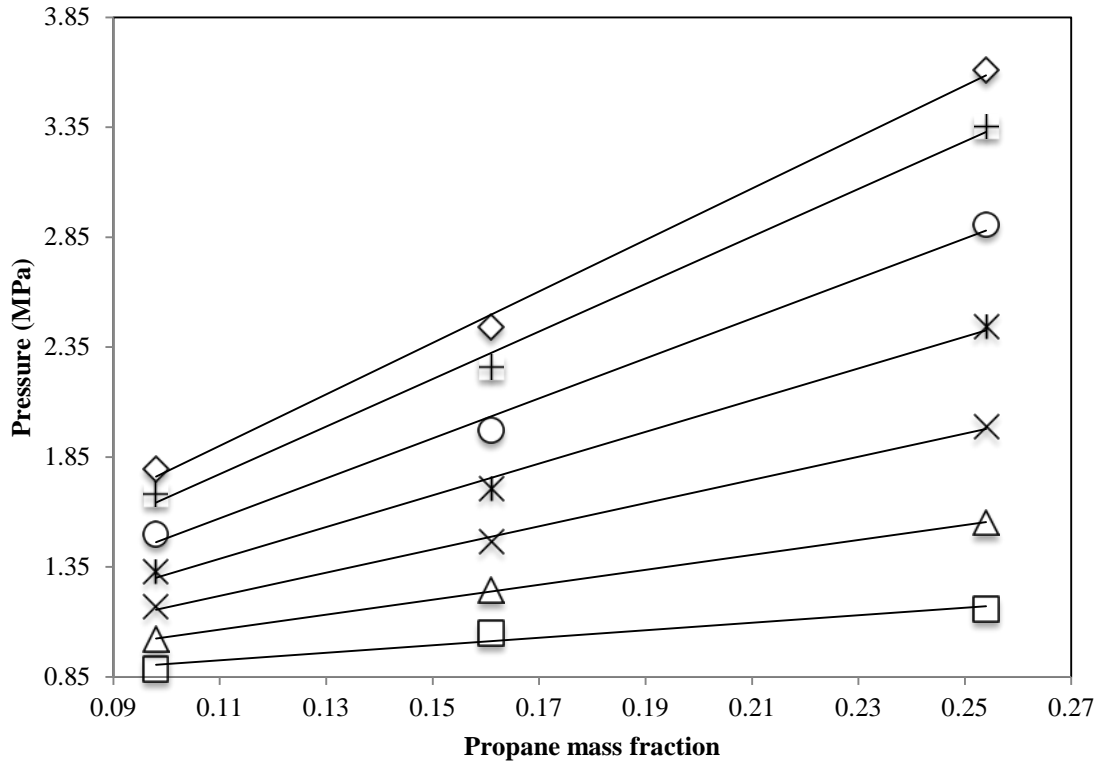
Figure 4.4. Pressure-Composition diagram for the L2V/L2 region. Square points are at 313, triangle points are at 323K, cross points are at 333K, star points are at 343K, circle points are at 353K, plus points are at 363K and diamond points are at 373K.

Table 4.4. Saturated propane mass fraction in Peace River bitumen

Temperature (K)	Propane mass fraction	Uncertainty
313	0.33	0.07
323	0.29	0.03
333	0.27	0.02
343	0.27	0.01
353	0.27	0.02
363	0.28	0.02
369	0.31	0.01
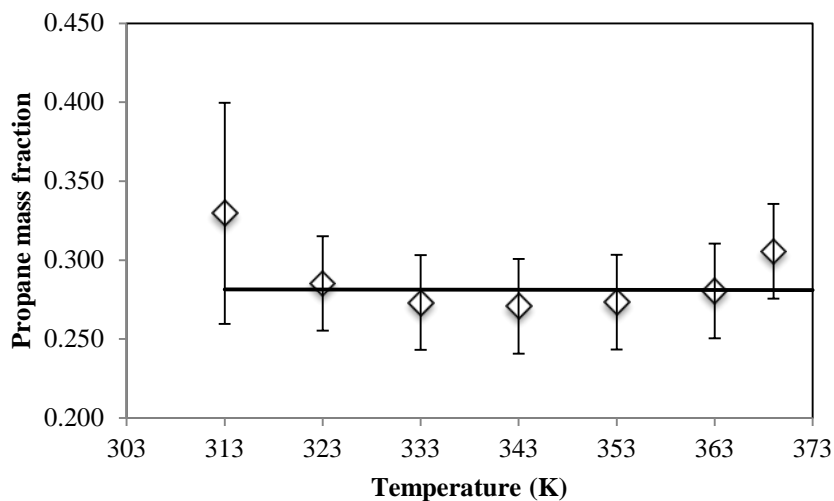
Figure 4.5. Saturated L2 compositions. Diamond points are experimental values for the L2/L1L2 boundary and the solid line represents the average value (0.281 wt. fraction propane) for this boundary over the temperature interval.

4.1.3 Saturated L1 Composition Identification

The method employed to define the L2/L1L2 boundary cannot be used to define the L1/L1L2 boundary because there is no significant pressure variation at this boundary. The pressure remains essentially at the vapor pressure of propane. This boundary is defined using a correlation between the mass fraction of propane in the liquid (based on the mass fraction charged to the view cell minus the mass in the gas phase – assumed to be pure propane) and the volume fraction of the L2 phase. The L1L2/L1 boundary is determined by extrapolating the L2 volume to zero. The global compositions within the three-phase region at each temperature and pressure (0.397 wt. fraction, 0.495 wt. fraction, 0.742 wt. fraction and 0.856 wt. fraction propane) are corrected individually. The mass of propane in the vapor is calculated by using the vapor density of pure propane from NIST [46] and the vapor volume is measured from the individual images based on the volume calibration (Chapter 3 section 3.7.1). Corrected liquid compositions and compositions for the L1L2/L1 boundary are given in Table 4.5 and plotted in Figure 4.6. The propane mass fraction at the L1L2/L1 phase boundary varies with temperature from 0.888 wt. fraction at 304 K to 0.807 wt. fraction at 354.2 K. The variation can be treated as linear with an uncertainty of ± 0.01 wt. fraction.

Table 4.5. L1L2/L1 boundary

Temperature (K)	Experiment Propane mass fraction	Corrected Propane mass fraction	L2 phase volume fraction	L1L2/L1 boundary propane mass fraction*	Deviation L1L2/L1 boundary propane
304.1	0.397	0.377	0.305	0.888	0.01
	0.495	0.459	0.282		
	0.742	0.732	0.098		
	0.857	0.852	0.021		
313.8	0.397	0.370	0.310	0.876	0.01
	0.495	0.451	0.304		
	0.742	0.729	0.091		
	0.857	0.850	0.020		
324.5	0.397	0.363	0.340	0.860	0.01
	0.495	0.435	0.337		
	0.742	0.724	0.099		
333.5	0.397	0.352	0.387	0.839	0.01
	0.495	0.415	0.394		
	0.742	0.720	0.103		
343.6	0.397	0.340	0.443	0.834	0.01
	0.495	0.382	0.459		
	0.742	0.713	0.117		
354.2	0.495	0.350	0.597	0.807	0.01
	0.742	0.699	0.142		

*Found by extrapolating L2 volume fractions to zero
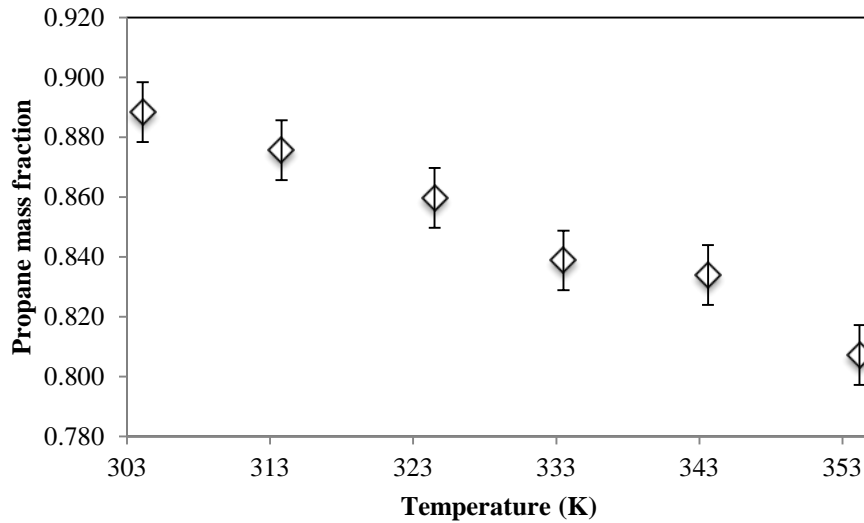
Figure 4.6. Saturated L1 compositions.

4.1.4 L1L2V/L2V Boundary Identification

The L1L2V/L2V boundary, which arises at pressures below the L1L2V/L1L2 boundary, is hard to detect experimentally because the volume of vapor needed to vaporize the L1 phase is very large. Consequently, only a few L1L2V/L1L2 boundary points were identified within the phase behavior observation data set presented in Table 4.6. For example, a transition from L1L2V to L2V behavior is observed for the 0.397 wt. fraction propane mixture between 342.6 K and 354.6 K, for the 0.495 wt. fraction propane mixture between 354.5 K and 364.8 K and for 0.742 wt. fraction propane mixture between 372.8 K and 381.1 K. Two other points can also be found from these experiments. The experiment with 0.397 wt. fraction of propane shows an L2V phase behavior at 354.6 K whereas at the same temperature 0.495 wt. fraction propane experiment shows an L1L2V phase behavior. There is therefore a point at 354.6 K between those two compositions and pressures. Similarly, there is a L1L2V/L2V boundary at 364.8 K between the 0.495 wt. fraction propane experiment and 0.742 wt. fraction propane experiment. These phase boundary points are presented in Table 4.7

with their uncertainties and they are included in the pressure-composition diagrams at fixed temperature.

Table 4.6. Phase behavior observations relevant to the identification of the L1L2V/L2V boundary

Bitumen + 0.397 wt. fraction propane			Bitumen + 0.495 wt. fraction propane			Bitumen + 0.742 wt. fraction propane		
T (K)	P (MPa)	Phase	T (K)	P (MPa)	Phase	T (K)	P (MPa)	Phase
303.9	1.00	L1L2V	304.8	1.05	L1L2V	304.4	1.06	L1L2V
303.9	1.00	L1L2V	304.8	1.05	L1L2V	304.4	1.06	L1L2V
303.9	1.00	L1L2V	304.9	1.05	L1L2V	304.3	1.06	L1L2V
314.5	1.30	L1L2V	313.1	1.29	L1L2V	314.1	1.35	L1L2V
314.5	1.30	L1L2V	312.8	1.28	L1L2V	313.9	1.34	L1L2V
314.2	1.29	L1L2V	312.4	1.26	L1L2V	313.8	1.34	L1L2V
325.1	1.66	L1L2V	323.9	1.65	L1L2V	324.1	1.70	L1L2V
325.1	1.66	L1L2V	324.0	1.65	L1L2V	324.1	1.70	L1L2V
324.8	1.64	L1L2V	323.9	1.64	L1L2V	324.0	1.70	L1L2V
334.0	2.01	L1L2V	333.0	2.00	L1L2V	333.1	2.07	L1L2V
334.0	2.00	L1L2V	332.8	1.99	L1L2V	333.1	2.07	L1L2V
333.6	1.98	L1L2V	332.4	1.97	L1L2V	333.0	2.05	L1L2V
342.6	2.39	L1L2V	344.6	2.52	L1L2V	343.4	2.56	L1L2V
342.4	2.37	L1L2V	344.8	2.53	L1L2V	343.5	2.56	L1L2V
342.3	2.36	L1L2V	345.0	2.52	L1L2V	343.3	2.56	L1L2V
354.8	2.99	L2V	354.5	3.04	L1L2V	354.0	3.14	L1L2V
354.7	2.97	L2V	354.5	3.03	L1L2V	354.3	3.15	L1L2V
354.6	2.95	L2V	354.5	3.01	L1L2V	354.1	3.12	L1L2V
362.9	3.46	L2V	365.0	3.57	L2V	363.2	3.70	L1L2V
363.2	3.45	L2V	364.8	3.50	L2V	363.0	3.69	L1L2V
363.1	3.42	L2V	365.1	3.39	L2V	363.0	3.69	L1L2V
375.2	4.14	L2V	372.8	3.89	L2V	372.9	4.39	L1L2V
375.3	4.10	L2V	372.8	3.78	L2V	372.9	4.39	L1L2V
374.8	4.05	L2V	372.6	3.67	L2V	372.8	4.38	L1L2V
383.2	4.57	L2V	382.4	4.26	L2V	381.5	5.12	L2V
383.2	4.50	L2V	382.2	4.12	L2V	381.1	5.05	L2V
383.3	4.46	L2V	382.1	4.02	L2V	381.2	5.02	L2V
392.5	5.02	L2V	393.0	4.63	L2V	392.1	6.07	L2V
392.5	4.95	L2V	392.8	4.49	L2V	392.2	5.93	L2V
392.5	4.88	L2V	392.7	4.41	L2V	392.1	5.81	L2V

Table 4.7. Points on the L1L2V/L2V boundary with their uncertainty

Temperature (K)	Propane mass fraction	Pressure (MPa)	Temperature uncertainty (K)	Propane mass fraction uncertainty	Pressure uncertainty (MPa)
349	0.40	2.7	6	0	0.3
355	0.45	3	0	0.05	0
360	0.50	3.2	5	0	0.2
373	0.62	4.1	0	0.1	0.3
377	0.74	4.7	4	0	0.3

4.1.5 Pressure-Composition diagrams at fixed temperature

Below the critical temperature of propane (369 K), the phase diagrams for Peace River bitumen + propane are qualitatively similar. A sketch is shown in Figure 4.7a. At pressures approaching 0 MPa, there is a vapor region at all propane mass fractions. Other phase behavior domains have the placements indicated. This distribution of phase domains is consistent with an extension of Type III phase behavior to a pseudo binary mixture. Above the critical temperature of propane, the vapor region extends to infinite pressure as the propane axis is approached, Figure 4.7b, and there is a critical point (L1=V) on the L1V/V boundary, and the L1V region shrinks. At higher temperatures still, the L1V region disappears and the L1=V critical point becomes a L1=V+L2 critical point on the L1L2V region surface, Figure 4.7c, and the L1L2V region shrinks. Once the L1L2V region disappears, only L2V and V domains remain in the diagram, Figure 4.7d, and the phase diagrams remain qualitatively similar until all of components reach their critical point or degrade thermally. For many pseudo binary mixtures, the transition from a pressure composition phase diagram such as the one shown in Figure 4.7a to one shown in Figure 4.7d can take place over a few degrees.
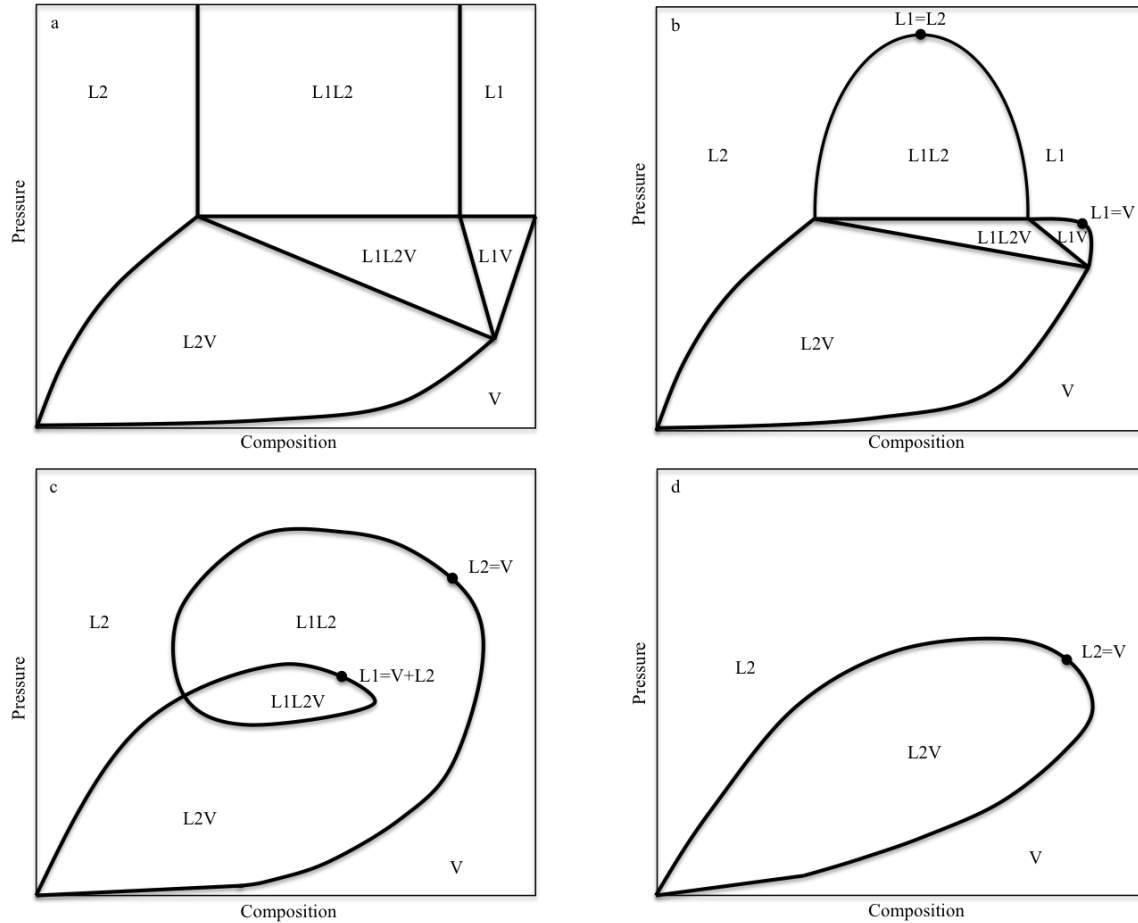
Figure 4.7. Sketches showing the sequence of expected pressure-composition phase diagrams at fixed temperature: below the critical temperature of the light component (a) and with increasing temperature above the critical temperature of the light component (b-d). Black circles denote critical points.

The experimental pressure-composition phase diagrams at fixed temperature for Peace River Bitumen + propane prepared on the observations and calculations noted above and shown in Figure 4.8 a-j reflect most but not all of the sketches in Figure 4.7. The transition from a phase diagram like Figure 4.7b to one like Figure 4.7d occurs over a temperature interval of less than 5 K for Peace River Bitumen + propane mixtures. Other key features of the phase diagram include the scale of the L1L2V region, which must almost reach the propane axis at low pressure, the scale of the L1L2 region, which spans a broad composition range, and the presence of a high-pressure vapor phase containing a significant wt. fraction of bitumen in the phase diagrams at temperatures exceeding 369 K. At 377 K this phase comprises 0.15 wt. fraction bitumen. This corresponds to an asphaltene content of more than 0.03 wt. fraction. A similar finding was obtained for

pentane and Athabasca vacuum residue (AVR). Above the critical temperature of pentane [39], a vapor phase with approximately 0.25 wt. fraction AVR (corresponding to 0.08 wt fraction asphaltenes) was identified at high pressure.
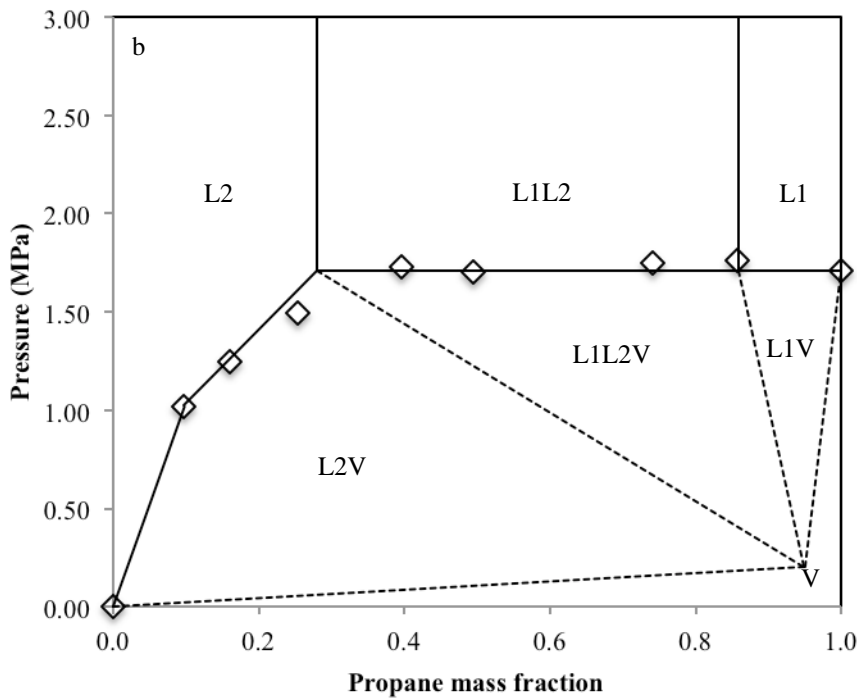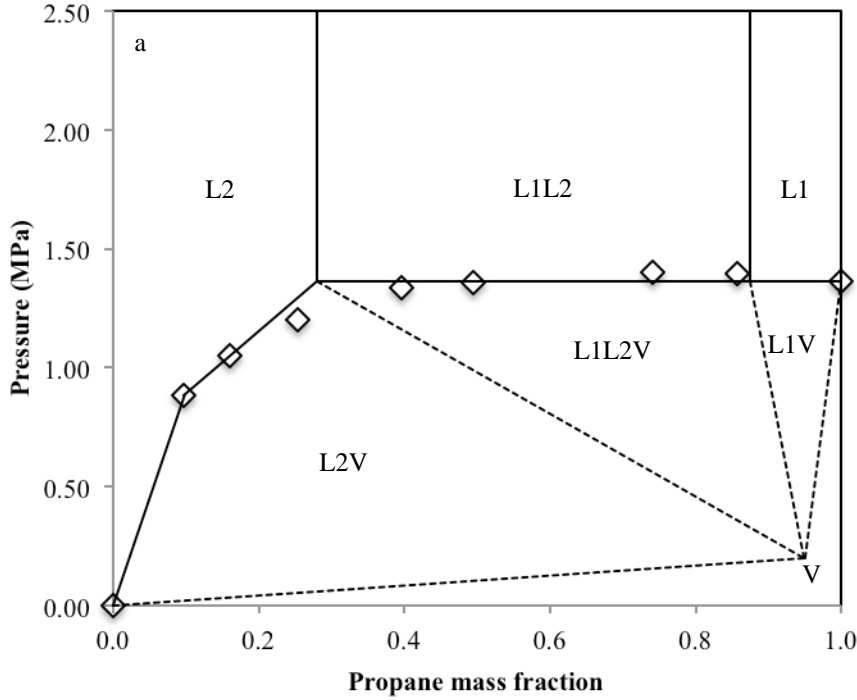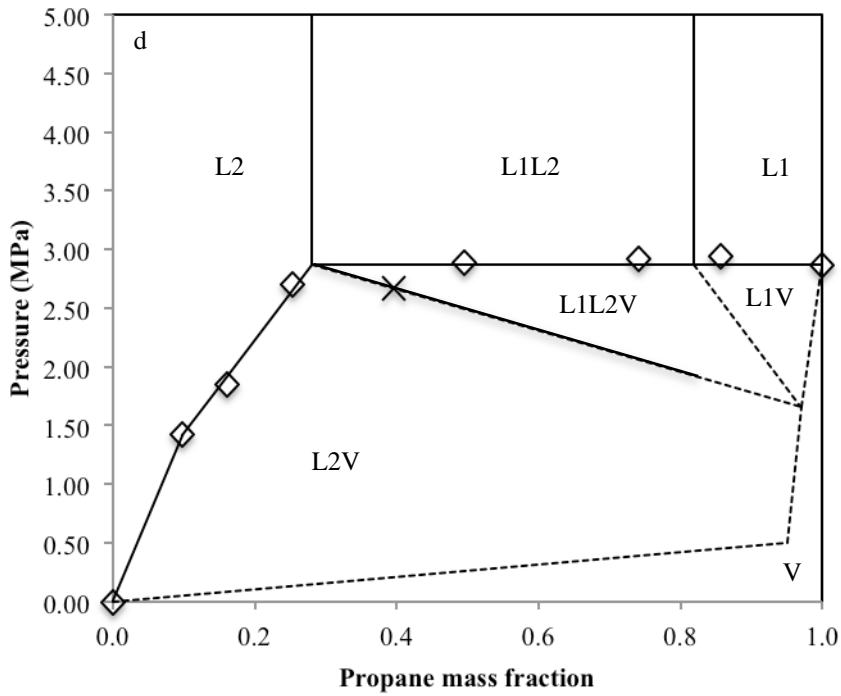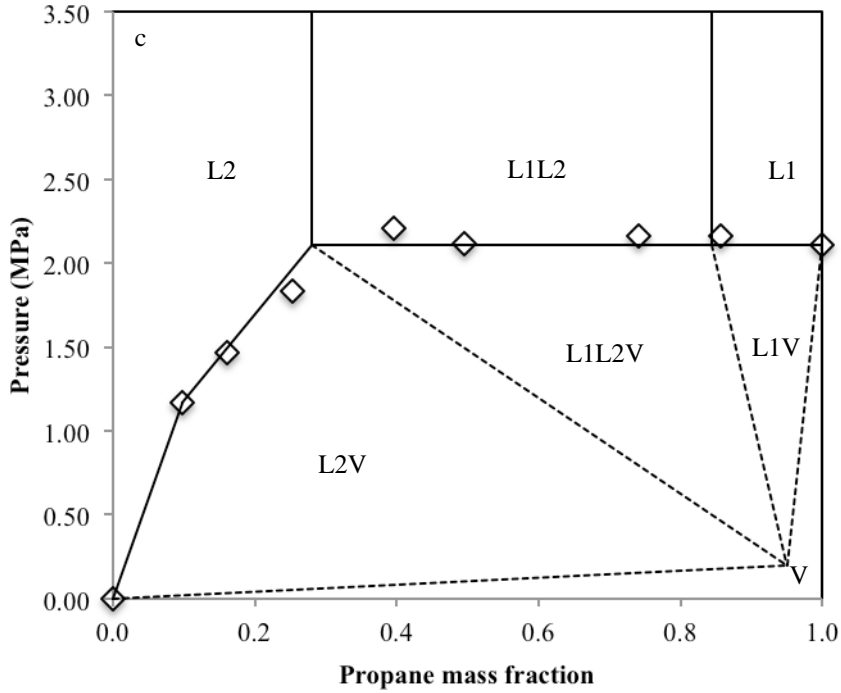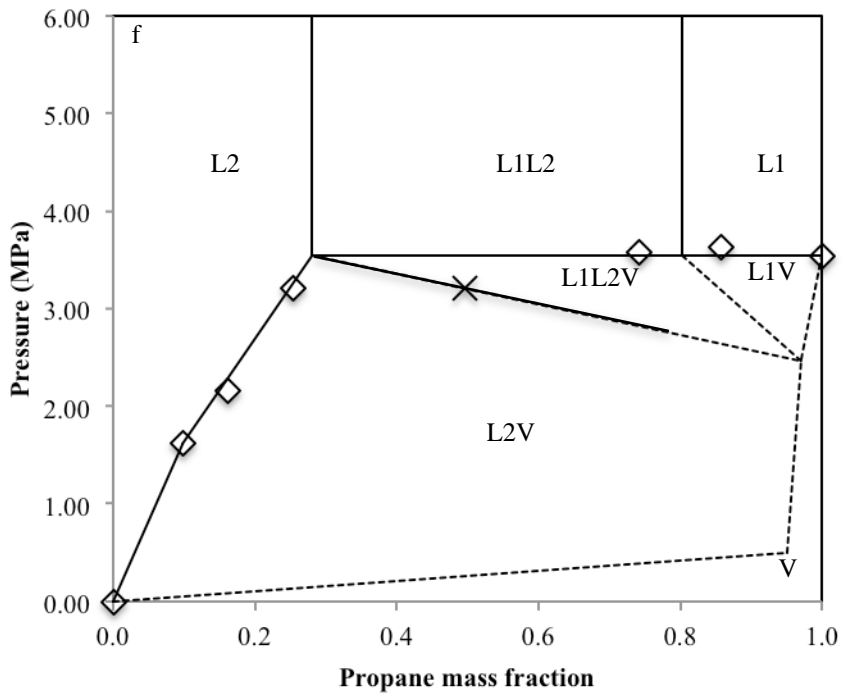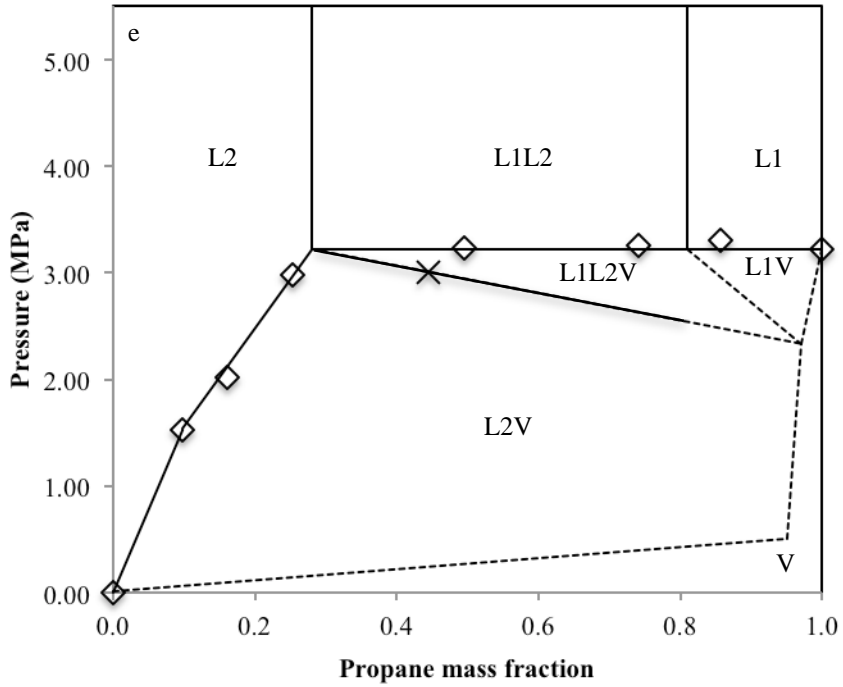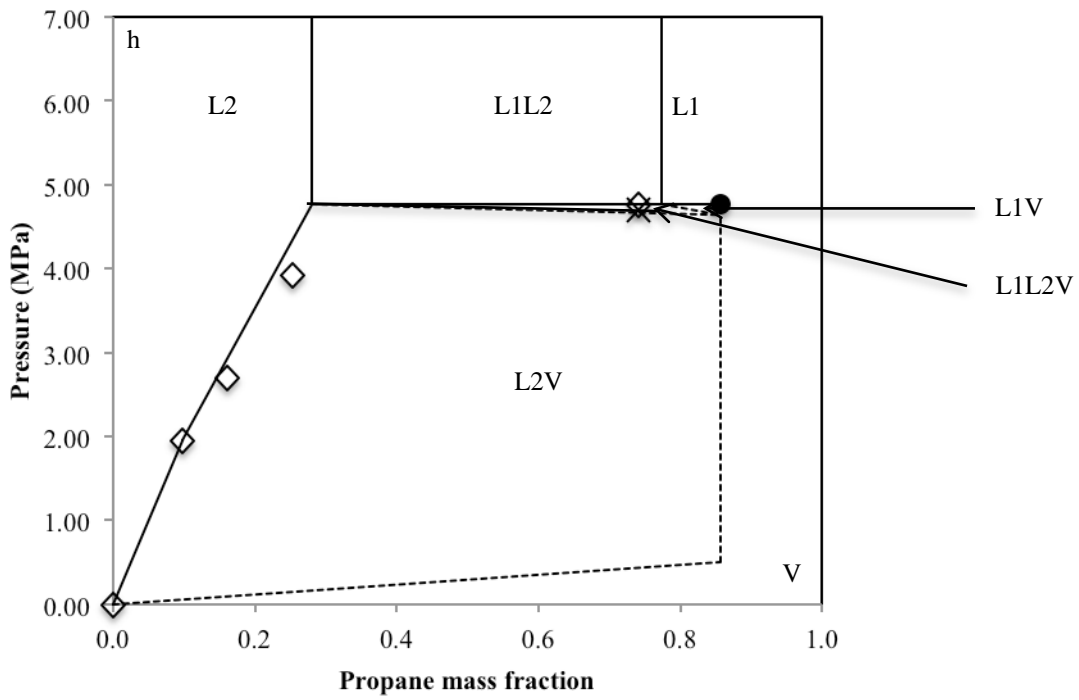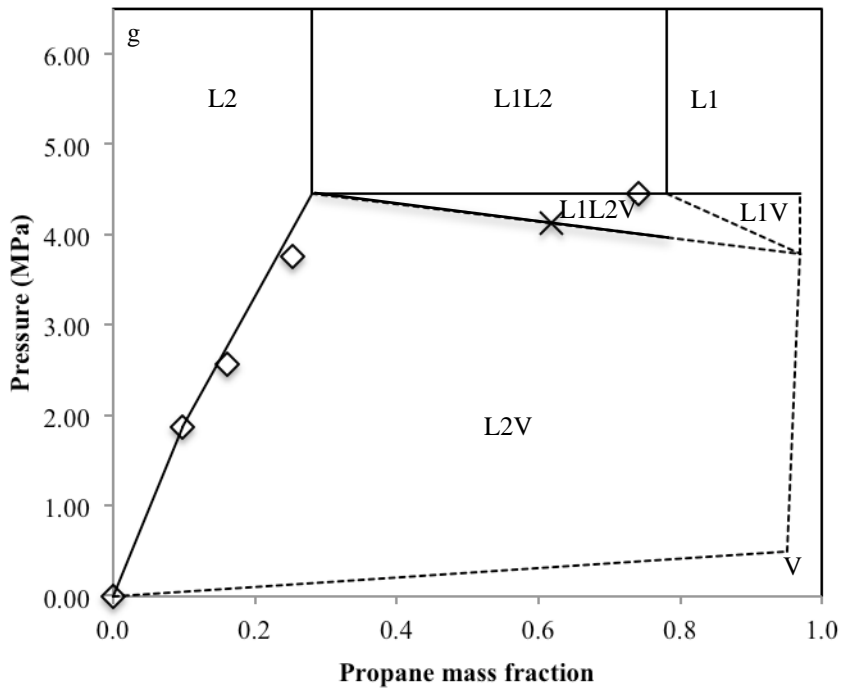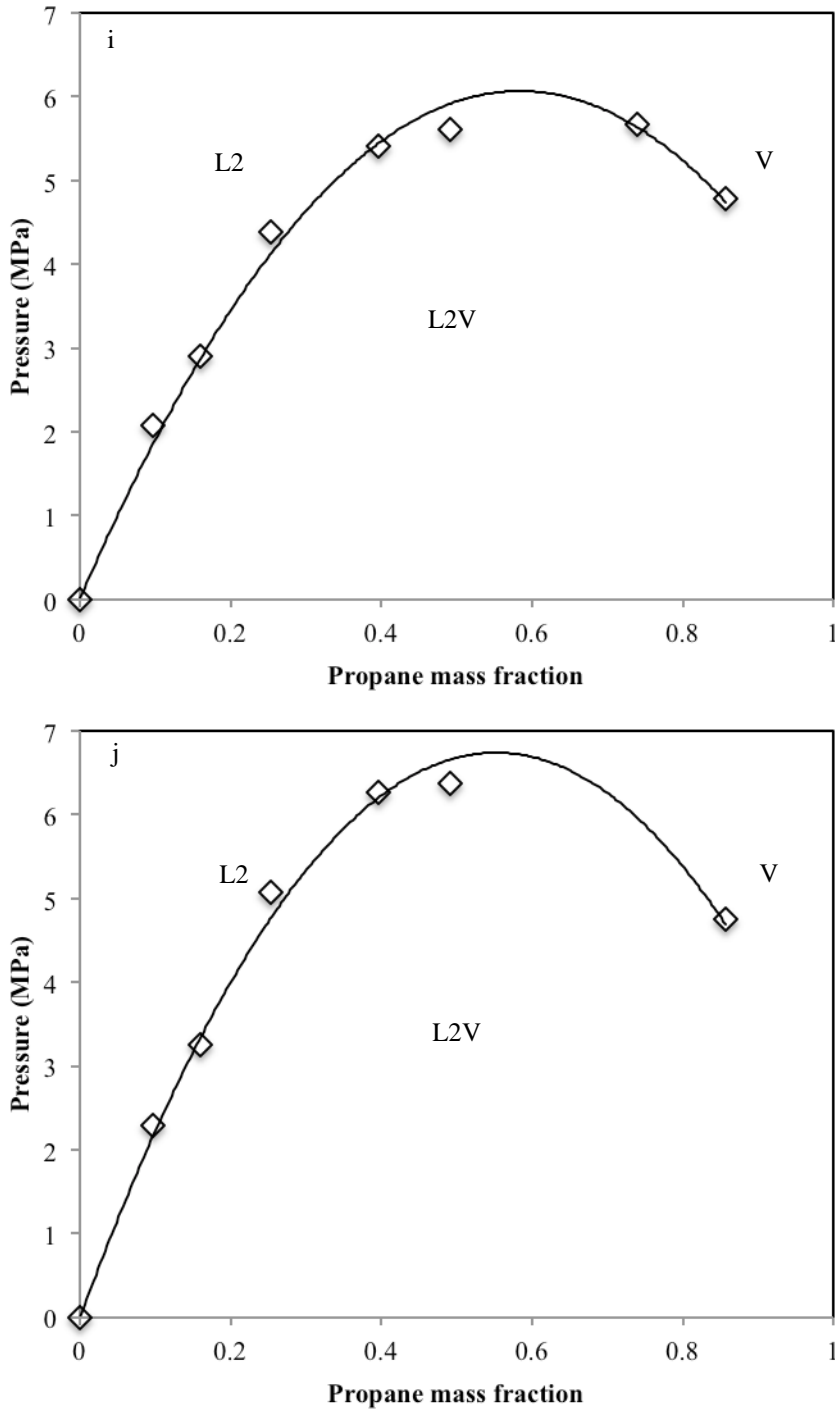
Figure 4.8. Pressure-composition diagrams for Peace River bitumen + propane mixtures at fixed temperature: a) 313 K, b) 323 K, c) 333 K, d) 348.6 K, e) 354.5 K, f) 359.8 K, g) 372.8 K, h) 377 K, i) 383 K, j) 393 K. Empty diamond points are saturated pressures. Solid lines show boundaries identified experimentally. Dashed lines are illustrative and are provided for completeness only. Cross points are the L1L2V/L2V pressures. The solid circle is a L1=V critical point.

59

4.2 Phase Density Measurement and Analysis

4.2.1 Asphaltene flocculation in propane + Peace River Bitumen mixtures

Asphaltene molecules are not soluble in n-alkane and are likely to flocculate in the propane + Peace River bitumen mixture. As already observed in Abedi's work [40], asphaltene flocculation will create dispersed solids in the liquid phases, which will absorb the X-ray intensity and decrease the measured intensity.

In order to be able to observe this phenomenon in the bitumen + propane experiments, the mass balance of the 0.857 wt. fraction propane experiment is made. This experiment has been chosen because only one L1 phase was observed and asphaltene molecules are very likely to flocculate in the propane rich phase. Bitumen + 0.857 wt. fraction propane mass balance is presented in Table 4.8.

Table 4.8. Mass balance for bitumen + 0.857 wt. fraction propane

Temperature (K)	Pressure (MPa)	Vapor Volume (mL)	L1 volume (mL)	L1 density (kg.m^{-3})	Density vapor propane (kg.m^{-3})	Mass balance (g)
323.5	1.63	49.7	58.2	600	35.6	4.0
323.5	1.62	51.3	58.9	600	35.5	4.5
323.4	1.62	52.7	58.9	601	35.4	4.5
334.2	2.04	51.2	58.1	584	46.0	3.6
334.2	2.04	52.5	58.2	584	45.9	3.7
334.1	2.03	53.6	58.1	584	45.7	3.7
343.7	2.47	50.3	58.1	566	57.7	3.1
343.7	2.46	51.6	58.1	567	57.5	3.2
343.4	2.45	53.2	58.1	566	57.1	3.2
352.4	2.91	50.8	58.1	546	71.2	2.7
352.3	2.90	51.7	58.0	547	71.2	2.7
362.6	3.48	50.6	57.4	525	91.4	2.1
362.6	3.47	52.4	57.3	527	90.8	2.2
362.2	3.45	53.5	57.4	529	89.7	2.4

For this experiment the mass balance is positive which means that the measured densities are too high compared to the real densities. Based on Abedi's work [40], this difference in density is explained by the aggregation of asphaltene molecules in the propane rich phase. In order to find the real value of the liquid density, densities are adjusted with a multiplying factor in a way that the mass balance is equal to zero.

Mass balances have also been performed in the L2 region on bitumen + 0.098 wt. fraction propane, bitumen + 0.161 wt. fraction propane and bitumen + 0.254 wt. fraction propane experiments. As for the 0.857 wt. fraction propane experiment, the mass balances of these three experiments, presented in Table 4.9 a), b), c), have been found positive but, lower than in the L1 region. This is due to the fact that the amount of propane in the L2 region is much lower than in the L1 region, which leads to less asphaltene flocculation. Densities in this region must also be corrected in order to have a mass balance equal to zero.

Table 4.9. Mass balances for a) bitumen + 0.098 wt. fraction propane, b) bitumen + 0.161 wt. fraction propane and c) bitumen + 0.254 wt. propane fraction

a) Bitumen + 0.098 wt. fraction propane

Temperature (K)	Pressure (MPa)	Vapor Volume (mL)	L2 volume (mL)	L2 density (kg.m^{-3})	Vapor propane density (kg.m^{-3})	Mass balance (g)
302.9	0.57	62.3	36.5	958	11.0	0.6
303.1	0.56	65.2	36.5	956	10.8	0.5
303.6	0.54	69.6	36.5	944	10.3	0.1
313.4	0.67	62.3	36.6	964	12.6	1.0
313.0	0.64	69.5	36.5	962	12.0	0.9
312.7	0.61	73.9	36.2	960	11.5	0.5
322.3	0.73	64.2	36.7	963	13.2	1.1
322.3	0.72	67.8	36.6	962	13.2	1.0
322.1	0.71	70.9	36.5	963	12.9	1.0
335.4	0.83	61.8	36.8	960	14.5	1.2
335.6	0.82	65.9	36.7	959	14.4	1.1
335.3	0.81	72.3	36.9	956	14.1	1.3
344.4	0.94	63.5	36.7	959	16.1	1.2
344.7	0.93	68.9	37.0	957	16.0	1.5
345.0	0.89	73.3	37.0	953	15.1	1.3

351.7	1.04	62.4	36.8	957	17.5	1.3
352.0	1.00	68.7	37.0	956	16.7	1.5
351.9	0.97	71.6	37.2	954	16.1	1.6
362.2	1.16	61.3	37.2	957	19.1	1.7
362.1	1.14	63.1	37.2	956	18.4	1.7
362.1	1.13	64.2	36.6	953	18.5	1.0
372.2	1.26	62.6	37.3	956	20.1	1.9
372.0	1.23	64.8	37.3	954	19.5	1.8
371.2	1.16	73.5	36.9	949	18.3	1.3
382.0	1.43	60.8	37.3	954	22.4	1.9
382.1	1.37	67.4	37.1	950	21.2	1.6
382.1	1.29	73.9	37.0	944	19.8	1.3
392.4	1.52	60.8	37.4	948	23.0	1.8
392.3	1.44	67.7	37.3	945	21.7	1.7
392.7	1.40	71.0	37.3	932	21.2	1.2

b) Bitumen + 0.161 wt. fraction propane

Temperature (K)	Pressure (MPa)	Vapor Volume (mL)	L2 volume (mL)	L2 density (kg.m^{-3})	Vapor propane density (kg.m^{-3})	Mass balance (g)
302.7	0.68	59.8	40.1	939	13.5	0.8
302.9	0.67	65.5	40.0	925	13.2	0.2
303.0	0.66	69.4	40.0	922	12.9	0.1
313.8	0.84	61.0	40.2	948	16.2	1.4
313.6	0.83	63.4	40.2	946	15.9	1.4
313.3	0.81	68.3	40.0	942	15.6	1.1
325.1	0.99	71.1	40.0	947	18.7	1.6
325.1	1.04	60.2	40.1	944	19.8	1.4
325.4	1.02	66.3	39.9	940	19.3	1.1
333.3	1.17	63.3	40.0	945	21.9	1.5
333.2	1.15	67.6	39.9	942	21.3	1.4
332.7	1.13	69.9	39.9	940	20.9	1.3
341.4	1.33	61.0	39.9	944	24.5	1.5
341.4	1.31	64.5	39.9	944	24.1	1.6
341.4	1.28	69.1	39.7	940	23.5	1.3
352.8	1.51	62.6	39.8	944	27.1	1.6
353.0	1.49	69.1	39.2	942	26.6	1.1
365.6	1.75	64.5	39.2	941	30.4	1.2

Temperature (K)	Pressure (MPa)	Vapor Volume (mL)	L2 volume (mL)	L2 density (kg.m⁻³)	Vapor propane density (kg.m⁻³)	Mass balance (g)
365.8	1.73	67.5	39.2	940	29.8	1.2
365.7	1.70	69.8	39.1	938	29.4	1.1
372.6	1.88	64.1	39.3	939	32.0	1.3
372.7	1.84	67.3	39.2	936	31.3	1.2
372.4	1.79	71.7	39.1	933	30.2	1.0
382.4	2.04	64.7	39.2	936	33.8	1.2
381.6	2.00	67.4	39.2	935	33.1	1.2
381.7	1.94	71.9	39.1	934	31.9	1.2
392.9	2.22	64.6	39.2	922	35.8	0.8
392.8	2.18	67.2	39.2	906	35.0	0.2
392.6	2.12	70.9	39.2	921	33.9	0.9

c) Bitumen + 0.254 wt. fraction propane

Temperature (K)	Pressure (MPa)	Vapor Volume (mL)	L2 volume (mL)	L2 density (kg.m⁻³)	Vapor propane density (kg.m⁻³)	Mass balance (g)
303.4	0.89	57.3	48.8	901	18.3	2.6
303.5	0.89	59.1	48.8	900	18.3	2.7
303.7	0.89	61.6	48.7	899	18.3	2.5
313.6	1.12	57.5	48.2	907	23.1	2.7
313.6	1.12	59.0	48.2	907	23.1	2.7
313.5	1.12	62.4	48.1	920	23.1	3.3
325.1	1.43	58.8	48.0	920	29.6	3.5
325.2	1.43	60.6	48.0	918	29.4	3.5
325.0	1.42	63.6	47.5	904	29.1	2.4
336.4	1.78	58.2	47.4	920	36.7	3.4
336.5	1.76	60.9	47.4	906	36.3	2.8
336.2	1.74	63.6	47.3	906	35.8	2.8
344.2	2.03	58.3	47.2	907	42.0	2.9
344.2	2.01	60.7	47.1	907	41.4	2.9
344.0	1.99	63.3	46.6	906	40.8	2.5
353.6	2.33	60.3	46.4	909	48.0	2.7
353.6	2.32	62.1	46.4	908	47.5	2.7
353.5	2.30	64.3	46.2	907	46.9	2.6
364.1	2.69	59.8	45.8	909	54.7	2.6
364.1	2.66	62.3	45.7	910	54.0	2.6
364.1	2.64	65.1	45.5	909	53.1	2.5

Temperature (K)	Pressure (MPa)	Vapor Volume (mL)	L2 volume (mL)	L2 density (kg.m^{-3})	Vapor propane density (kg.m^{-3})	Mass balance (g)
372.8	2.96	61.6	45.5	911	59.3	2.8
373.3	3.00	59.2	45.1	910	60.3	2.2
373.3	2.90	66.2	44.9	910	57.1	2.3
381.6	3.26	60.5	44.9	912	63.9	2.4
381.2	3.21	63.2	44.8	911	62.7	2.4
381.4	3.16	66.2	44.8	910	61.2	2.5
394.8	3.62	61.0	44.8	912	67.8	2.6
395.0	3.54	67.0	44.1	909	65.6	2.1

4.2.2 Density of the L2 phase

All densities for 0.098, 0.161 and 0.254 wt. fraction propane experiments were measured in the L2V region. Therefore, some of the propane is in the vapor phase. As in section 4.1.3, the mass fraction of propane in the liquid phase is corrected at each condition. The values for unsaturated L2 densities are shown in Table 4.10. To a first approximation L2 densities are linear in composition at fixed temperature as shown Figure 4.9 a-j.

Table 4.10. Unsaturated L2 density data (at corrected compositions)

Temperature (K)	Propane mass fraction in liquid phase	Corrected L2 density (kg.m^{-3})
303.2	0.000	1009
302.9	0.080	925
303.1	0.080	923
303.6	0.079	912
302.7	0.143	912
302.9	0.141	898
303.0	0.141	896
303.4	0.235	847
303.5	0.234	846
303.7	0.233	845
313.3	0.000	1002
313.4	0.077	931
313.0	0.076	929
312.7	0.076	927
313.6	0.138	918
313.3	0.137	915

Temperature (K)	Propane mass fraction in liquid phase	Corrected L2 density (kg.m^{-3})
313.6	0.229	853
313.5	0.228	865
323.7	0.000	996
322.3	0.076	930
322.3	0.075	928
322.1	0.074	930
325.1	0.130	919
325.1	0.134	916
325.4	0.132	913
325.1	0.222	865
325.2	0.221	863
325.0	0.220	850
334.6	0.000	989
335.4	0.074	927
335.6	0.073	926
335.3	0.071	923
333.3	0.129	918
333.2	0.128	915
332.7	0.127	913
336.4	0.214	865
336.5	0.213	852
336.2	0.212	852
343.2	0.000	983
344.4	0.071	926
344.7	0.069	924
345.0	0.069	920
341.4	0.126	917
341.4	0.125	916
341.4	0.123	912
344.2	0.208	853
344.2	0.207	853
344.0	0.206	852
352.6	0.000	977
351.7	0.069	925
352.0	0.068	923
351.9	0.067	921
352.8	0.122	916
353.0	0.118	914
353.6	0.199	854
353.6	0.198	854
353.5	0.197	853
363.9	0.000	970
362.2	0.067	924

Temperature (K)	Propane mass fraction in liquid phase	Corrected L2 density (kg.m^{-3})
362.1	0.067	923
362.1	0.067	920
365.6	0.115	914
365.8	0.114	913
365.7	0.113	911
364.1	0.191	855
364.1	0.190	855
364.1	0.188	855
372.3	0.000	965
372.2	0.065	923
372.0	0.064	922
371.2	0.062	916
372.6	0.113	912
372.7	0.111	909
372.4	0.110	906
372.8	0.184	857
373.3	0.185	855
373.3	0.181	855
381.8	0.000	959
382.0	0.062	921
382.1	0.060	917
382.1	0.059	912
382.4	0.109	909
381.6	0.108	908
381.7	0.107	907
381.6	0.179	857
381.2	0.177	856
381.4	0.175	856
393.7	0.000	951
392.4	0.061	915
392.3	0.059	913
392.7	0.058	900
392.9	0.106	895
392.8	0.105	880
392.6	0.104	895
394.8	0.173	857
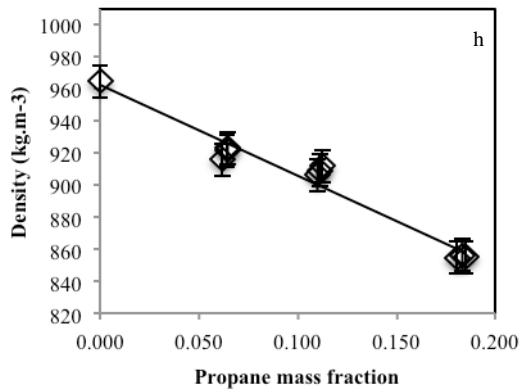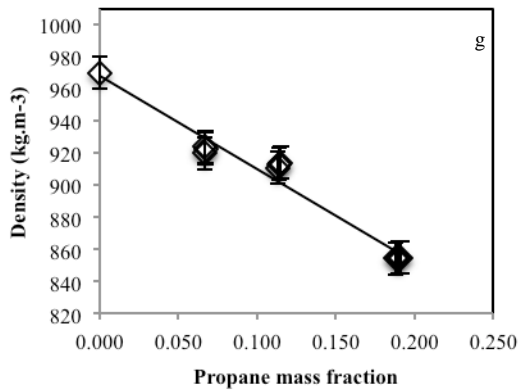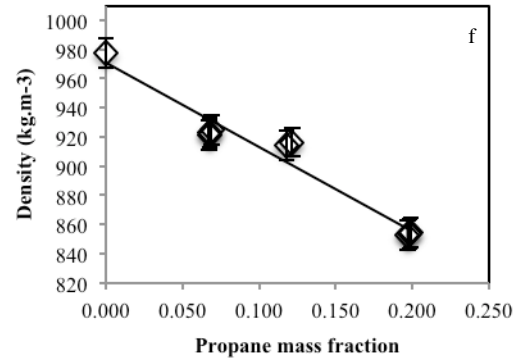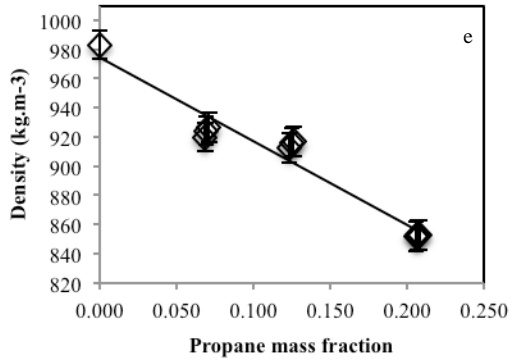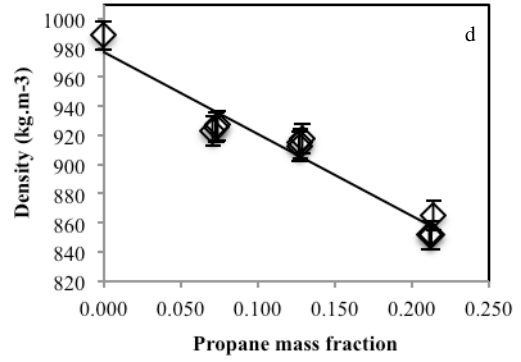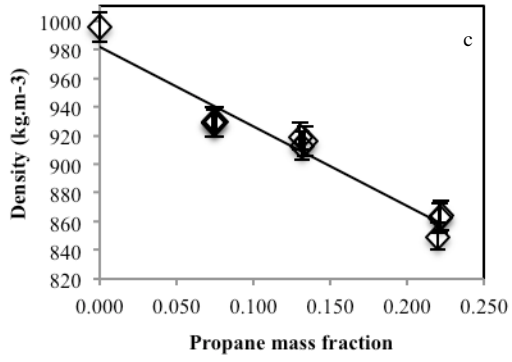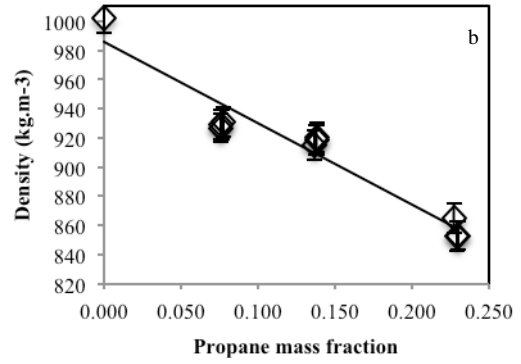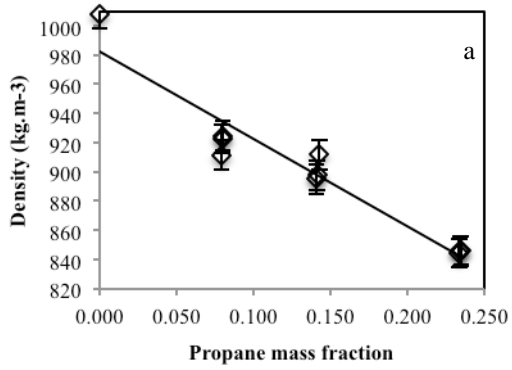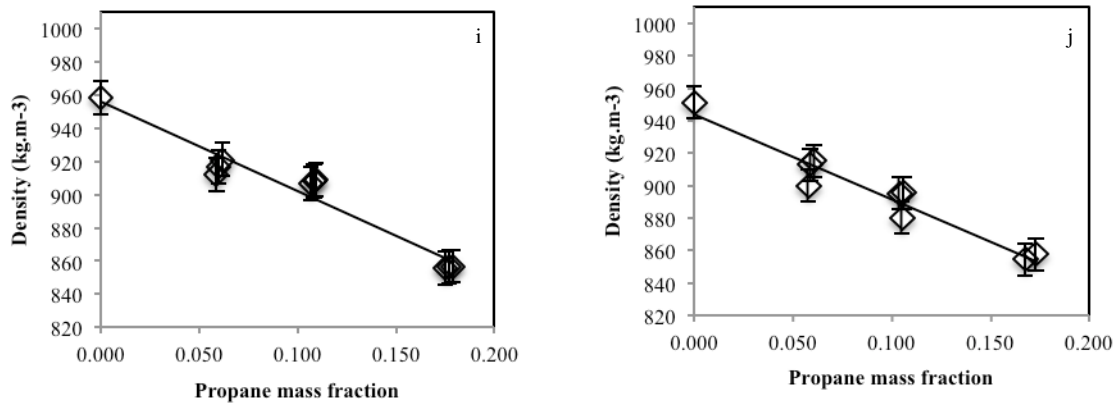
Figure 4.9. Impact of the propane mass fraction on the L2 density at: a) 303 K, b) 313 K, c) 324 K, d) 335 K, e) 343 K, f) 353 K, g) 364 K, h) 372 K, i) 382 K and j) 394 K. The solid line is a fitted linear model extrapolated to obtain the saturated L2 density.

The linear model falls within the uncertainty of the measurements. Extrapolation to the L2/L1L2 boundary, 0.281 wt. fraction of propane between 303 K and 369 K, yields the saturated L2 phase densities shown in Table 4.11 and presented in Figure 4.10. The uncertainty on the saturated L2 densities is at least $\pm$ 15 kg.m^{-3}. The density of the saturated L2 phase decreases with the increase of temperature in the interval but a constant value of 815 kg.m^{-3} fits the data within the combined measurement and extrapolation uncertainty.

Table 4.11. Extrapolated densities of saturated L2 (L2/L1L2 boundary)

Temperature (K)	Composition L2/L1L2 boundary	L2 Density (kg.m^{-3})
303.2	0.281	815
313.3	0.281	829
323.7	0.281	826
334.6	0.281	820
343.2	0.281	813
352.6	0.281	809
363.9	0.281	805
372.3	0.281	804
381.8	0.281	804
393.7	0.281	797
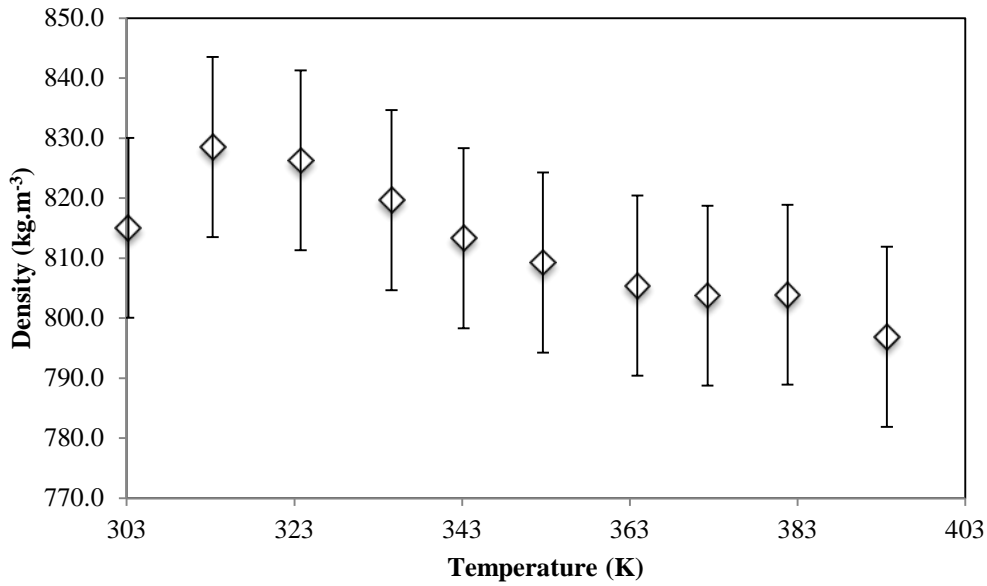
Figure 4.10. Saturated L2 phase density

4.2.3 Density of the L1 phase

Due the small size of the L1V region, only two experiments were performed, one with 0.857 wt. fraction propane and the other with pure propane. However the global composition of the 0.857 wt. fraction experiment is close to the composition at the L1/L1L2 boundary. Again the global composition is corrected and linear extrapolation to the boundary is performed. Measured densities are reported in Table 4.12. The uncertainty for these extrapolated densities is $\pm$ 12 kg.m^{-3}. The saturated L1 density values are shown in Table 4.13 and plotted in Figure 4.11. The saturated L1 density decreases with temperature, but like the saturated L2 density, temperature variation has a small impact on the saturated L1 density over the temperature range investigated.

Table 4.12. Unsaturated L1 density data (with composition correction)

Temperature (K)	Propane mass fraction in liquid	L1 density (kg.m^{-3})
303.4	1.000	484
303.3	0.853	606
303.4	0.852	606
314.3	1.000	465

Temperature (K)	Propane mass fraction in liquid	L1 density (kg.m^{-3})
314.4	0.851	581
314.2	0.851	580
314.0	0.851	581
323.5	1.000	448
323.5	0.849	567
323.5	0.849	567
323.4	0.849	567
334.2	1.000	426
334.2	0.846	552
334.2	0.846	552
334.1	0.846	552
343.7	1.000	402
343.7	0.844	535
343.7	0.843	535
343.4	0.843	535
352.3	1.000	376
352.4	0.840	516
352.3	0.839	517
362.6	1.000	332
362.6	0.834	496
362.6	0.833	498
362.2	0.833	500

Table 4.13. Extrapolated densities - saturated L1 (L1/L1L2 boundary)

Temperature (K)	L1/L1L2 Composition	L1 Density (kg.m^{-3})
303.4	0.891	574
314.3	0.874	563
323.5	0.859	559
334.2	0.842	555
343.7	0.827	549
352.3	0.814	542
362.6	0.797	534
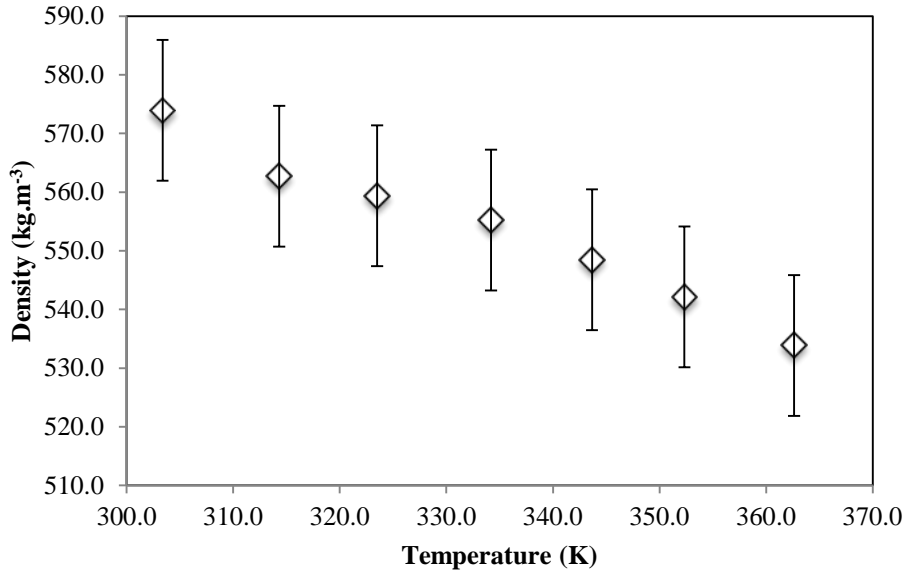
Figure 4.11. Evolution of the saturated L1 phase density with temperature (L1/L1L2 boundary)

4.2.4 Specific excess volumes

The excess volume ΔV:

$$\Delta V = \frac{1}{\rho} - \left(\frac{\omega}{\rho_p} + \frac{1-\omega}{\rho_b} \right)$$

(4-1)

where ρ is the measured mixture density, ρ_p is the propane density, ρ_b is the bitumen density and ω is the propane mass fraction, is a measure of how the unit volume of mixtures deviates from the volume expected using the ideal mixing rule based on the density of the components. By definition, the specific excess volumes for propane and bitumen are zero. Specific excess volume values for propane + bitumen mixtures are reported in Table 4.12 and isotherms are plotted in Figure 4.12. In all cases excess volumes are negative. This means that density values predicted using the ideal mixing model are lower than the measured densities. The absolute value of the excess volumes is large and a maximum value is reached, at fixed temperature, in the saturated L1 phase. The absolute value of the maximum impact also increases with temperature in the range

71

investigated. This behavior is observed because propane and bitumen have a large difference in critical temperature values. The experiment temperatures are close to the critical temperature of propane (a high reduced temperature $Tr = T/Tc$) but the mixtures are at a lower reduced temperature relative to the mixture critical point. Consequently, the apparent density of propane in the liquid is higher than anticipated by the ideal mixing rule.

Table 4.14. Specific excess volumes for Peace River Bitumen + propane mixtures

Temperature (K)	Propane mass fraction	Excess volume (mL.kg^{-1})	Phase State
303.2	0.000	0.0	L2
303.2	0.080	10.2	L2
302.9	0.142	-34.0	L2
303.5	0.234	-61.3	L2
303.2	0.281	-66.1	L2/L1L2
303.4	0.891	-206.8	L1/L1L2
303.4	1.000	0.0	L1
313.0	0.000	0.0	L2
313.0	0.077	-8.3	L2
313.6	0.138	-65.8	L2
313.6	0.229	-92.6	L2
313.3	0.281	-111.8	L2/L1L2
314.3	0.874	-226.2	L1/L1L2
314.3	1.000	0.0	L1
322.2	0.000	0.0	L2
322.2	0.075	-18.0	L2
325.2	0.132	-77.6	L2
325.1	0.221	-115.5	L2
323.7	0.281	-139.5	L2/L1L2
323.5	0.859	-270.6	L1/L1L2
323.5	1.000	0.0	L1
334.2	0.000	0.0	L2
335.4	0.074	-30.0	L2
333.1	0.128	-87.1	L2
336.4	0.213	-135.1	L2
334.6	0.281	-168.8	L2/L1L2
334.2	0.846	-332.0	L1/L1L2
334.2	0.842	-337.5	L1
334.2	1.000	0.0	L1
344.7	0.000	0.0	L2

Temperature (K)	Propane mass fraction	Excess volume (mL.kg^{-1})	Phase State
344.7	0.070	-38.4	L2
341.4	0.125	-102.4	L2
344.1	0.207	-149.9	L2
343.2	0.281	-198.1	L2/L1L2
343.6	0.843	-385.7	L1/L1L2
343.7	0.827	-409.5	L1
343.7	1.000	0.0	L1
351.8	0.000	0.0	L2
351.8	0.068	-50.0	L2
352.9	0.121	-128.6	L2
353.6	0.198	-182.3	L2
357.8	0.281	-293.1	L2/L1L2
352.3	0.814	-498.9	L1/L1L2
352.3	0.840	-460.7	L1
352.3	1.000	0.0	L1
362.1	0.000	0.0	L2
362.1	0.067	-76.9	L2
365.7	0.114	-184.4	L2
364.1	0.190	-252.8	L2
363.9	0.281	-366.4	L2/L1L2
362.5	0.833	-667.3	L1/L1L2
362.6	0.797	-736.3	L1
362.6	1.000	0.0	L1

a

b

c

d

e

f

75

g
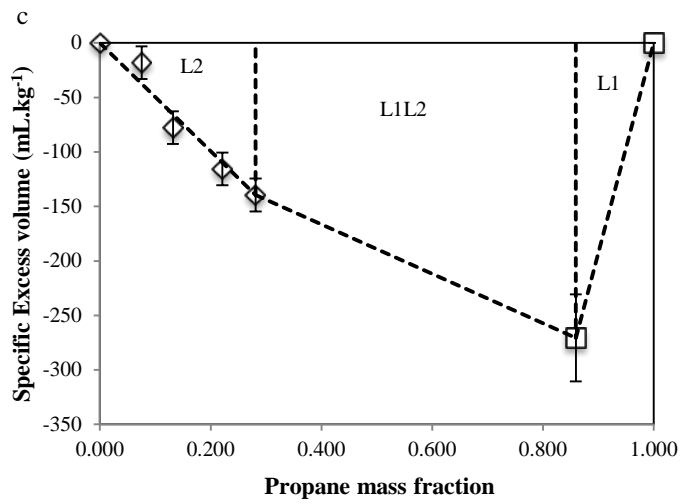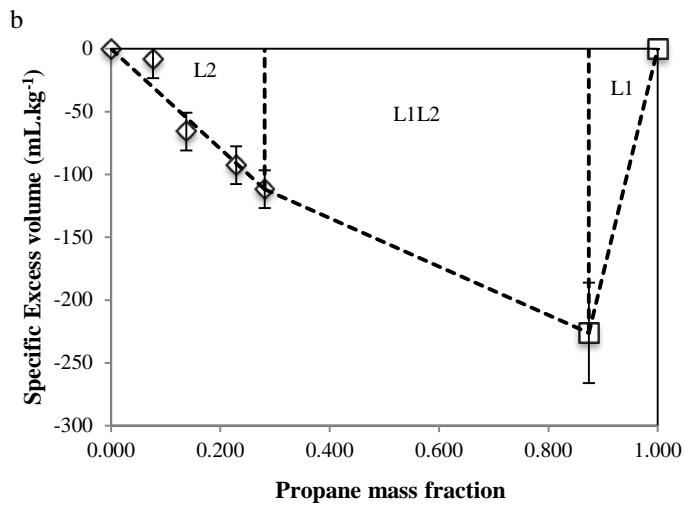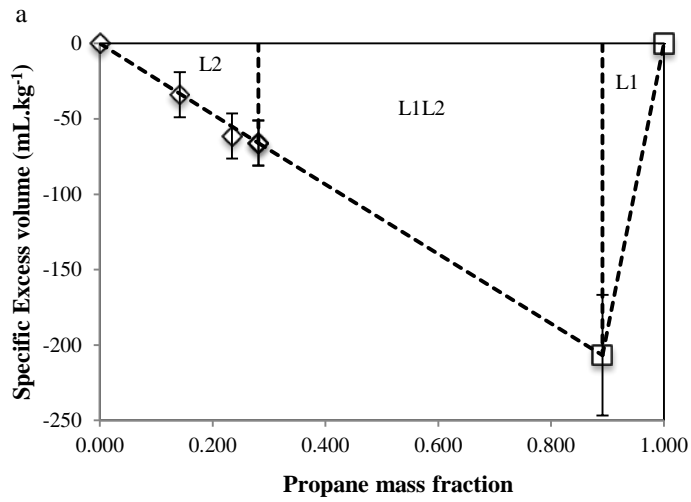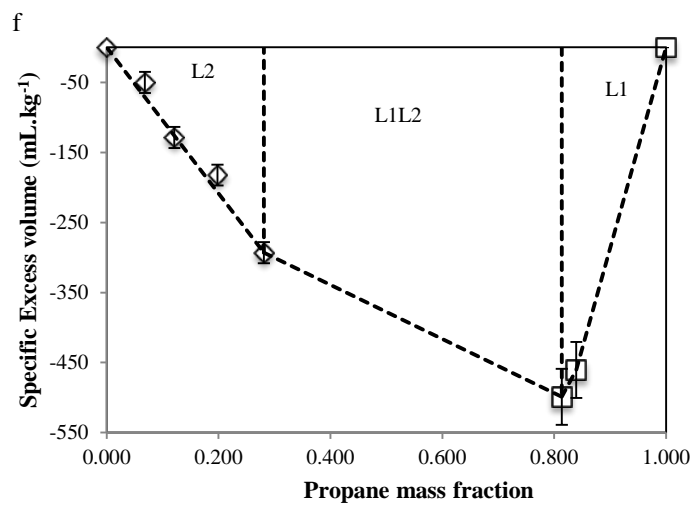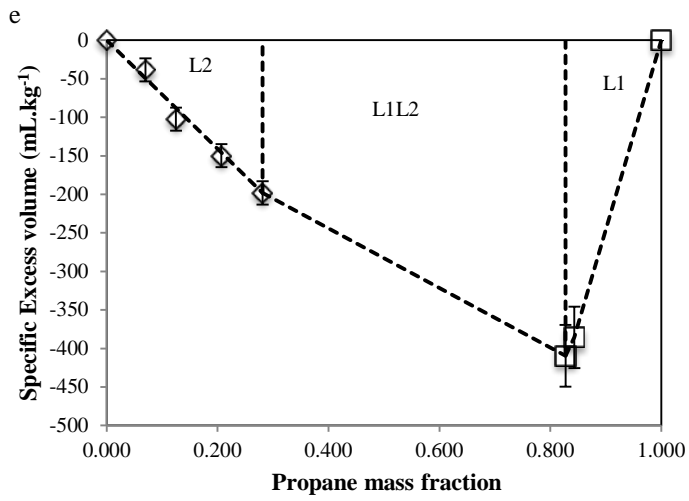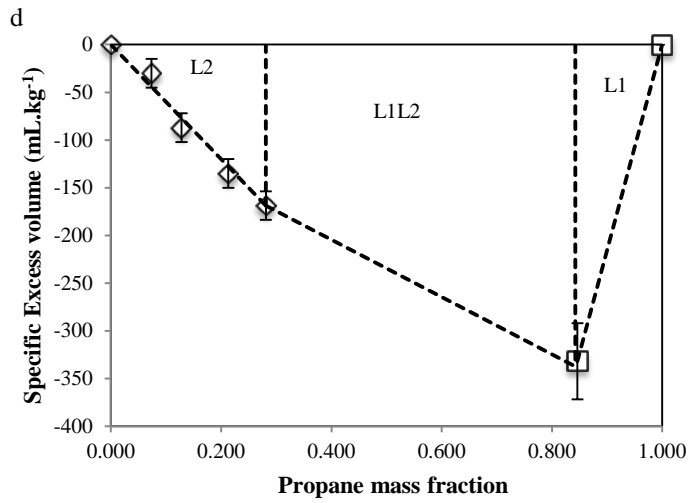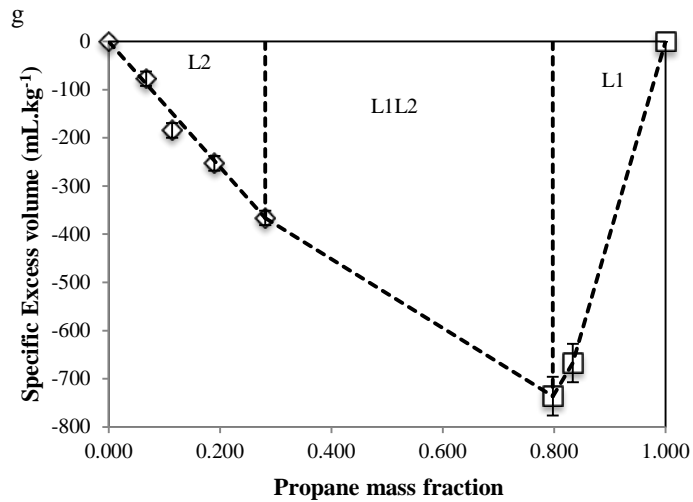
Figure 4.12. Excess volumes of bitumen + propane mixtures at: a) 303 K b) 313 K, c) 322.2 K, d) 335.4 K, e) 344.7 K, f) 351.8 K, g) 362.1 K. Empty diamond points correspond to the L2 region and square points correspond to the L1 region. Dashed lines show the boundaries between the different phase regions.

Chapter 5 Conclusion and Future Work

5.1 Conclusions

1. This work presents reliable and accurate phase diagrams and phase density data for Peace River bitumen + propane mixtures. The X-ray view cell apparatus was calibrated and validated with pure propane and a binary mixture of propane + n-decane. In the experimental range of temperature 303 K to 393 K and pressure 0 MPa to 7 MPa, the accuracy on the pressure and temperature measurements is 0.7% ($\pm$ 0.02 MPa) and 0.1% ($\pm$ 0.4K) respectively.

2. Phase diagrams for Peace River Bitumen + propane were constructed by studying the phase behavior of mixtures at fixed composition. Vapor (V), low-density liquid (L1) and high-density liquid (L2) phases were observed singly and in combination.

3. Based on the pressure-composition diagrams at fixed temperature and the pressure-temperature diagrams at fixed composition, the phase behavior of the Peace River bitumen + propane mixture is consistent with expected behaviors for a Type III pseudo binary mixture, according to the van Konynenburg and Scott classification scheme for phase behavior.

4. Type III phase behavior is characterized by a L1L2V region extending from the freezing point up to a temperature exceeding the critical point of one of the components, in this case propane.

5. The saturated mass fraction of propane in the Peace River Bitumen rich L2 phase between 303 K and 369 K is shown to be temperature independent (0.28 $\pm$ 0.03 wt. fraction)

6. The saturated mass fraction bitumen in the propane-rich L1 phase increases with temperature from 0.11 wt. fraction at 304 K to 0.20 wt. fraction at 354 K.

7. A second characteristic of Type III phase behavior, but one shared with other phase behavior Types, is the presence of high-pressure vapor phases that are rich in the high molar mass component, in this case Peace River Bitumen. For non-

experts, the existence of a propane-rich vapor phase with a bitumen mass fraction exceeding 0.20, at only 380 K is unexpected.

8. Densities of the low-density liquid (L1) and the high-density liquid (L2) phases were measured and specific excess volumes were determined. In all cases excess volumes were found to be negative and to possess large absolute values. Maximum absolute values, at fixed temperature, arise in the saturated L1 phase. The absolute value of the maximum also increases with temperature in the range investigated (303 to 362 K).

9. Potentially promising regions of pressure, temperature and composition for production process development that make use of the high-pressure and high-temperature V region, where Peace River bitumen has a significant solubility, for production combined with the high temperature transition from V to L2V for propane recovery are identified.

5.2 Future work

1. These data are expected to be important for applications in the heavy oil/bitumen production, transport, and refining sectors. Development and testing of process models that include these data is one avenue for further study.

2. Further investigation of the solubility of bitumen in the high-pressure propane vapor rich phase, in particular, is warranted.

3. In order to have a better understanding of the Expanded-Solvent SAGD process, a phase behavior study of the ternary mixture propane + water + bitumen is warranted.

4. The transport properties of saturated L1 and L2 phases arising in the propane + bitumen mixture, and their viscosities in particular, warrant further investigation.

5. A phase behavior study involving other light n-alkanes such as butane, or mixtures of light n-alkanes is warranted as these could be used to tailor critical phenomena for specific applications or to optimize the impact of critical phenomena on process chemistry.

References

[1]   R. M. Butler, G. S. McNab, and H. Y. Lo, "Theoretical-studies on the gravity drainage of heavy oil during insitu steam heating", Canadian Journal of Chemical Engineering, vol. 59, pp. 455-460, 1981.

[2]   R. M. Butler and D. J. Stephens, "The gravity drainage of steam- heated heavy oil to parallel horizontal wells", Journal of Canadian Petroleum Technology, vol. 20, pp. 90-96, 1981.

[3]   Brian Hitchon, "Geochemical studies-4 Physical and Chemical Properties of Sediments and Bitumen from some Alberta oil sand deposits", Alberta Research Council Open File Report 1993-25.

[4]   Stewart, Robert A., Wood, Caitlin V., Murowchuck, Steven J., Shaw, John M., "Phase Order Inversion During Heavy Oil and Bitumen Production with Solvent Addition", Energy & Fuels, 2014, 28(7), pp 4835-4848

[5]   R. M. Butler, "The gravity drainage of steam- heated heavy oil to parallel horizontal wells", Journal of Canadian Petroleum Technology, vol. 33, No 2, pp. 44-50, 1994.

[6]   Nasr, T. and Isaacs, E. "Process For Enhancing Hydrocarbon Mobility Using a Steam Additive", U.S. Patent 6230814, 2001

[7]   Ayodele, O. R., Nasr, T. N., Beaulieu, G., & Heck, G., "Laboratory Experimental Testing and Development of an Efficient Low Pressure ES-SAGD Process", Journal of Canadian Petroleum Technology, vol. 48, No 9, pp. 54-61, 2009

[8]   H. Matsuda, K. Ochi, "Liquid–liquid equilibrium data for binary alcohol + n-alkane (C10–C16) systems: methanol + decane, ethanol + tetradecane, and ethanol + hexadecane" Fluid Phase Equilibr 224 31–37, 2004

[9]   Sen, S. C.; Maity, S.; Ganguli, K.; Goswami, K.; Ray, P. "Binary Liquid-Liquid Equilibria of Aniline-Paraffin and Furfural-Paraffin Systems" Can. J. Chem. Eng., 69, 1367-1373, 1991

[10]   A. Pourmohammadbagher, John M. Shaw "On probing contaminant transport to and from clay surfaces in organic solvents and water using solution calorimetry", Environmental Science & Technology, in press 2015.

[11]   Transmountain.com, 'Product | Trans Mountain'. 2015. Web. May 2015.

[12]   Crudemonitor.ca, 'Crudemonitor.Ca - Canadian Crude Quality Monitoring Program'. 2015. Web. May 2015.

[13]   A. Badamchi-Zadeh, H.W. Yarranton, W.Y. Svrcek, B.B. Maini, "Phase Behaviour and Physical Property Measurements for VAPEX Solvents: Part I. Propane and Athabasca Bitumen", Journal of Canadian Petroleum Technology, Volume 48, No. 1, 54-61, January 2009

[14]   Frauenfeld, T.W.J., Kissel, G. and Zhou, S.W., "PVT and Viscosity Measurements for Lloydmister-Aberfeldy and Cold Lake Blended Oil Systems", paper SPE 79018 presented at the SPE International Thermal Operations and Heavy Oil Symposium and International Horizontal Well Technology Conference, Calgary, AB, 4-7 November 2002.

[15]   P. H. Vankonynenburg and R. L. Scott, "Critical Lines and Phase-Equilibria in Binary Vanderwaals Mixtures", Philosophical Transactions of the Royal Society of London Series a-Mathematical Physical and Engineering Sciences, vol. 298, pp. 495-540, 1980.

[16]   Schouten, J. A., Deerenberg, A., and Trappeniers, N. J., "Vapour-Liquid and Gas-Gas Equilibriums in Simple Systems. IV. System Argon-Krypton". Physica, **81A**, 151-160, 1975

[17]   Wichterle, I. and Kobayashi, R. "Vapour-Liquid Equilibrium of Methane-Ethane System at Low Temperatures and High Pressures", J. Chem. Eng. Data, **17**, 9-12, 1972

[18]   Wichterle, I. and Kobayashi, R. "Vapour-Liquid Equilibrium of Methane-Propane System at Low Temperatures and High Pressures" J. Chem. Eng. Data, **17**, 4-8, 1972

[19]   G.J. Besserer, D.B. Robinson, "Equilibrium-phase properties of n-pentane- carbon dioxide system", Journal of Chemical and Engineering Data 18, 416–419, 1973.

[20]   W.L. Weng, M.J. Lee, "Vapor-liquid-equilibrium of the octane/carbon dioxide, octane/ethane, and octane/ethylene systems", Journal of Chemical and Engineering Data 37, 213–215, 1992

[21]   Hottovy, J.D., Luks, K.D. and Kohn, J.P., "Three phase liquid-liquid-vapor equilibria of certain binary CO-n-paraffin systems" J. Chem. Eng. Data, 26: 256-258, 1981.

[22]   Brunner, E., "Fluid Mixtures at High Pressures VI. Phase Separations and Critical Phenomena in 18 (n-alkane + ammonia) and 4 (n-alkane + methanol) Mixtures" J. Chem. Thermodynamics, **2 0**, 273-297, 1988a.

[23]   Brunner, E. "Fluid Mixtures at High Pressures II. Phase Separations and Critical Phenomena of (ethane + an n-alkanol) and of (ethane + methanol) and of (propane + methanol)", J. Chem. Thermodynamics, **17** , 871-885, 1985

[24]   T. W. De Loos, A. J. M. Wijen, and G. A. M. Diepen, "Phase equilibria and critical phenomena in fluid (propane + water) at high pressures and temperatures", The Journal of Chemical Thermodynamics, vol. 12, pp. 193-204, 1980.

[25] R.Enick, G.D.Holder and B.I. Morsi, "Critical and Three Phase Behavior in the Carbon Dioxide/Tridecane System", Fluid Phase Equilibria, **22**, pp. 209-224, 1985

[26] Davenport, A. J., Rowlinson, J. S. and Saville, G., "Solution of Three Hydrocarbons in Liquid Methane", Trans. Faraday Soc., 62, 322-327. 1966.

[27] A. J. Davenport and J. S. Rowlinson, "The Solubility of Hydrocarbons in Liquid Methane", Trans. Faraday SOC.,59, 78-84, 1963

[28] Kuenen, J. P.; Robson, W. G. "On the Mutual Solubility of LiquidsVapour-Pressure and Critical Points", Philos. Mag., 148, Ser.5, 180-203, 1899

[29] Schneider, G. M. "Pressure Influence on the Separation of Liquid Systems. I. Closed Miscibility Gaps up to 5000 bars", Z. Phys. Chem. N. F., 37, 333-352. 1963.

[30] C.J Peters, H.J. Van Der Kooi, J.L. De Roo, J. De Swaan Arons, "The search for tricriticality in binary mixtures of near-critical propane and normal paraffins" Fluid Phase Equilibria, Volume 51, pp. 339–351, 1989

[31] C.J. Peters, M.P.W.M. Rjkers, J.L. De Roo and J. De Swaan Arons, "Phase equilibria in binary mixtures of near-critical propane and poly-aromatic hydrocarbons", Fluid Phase Equilibria, Volume 52, Pages 373–387, 1989

[32] Bianca Breure, Eugene J. M. Straver, Louw J. Florusse, Marijn P. W. M. Rijkers, Ioannis G. Economou, Francisco M. Vargas, and Cor J. Peters, "Phase Equilibria in Binary Mixtures of Propane and Phenanthrene: Experimental Data and Modeling with the GC-EoS", J. Chem. Eng. Data, 56, 1407–141, 2011

[33] C.J. Peters, J.L. de Roo, J. de Swaan Arons, "Phase equilibria in binary mixtures of propane and triphenylmethane", Fluid Phase Equilibria 109, 99-111, 1995

[34] Fabiola Martínez, Alicia Martín, and Jesusa Rincón, "Solubility of Dibenzothiophene in Sub- and Supercritical Propane", J. Chem. Eng. Data, 56, 4364–4370, 2011

[35] Melchior A. Meilchen, Bruce M. Hasch, and Mark A. McHugh, "Effect of Copolymer Composition on the Phase Behavior of Mixtures of Poly(ethy1ene-co-methyl acrylate) with Propane and Chlorodifluoromethane", Macromolecules, 24, 4874-4882, 1991

[36] Christopher J. Gregg, Fred P.Stein, and Maciej Radosz, "Phase Behavior of Telechelic Polyisobutylene (PIB) in Subcritical and Supercritical Fluids. 1. Inter- and Intra-Association Effects for Blank, Monohydroxy, and Dihydroxy PIB(1K) in Ethane, Propane, Dimethyl Ether, Carbon Dioxide, and Chlorodifluoromethane", Macromolecules, Vol.27, No.18, 4972-4980, 1994

[37] A. K. Mehrotra, W. Y. Svrcek, "Properties of Cold Lake Bitumen Saturated with Pure Gases and Gas Mixtures", The canadian Journal of Chemical Engineering, Vol 66, 656-665, 1988

[38] Keivan Khaleghi: "Experimental PVT Study of the Phase Behavior of CO2 + Heavy Oil Mixtures", 2011 MSc

[39] Zou, X., Zhang X. and Shaw, J.M. "The Phase behavior of Athabasca Vacuum Bottoms +n-Alkane Mixtures, SPE Production & Operations," 22 (2), May 2007, 265-272

[40] S.J. Abedi, S Seyfaie, and J.M. Shaw, "Unusual Retrograde Condensation and Asphaltene Precipitation in a Model Heavy Oil Systems", Petroleum Science and Technology, 16 (3&4), 209-226, 1998

[41]   S.J. Abedi, H.Y. Cai, S. Seyfaie, J.M. Shaw, "Simultaneous phase behaviour, elemental composition and density measurement using X-ray imaging", Fluid Phase Equilibria, 158, 775–781, 1999

[42]   Mohammad Javad Amani, "Phase Behavior and Thermophysical Properties of Athabasca Bitumen and Athabasca Bitumen + Toluene Mixtures in Near-critical Water", 2013 PhD

[43]   E. W. Lemmon, M. O. McLinden, and D. G. Friend, "Thermophysical Properties of Fluid Systems", in NIST Chemistry WebBook, NIST Standard Reference Database Number 69, P. J. Linstrom and W. G. Mallard, Eds., ed Gaithersburg MD, http://webbook.nist.gov: National Institute of Standards and Technology, 2015.

[44]   Amani, Mohammad, Gray, M.R. and Shaw, J.M., "Phase Behavior of Athabasca Bitumen + Water Mixtures at High Temperatures and Pressure", Journal of Supercritical Fluids, 77(2013) 142-152.

[45]   Reamer, H. H.; Sage, B. H. "Phase equilibria in hydrocarbon systems. Volumetric and phase behavior of the propane−n-decane system." J. Chem. Eng. Data, 11, 17−24, 1966

[46]   Wtt-pro.nist.gov, 'NIST/TRC Web Thermo Tables (WTT): Critically Evaluated Thermophysical Property Data', June 2015

Appendix 1. Supplementary data

Detailed data of the propane + bitumen mixtures are provided in this section. Initial inserted mass, temperature, pressure, L1, L2 and vapor volumes, X-ray intensity and densities.

Table 1. Initial inserted mass

Mixtures	Propane mass (g)	Bitumen mass (g)
Bitumen + 0.098 wt. fraction propane	3.4	31.7
Bitumen + 0.161 wt. fraction propane	6.1	31.6
Bitumen + 0.254 wt. fraction propane	10.8	31.6
Bitumen + 0.397 wt. fraction propane	14.7	22.2
Bitumen + 0.495 wt. fraction propane	11.0	11.2
Bitumen + 0.742 wt. fraction propane	24.3	8.5
Bitumen + 0.857 wt. fraction propane	28.0	4.7

Table 2. Bitumen + 0.098 wt. fraction propane

Temperature (K)	Pressure (MPa)	Vapor Volume (mL)	Liquid volume (mL)	Liquid intensity	Beryllium intensity	Liquid density (kg.m^{-3})	Phase
302.9	0.57	62.3	36.5	102	88	958	L2V
303.1	0.56	65.2	36.5	100	86	956	L2V
303.6	0.54	69.6	36.5	95	81	944	L2V
313.4	0.67	62.3	36.6	95	83	964	L2V
313.0	0.64	69.5	36.5	96	84	962	L2V
312.7	0.61	73.9	36.2	94	81	960	L2V
322.3	0.73	64.2	36.7	95	83	963	L2V
322.3	0.72	67.8	36.6	96	83	962	L2V
322.1	0.71	70.9	36.5	97	84	963	L2V
335.4	0.83	61.8	36.8	95	83	960	L2V
335.6	0.82	65.9	36.7	96	83	959	L2V
335.3	0.81	72.3	36.9	97	84	956	L2V
344.4	0.94	63.5	36.7	96	83	959	L2V
344.7	0.93	68.9	37.0	97	84	957	L2V
345.0	0.89	73.3	37.0	95	82	953	L2V
351.7	1.04	62.4	36.8	95	82	957	L2V
352.0	1.00	68.7	37.0	96	83	956	L2V
351.9	0.97	71.6	37.2	97	83	954	L2V
362.2	1.16	61.3	37.2	99	86	957	L2V
362.1	1.14	63.1	37.2	96	83	956	L2V
362.1	1.13	64.2	36.6	95	81	953	L2V
372.2	1.26	62.6	37.3	96	83	956	L2V
372.0	1.23	64.8	37.3	97	83	954	L2V
371.2	1.16	73.5	36.9	96	82	949	L2V
382.0	1.43	60.8	37.3	97	84	954	L2V
382.1	1.37	67.4	37.1	99	85	950	L2V
382.1	1.29	73.9	37.0	98	83	944	L2V
392.4	1.52	60.8	37.4	101	86	948	L2V
392.3	1.44	67.7	37.3	99	83	945	L2V
392.7	1.40	71.0	37.3	93	77	932	L2V

Table 3. Bitumen + 0.161 wt. fraction propane

Temperature (K)	Pressure (MPa)	Vapor Volume (mL)	Liquid volume (mL)	Liquid intensity	Beryllium intensity	Liquid density (kg.m^{-3})	Phase
302.7	0.68	59.8	40.1	106	89	939	L2V
302.9	0.67	65.5	40.0	99	81	925	L2V
303.0	0.66	69.4	40.0	100	81	922	L2V
313.8	0.84	61.0	40.2	98	83	948	L2V
313.6	0.83	63.4	40.2	99	84	946	L2V
313.3	0.81	68.3	40.0	100	84	942	L2V
325.1	0.99	71.1	40.0	97	83	947	L2V
325.1	1.04	60.2	40.1	99	84	944	L2V
325.4	1.02	66.3	39.9	97	81	940	L2V
333.3	1.17	63.3	40.0	98	83	945	L2V
333.2	1.15	67.6	39.9	99	84	942	L2V
332.7	1.13	69.9	39.9	97	81	940	L2V
341.4	1.33	61.0	39.9	98	83	944	L2V
341.4	1.31	64.5	39.9	99	84	944	L2V
341.4	1.28	69.1	39.7	100	84	940	L2V
352.8	1.51	62.6	39.8	98	83	944	L2V
353.0	1.49	69.1	39.2	99	83	942	L2V
365.6	1.75	64.5	39.2	99	83	941	L2V
365.8	1.73	67.5	39.2	99	84	940	L2V
365.7	1.70	69.8	39.1	100	84	938	L2V
372.6	1.88	64.1	39.3	100	84	939	L2V
372.7	1.84	67.3	39.2	101	85	936	L2V
372.4	1.79	71.7	39.1	99	82	933	L2V
382.4	2.04	64.7	39.2	102	85	936	L2V
381.6	2.00	67.4	39.2	103	86	935	L2V
381.7	1.94	71.9	39.1	100	84	934	L2V
392.9	2.22	64.6	39.2	98	80	922	L2V
392.8	2.18	67.2	39.2	100	80	906	L2V
392.6	2.12	70.9	39.2	96	78	921	L2V

Table 4. Bitumen + 0.254 wt. fraction propane

Temperature (K)	Pressure (MPa)	Vapor Volume (mL)	Liquid volume (mL)	Liquid intensity	Beryllium intensity	Liquid density (kg.m^{-3})	Phase
303.4	0.89	57.3	48.8	112	88	901	L2V
303.5	0.89	59.1	48.8	112	89	900	L2V
303.7	0.89	61.6	48.7	113	89	899	L2V
313.6	1.12	57.5	48.2	107	85	907	L2V
313.6	1.12	59.0	48.2	107	85	907	L2V
313.5	1.12	62.4	48.1	109	89	920	L2V
325.1	1.43	58.8	48.0	112	91	920	L2V
325.2	1.43	60.6	48.0	113	92	918	L2V
325.0	1.42	63.6	47.5	104	83	904	L2V
336.4	1.78	58.2	47.4	112	92	920	L2V
336.5	1.76	60.9	47.4	107	85	906	L2V
336.2	1.74	63.6	47.3	100	80	906	L2V
344.2	2.03	58.3	47.2	107	85	907	L2V
344.2	2.01	60.7	47.1	107	86	907	L2V
344.0	1.99	63.3	46.6	104	83	906	L2V
353.6	2.33	60.3	46.4	107	86	909	L2V
353.6	2.32	62.1	46.4	108	86	908	L2V
353.5	2.30	64.3	46.2	104	83	907	L2V
364.1	2.69	59.8	45.8	108	86	909	L2V
364.1	2.66	62.3	45.7	108	87	910	L2V
364.1	2.64	65.1	45.5	105	84	909	L2V
372.8	2.96	61.6	45.5	108	86	911	L2V
373.3	3.00	59.2	45.1	112	90	910	L2V
373.3	2.90	66.2	44.9	105	84	910	L2V
381.6	3.26	60.5	44.9	108	87	912	L2V
381.2	3.21	63.2	44.8	109	87	911	L2V
381.4	3.16	66.2	44.8	106	85	910	L2V
394.8	3.62	61.0	44.8	110	88	912	L2V
395.0	3.54	67.0	44.1	108	86	909	L2V

Table 5. Bitumen + 0.397 wt. fraction propane

Temperature (K)	Pressure (MPa)	Vapor Volume (mL)	L1 volume (mL)	L2 volume (mL)	Phase
303.9	1.00	56.1	34.9	15.3	L1L2V
303.9	1.00	58.8	34.7	15.5	L1L2V
303.9	1.00	60.9	34.7	15.5	L1L2V
314.5	1.30	56.8	34.6	15.5	L1L2V
314.5	1.30	61.3	33.9	15.5	L1L2V
314.2	1.29	62.9	34.0	15.4	L1L2V
325.1	1.66	53.3	33.1	17.0	L1L2V
325.1	1.66	58.4	32.3	17.1	L1L2V
324.8	1.64	62.5	32.6	16.7	L1L2V
334.0	2.01	57.5	29.8	18.8	L1L2V
334.0	2.00	59.8	29.9	18.7	L1L2V
333.6	1.98	63.8	29.3	18.6	L1L2V
342.6	2.39	58.5	26.6	21.1	L1L2V
342.4	2.37	60.1	26.7	21.0	L1L2V
342.3	2.36	62.3	27.3	20.3	L1L2V
354.8	2.99	60.3		45.3	L2V
354.7	2.97	65.3		44.5	L2V
354.6	2.95	67.4		44.4	L2V
362.9	3.46	62.1		42.9	L2V
363.2	3.45	66.0		42.2	L2V
363.1	3.42	69.5		41.9	L2V
375.2	4.14	64.2		39.0	L2V
375.3	4.10	66.5		38.8	L2V
374.8	4.05	70.0		38.6	L2V
383.2	4.57	64.3		37.3	L2V
383.2	4.50	68.8		37.1	L2V
383.3	4.46	72.8		36.5	L2V
392.5	5.02	66.5		35.6	L2V
392.5	4.95	69.8		35.5	L2V
392.5	4.88	74.0		35.1	L2V

Table 6. Bitumen + 0.495 wt. fraction propane

Temperature (K)	Pressure (MPa)	Vapor Volume (mL)	L1 volume (mL)	L2 volume (mL)	Phase
304.8	1.05	67.0	7.9	20.2	L1L2V
304.8	1.05	71.6	8.1	20.0	L1L2V
304.9	1.05	80.0	7.9	19.7	L1L2V
313.1	1.29	65.0	8.5	19.5	L1L2V
312.8	1.28	70.4	8.5	19.1	L1L2V
312.4	1.26	79.0	8.5	18.7	L1L2V
323.9	1.65	64.9	9.2	18.1	L1L2V
324.0	1.65	68.7	9.2	17.7	L1L2V
323.9	1.64	77.2	9.2	17.1	L1L2V
333.0	2.00	67.2	10.2	15.7	L1L2V
332.8	1.99	71.6	10.2	15.4	L1L2V
332.4	1.97	79.0	10.2	14.9	L1L2V
344.6	2.52	68.1	11.1	13.1	L1L2V
344.8	2.53	73.2	11.1	12.3	L1L2V
345.0	2.52	80.4	11.2	11.4	L1L2V
354.5	3.04	65.1	13.1	8.8	L1L2V
354.5	3.03	68.1	13.1	9.1	L1L2V
354.5	3.01	73.8	13.1	8.1	L1L2V
365.0	3.57	66.7		19.7	L2V
364.8	3.50	73.2		19.0	L2V
365.1	3.39	82.9		18.3	L2V
372.8	3.89	69.2		18.3	L2V
372.8	3.78	75.9		18.0	L2V
372.6	3.67	83.4		17.4	L2V
382.4	4.26	69.3		17.5	L2V
382.2	4.12	76.0		17.3	L2V
382.1	4.02	81.6		16.9	L2V
393.0	4.63	69.6		16.9	L2V
392.8	4.49	75.3		16.6	L2V
392.7	4.41	78.4		16.6	L2V

Table 7. Bitumen + 0.742 wt. fraction propane

Temperature (K)	Pressure (MPa)	Vapor Volume (mL)	L1 volume (mL)	L2 volume (mL)	Phase
304.4	1.06	54.2	47.6	5.2	L1L2V
304.4	1.06	57.4	48.2	5.2	L1L2V
304.3	1.06	59.6	47.8	5.1	L1L2V
314.1	1.35	54.2	48.7	4.9	L1L2V
313.9	1.34	56.9	49.3	5.0	L1L2V
313.8	1.34	57.9	49.3	4.9	L1L2V
324.1	1.70	54.3	49.0	5.3	L1L2V
324.1	1.70	56.8	49.0	5.3	L1L2V
324.0	1.70	58.2	48.9	5.3	L1L2V
333.1	2.07	53.8	48.6	5.6	L1L2V
333.1	2.07	57.0	48.0	5.6	L1L2V
333.0	2.05	59.0	47.8	5.6	L1L2V
343.4	2.56	53.2	48.0	6.4	L1L2V
343.5	2.56	56.2	47.0	6.5	L1L2V
343.3	2.56	59.6	46.2	6.6	L1L2V
354.0	3.14	56.2	45.3	7.5	L1L2V
354.3	3.15	59.1	44.4	7.6	L1L2V
354.1	3.12	63.0	42.0	7.6	L1L2V
363.2	3.70	54.2	43.5	8.5	L1L2V
363.0	3.69	57.5	43.3	8.6	L1L2V
363.0	3.69	62.6	40.9	8.7	L1L2V
372.9	4.39	55.8	38.9	9.9	L1L2V
372.9	4.39	60.9	36.2	10.3	L1L2V
372.8	4.38	70.8	31.3	10.5	L1L2V
381.5	5.12	82.9		18.0	L2V
381.1	5.05	88.5		18.0	L2V
381.2	5.02	97.6		18.0	L2V
392.1	6.07	82.2		19.3	L2V
392.2	5.93	90.6		19.3	L2V
392.1	5.81	98.5		19.3	L2V

Table 8. Bitumen + 0.857 wt. fraction propane

Temperature (K)	Pressure (MPa)	Vapor Volume (mL)	Liquid volume (mL)	L1 volume (mL)	L2 volume (mL)	Liquid intensity	Beryllium intensity	L1 density (kg.m^{-3})	Phase
303.3	1.01	50.3	58.2	57.0	1.2	169	99		L1L2V
303.4	1.01	51.7	58.2	57.0	1.2	158	92		L1L2V
314.4	1.32	51.6	58.9	57.7	1.2	153	87		L1L2V
314.2	1.31	52.1	58.9	57.7	1.2	153	87		L1L2V
314.0	1.30	53.4	58.9	57.7	1.2	149	85		L1L2V
323.5	1.63	49.7	58.2			172	97	600	L1V
323.5	1.62	51.3	58.9			155	87	600	L1V
323.4	1.62	52.7	58.9			155	87	601	L1V
334.2	2.04	51.2	58.1			157	87	584	L1V
334.2	2.04	52.5	58.2			158	87	584	L1V
334.1	2.03	53.6	58.1			158	87	584	L1V
343.7	2.47	50.3	58.1			166	90	566	L1V
343.7	2.46	51.6	58.1			161	87	567	L1V
343.4	2.45	53.2	58.1			161	88	566	L1V
352.4	2.91	50.8	58.1			169	90	546	L1V
352.3	2.90	51.7	58.0			170	90	547	L1V
362.6	3.48	50.6	57.4			174	91	525	L1V
362.6	3.47	52.4	57.3			174	92	527	L1V
362.2	3.45	53.5	57.4			175	92	529	L1V
372.7	4.29	94.4	0.0						V
373.0	4.21	99.9	1.2						L2V
372.8	4.13	106.5	2.5						L2V
380.9	4.84	94.4	0.0						V
380.7	4.71	101.0	1.2						L2V
380.6	4.63	109.5	2.2						L2V
389.8	5.60	90.9	2.4						L2V
389.8	5.47	94.5	4.3						L2V
390.0	5.39	100.1	5.7						L2V

Appendix 2. Image processing code in MATLAB

Example of Matlab code used for the image processing is presented in this section. The code may change depending on the desired parameters of the images. This code allows to detect the liquid-liquid and liquid-vapor interfaces, the bellows position and the intensity of a specific area.

```
clc
clear all,
close all
tic
javaaddpath('/Users/Yoann/Documents/MATLAB/poi_library/poi-3.8-20120326.jar');
javaaddpath('/Users/Yoann/Documents/MATLAB/poi_library/poi-ooxml-3.8-
20120326.jar');
javaaddpath('/Users/Yoann/Documents/MATLAB/poi_library/poi-ooxml-schemas-3.8-
20120326.jar');
javaaddpath('/Users/Yoann/Documents/MATLAB/poi_library/xmlbeans-2.3.0.jar');
javaaddpath('/Users/Yoann/Documents/MATLAB/poi_library/dom4j-1.6.1.jar');
javaaddpath('/Users/Yoann/Documents/MATLAB/poi_library/stax-api-1.0.1.jar');

offset1 = 1;
offset2 = 1;
run=0;
imagefiles = dir('*.tif');
nfiles = length(imagefiles);
for ii=1:nfiles
Address=imagefiles(ii).name;
image001 = double(imread(Address));
image001 = mat2gray(image001);
image001= imrotate((image001),-90,'bicubic');
image001= imrotate((image001),-1,'bicubic','crop');
imagesize=size(image001);
image= image001;
imagesize=size(image);
imageaverage = zeros(1,imagesize(2));

% Phase detection (Edge)average
% Swap horizentally from YE1 to YE2 along XE1 to XE2
```

```matlab
% Green Box
                XE2=imagesize(2);
                  YE2=320;


XE1=1;
   YE1=240;


for x = XE1:imagesize(2)  % swap vertically 765
     counter = 0; sum=0;
    for y = YE1 :YE2%170
        % 260 to 290 for bolt_vol_calib
        % swap horizentally
        if image(y,x)==0
           %a=a+1;
        else
           sum = sum + image(y,x);
           counter=counter+1;
        end
    end

    imageaverage(1,x) = sum/counter;
    if x<imagesize(2)
    t(1,x)=x;
    end
end


for i=XE1+1:XE2-1
   dimage1(i)=(imageaverage(1,i+1)-imageaverage(1,i-1))/2;
   f=0;b=0;

   if i<21
     dimage3(i)=dimage1(i);
   else
     for z=1:20

     if ( i>imagesize(2)-20)
     dimage3(i)=dimage1(i);
     else

     f= f + imageaverage(1,i+z);
     b = b + imageaverage(1,i-z);
     dimage3(i)=(f/20 - b/20);
     end
```

94

```
   end
      end

   end

%  Peaks
[maxtab, mintab] = peakdet(dimage3,0.06,t);

%Figure
%if run<1 run=1; end
z=sprintf('%s',Address);

figure('Name',z);
hold on
subplot(3,1,1),
plot(imageaverage,'black')
%axis([0 750 0 10])
subplot(3,1,3),
plot(dimage3,'black')

%  Print Peaks

%And from here we continue like before, but note that the X axis represents "t" and not
indices.
hold on; plot(mintab(:,1), mintab(:,2), 'g*');
plot(maxtab(:,1), maxtab(:,2), 'r*');

subplot(3,1,2),
image001=image(YE1:YE2,XE1:XE2);
pcolor(image001);
shading interp
colormap gray

% Initialisation of POI Libs
% Add Java POI Libs to matlab javapath


% Data Generation for XLSX
% Define an xls name

if offset1<1
offset=1;
end

if offset2<1
offset2=1;
```

```matlab
    end

    fileName = 'test_xlwrite.xlsx';
    sheetName = 'this_is_sheetname';

    % Generate some data
    startRange = sprintf('E%d',offset1);
    xlsData1 = {sprintf('%s',Address) };
    offset1 = offset1 + 2;
    xlwrite(fileName, xlsData1, sheetName, startRange);

    startRange = sprintf('G%d',offset1);
    xlsData4 = {'Peak Pixel Position(min)' [] };
    offset2 = offset1 + 1;
    xlwrite(fileName, xlsData4, sheetName, startRange);

    startRange = sprintf('G%d',offset2);
    xlsData5 = [ mintab ];
    offset2 = offset2 + length(mintab)+2;
    xlwrite(fileName, xlsData5, sheetName, startRange);

    startRange = sprintf('B%d',offset1);
    xlsData2 = {'Peak Pixel Position(max)' [] };
    offset1 = offset1 + 1;
    xlwrite(fileName, xlsData2, sheetName, startRange);

    startRange = sprintf('B%d',offset1);
    xlsData3 = [ maxtab ];
    offset1 = offset1 + length(maxtab)+2;
    xlwrite(fileName, xlsData3, sheetName, startRange);


    if offset2<offset1
    offset2=offset1;
    else
    offset1=offset2;
    end

    run=run+1;

    end
    toc
```